Mechanistic role of forces in the regulation of morphogenetic movements during gastrulation.

Pooja Rajendra Sonavane

Pune, India

M.S., University of Pune, 2010

A Dissertation Presented to the Graduate Faculty of the University of Virginia in Candidacy for the Degree of Doctor of Philosophy

Department of Cell Biology

University of Virginia
May 2018

Abstract

The coordinated cellular movements are crucial for the assembly and morphogenesis of tissue during embryonic development. These movements are governed by chemical and mechanical inputs from the surrounding microenvironment. Mechanical forces are generated and sensed at cell-cell and cell-extracellular matrix (ECM) junctions. Cytoskeletal linkages at these junctions are essential for transduction of mechanical inputs. These mechanical cues are essential for guiding directed migration during morphogenesis. In this dissertation, I have investigated the mechanism by which cells balance forces between cadherin-based cell-cell adhesions and integrin-based focal adhesions (FAs) during collective migration in *Xenopus* embryos.

Xenopus mesendoderm cells migrate collectively along a fibronectin substrate at gastrulation, but how the adhesive and mechanical forces required for these movements are generated and transmitted is unclear. I demonstrated that mesendoderm cells organize into leader and follower cells. The traction forces are limited primarily to leading edge cells in mesendoderm explants, and that these forces are balanced by intercellular stresses in follower rows. This is further reflected in the morphology of these cells, with broad lamellipodial protrusions, mature focal adhesions and a gradient of activated Rac1 evident at the leading edge, while small protrusions, rapid turnover of immature focal adhesions and lack of a Rac1 activity gradient characterize cells in following rows. I established that keratin intermediate filaments (IFs) are necessary for the maintenance of the organization of mesendoderm tissue and loss of keratin IFs results in high traction stresses in follower row cells, misdirected protrusions and the formation of actin stress fibers anchored in

streak-like focal adhesions. I propose that maintenance of mechanical integrity in the mesendoderm by keratin intermediate filaments is required to balance forces within the tissue to regulate collective cell movements. I also show that cadherin-associated protein, plakoglobin (PG; also known as γ-catenin) is also essential to proper mesendoderm migration. PG is required for regulating the dynamics of FAs, the organization of actin and keratin IF network during mesendoderm migration. I propose that PG acts by maintaining forces balance between cadherin and integrin adhesions required for polarization of mesendoderm cells during migration.

The data presented in this study focuses on understanding the role of forces in the regulation of morphogenetic processes. I have identified a unique role for keratin IFs and PG in maintaining crosstalk between cadherin and integrin adhesions. Taken together these findings indicate that achieving the balance of forces between cellular junctions is integral to tissue morphogenesis.

Acknowledgements

My journey to the completion of this degree would not have been possible without the constant support and encouragement of many people. First, I would like to thank my mentor, Doug DeSimone who guided me through the ups and downs of my graduate career with patience, enthusiasm and dedication. He has provided me with the opportunity to learn, to think, to critique and to explore. His guidance over the years, I believe, has truly helped me become a better scientist. I am also grateful for the support and guidance of my committee members Ann Sutherland, David Castle and Dorothy Schafer.

I am thankful to all past and present lab members of the DeSimone lab. I thank Bette for guiding me, providing critical feedback and most importantly for all the advice and help with writing. Bette is not only an amazing colleague but she is a very supportive friend as well. Next, I thank Fred and Kara for excellent frog care, lab management and day-to-day life advice. I would like to thank Glen and Crystal for discussing new ideas and experiments, for cheering me when all my experiments failed and celebrating with me when they succeeded. I also thank Greg, Maureen, Chong, Tania, Claire, Dave and Wiktor for making my time spent in lab fun-filled and memorable. I would like to extend my gratitude to all the current and past members of the Cell Biology department for the inspiring hallway conversations. I would especially like to thank Ryan D'Souza and Karen Litwa for their guidance and technical advice.

I thank the friendly staff at PeachMac store in Charlottesville especially Vanya Grove for the help with data recovery.

I am grateful for the encouragement and support of my friends and family. I am thankful to my friends Jaamun, Ramya, Lakme, Chhavi, Budha, Mandovi, Manisha, Ankit,

Kunal and Ez from Charlottesville for their supports outside of the lab. I would like to acknowledge my friends Tanvi, Ankita and Neha for their inspiration and motivation over the years. I would like to thank my aunt Uma Pawar, uncle Sanjay Pawar and their kids Sachi and Amogh for welcoming me in their lives and never making me miss my own family since the day I moved to the US.

Finally, I owe never-ending gratitude to my sister Aarti, my parents Manjusha and Rajendra, and Prasad for always being there by my side. Without their support, love and constant encouragement none of this would have been possible!

Table of Contents

List of Abbreviations

AJs	Adherens Junctions
AFM	Atomic Force Microscopy
BCR	Blastocoel Roof
BSA	Bovine Serum Albumin
C-CadFc	Extracellular domain of C-cadherin
CE	Convergence and Extension
CMF MBS	Ca^{2+}/Mg^{2+} free MBS
DIC	Differential Interference Contrast
DP	Desmoplakin
DMZ	Dorsal Marginal Zone
ECM	Extracellular Matrix
EGFP	Enhanced Green Fluorescent Protein
EMT	Epithelial to Mesenchymal Transition
EVL	Enveloping Layer
FAs	Focal Adhesions
FAK	Focal adhesion kinase
FN	Fibronectin

fr	following row
FRET	Fluorescent Resonance Energy Transfer
GST	Glutathione S transferase
HepII	Heparin binding domain
IP	Immunoprecipitation
IFs	Intermediate Filaments
Krt8	Keratin(8)
LINC	Linker of nucleoskeleton and cytoskeleton
lr	leading row
MBS	Modified Barth's Saline
MMPs	Matrix Metalloproteinases
MSCs	Mesenchymal stem cells
MO	Morpholino Oligodeoxynucleotides
PDGF	Platelet Derived Growth Factor
PG	Plakoglobin
PLL	Poly-L-Lysine
pLLP	posterior Lateral Line Primordium
pMLC	phosphorylated Myosin Light Chain
RGD	Arginine-Glycine-Aspartic Acid

ROS	Reactive Oxygen Species
TFM	Traction Force Microscopy
TGF-β	Transforming Growth Factor β
TIRF	Total Internal Reflection Microscopy
UFR	upper following row

List of Tables

List of Figures

Note to reader:

Unless otherwise mentioned in the figure legends, all data were generated and analyzed by the author, Pooja Sonavane. Data for few figures were generated in collaboration with other whereas on other instances, data were generated wholly by other. However, even in these instances, the design and analysis of the experiments were conducted cooperatively.

Chapter 1

Introduction: Forces in embryonic development

1.1 Mechanical forces in tissue morphogenesis

Tissue morphogenesis involves cell proliferation (Morrison and Kimble, 2006), differentiation (Przybyla et al., 2016) and coordinated cell movements (Hunter and Fernandez-Gonzalez, 2017; Keller et al., 2003). In order to achieve morphogenesis, cells have to dynamically interact with neighboring cells and the surrounding microenvironment by forming either cell-cell junctions or cell-extracellular matrix (ECM) junctions (Collins and Nelson, 2015; Gumbiner, 2005; Weber et al., 2011) respectively. Work done for well over a century has established the importance of tissue morphogenesis in physiological processes such as embryogenesis and maintenance of tissue homeostasis. Although signaling networks essential for tissue morphogenesis have been well characterized (Albert Basson, 2012), mechanical forces that regulate cellular behavior during morphogenesis are just starting to be understood (Heisenberg and Bellaïche, 2013; Lecuit et al., 2011). However, the concept that forces shape embryos was introduced by Wilhelm Roux in 1895 and that mechanical forces have an instructive role during morphogenesis was further highlighted by D'Arcy Thompson in 1917 (Thompson 1917). It is only with advancements in biophysical and biochemical techniques, that help to measure the forces generated and experienced by the cells, that we have now begun to appreciate the mechanistic role of forces in regulating cell and tissue behavior.

1.2 What is mechanotransduction?

The question how cells generate and resist forces that are necessary to shape tissue during morphogenesis has raised a lot of interest in the recent years. Moreover, the

machinery cells utilize to do so has been studied extensively. Cells can sense mechanical cues from neighboring cells as well as the surrounding microenvironment by a process called mechanosensing. A response to the changing mechanical environment by altering biochemical signals occurs through a process called mechanotransduction (Chen et al., 2004; Iskratsch et al., 2014). Cell junctional proteins like cadherins and integrins that are essential to maintain tissue cohesion in metazoans also link cytoskeletal networks to the neighboring cells and ECM (Collins and Nelson, 2015; Gumbiner, 2005; Weber et al., 2011). These junctional proteins thus facilitate the crosstalk between cell intrinsic and extrinsic factor during mechanotransduction and can be classified as mechanosensor/mechanotransducer proteins (Chen et al., 2004). Although a lot is known about how integrins and cadherins carry out mechanotransduction, the mechanical crosstalk between signaling event at integrins and cadherin is just starting to be understood. Here, I will focus on how cell intrinsic and extrinsic mechanical forces activate mechanosensor and downstream effects of mechanotransduction such as changes in cytoskeletal networks. Furthermore, I will discuss the mechanism by which cells generate forces that are essential for proper morphogenesis and how these mechanical stimuli drive tissue morphogenesis during embryonic development.

1.3 Mechanotransduction at cell junctions.

Cells in a tissue experience mechanical forces such as shear stress, pulling or stretching forces, compression or tensile forces from the surrounding environment; whereas hydrostatic forces act from within the cells (Figure 1.1A-E; Schwartz and DeSimone, 2008). The stiffness of ECM also plays a critical role in mechanotransduction.

Cells establish contact with neighboring cells and surrounding matrix by forming cadherin and integrin-based adhesions respectively and these proteins help to propagate mechanical signal throughout the tissue. These mechanosensors recruit signaling molecules like kinases and phosphatases to the site of cellular contact (Aplin, 2003). Integrins and cadherins also undergo conformational changes in order to activate downstream signaling. Conformational changes can be regulated either by the stiffness of ECM (outside-in signaling) or changes in signaling within the cells (inside-out signaling; Barry et al., 2014). ECM stiffness can limit the accessibility of the morphogens to the cells (Lu et al., 2011; Rozario and DeSimone, 2010) thus, regulating the response of the cells to mechanical cues (Figure 1.1F). In this section, I will discuss how cells sense mechanical variation and how this leads to activation of mechanosensor and changes in cytoskeletal networks.

Mechanotransduction at cell-ECM adhesions: Integrin activation

Adhesion of cells to the ECM is facilitated by heterodimeric integrin receptors (Figure1.2A). Integrin receptors are composed of an α and β transmembrane glycoprotein subunits. Each subunit consists of a large extracellular head domain, a single pass transmembrane domain and a short cytoplasmic tail. Integrin receptors link ECM to the cytoskeletal networks in the cells and can transmit signals in a bidirectional manner (Figure 1.2B; Campbell and Humphries, 2011; Hynes, 2002). Integrins exist in a "low-affinity" state characterized by the V-shaped or bent conformation of the integrins and are stabilized in this conformation by the presence of a salt bridge between the two subunits (Chen et al., 2001; Mould et al., 2002; Yan and Smith, 2001). Conformational changes necessary for integrin activation can be achieved through association of the integrin head domain with

appropriate ECM ligand referred to as "outside-in signaling" or through binding of talins and kindlins to the cytoplasmic domains of the β subunit referred to as inside-out signaling (Figure 1.2B; (Du et al., 1991; Humphries, 2002; Patil et al., 1999). Outside-in or inside-out signaling causes breakage of the salt bridge and extension of integrin receptor by a switchblade-like motion to adopt an open conformation or "high-affinity" state (Figure 1.2B; Diaz-Gonzalez et al., 1996; Tsuchida et al., 1998). The physical state of the ECM has been demonstrated to regulate the activation of integrins (Choquet et al., 1997; Friedland et al., 2009; Paszek et al., 2009). On softer substrate cells form week integrin adhesion whereas on stiffer matrix adhesions formed are stronger. This is because cells on a softer substrate are unable to transmit forces via integrin adhesions. Integrins-based adhesions increase in strength upon applying external forces (Figure 1.1F; Friedland et al., 2009). These types of adhesions are known as catch-bond, adhesions that increase in strength upon force application.

Integrin adhesion and actin linkage

Once activated, integrin receptors cluster to form focal adhesion (FA) complexes and connect ECM to the actin network in the cell (Figure 1.2C). FAs are well-characterized mechanosensitive structures bearing high stresses. During migration, cells exert traction forces on the underlying matrix via FA complexes (Beningo et al., 2001). FA dynamics are regulated by matrix stiffness and are essential for proper migration of cells (Prager-Khoutorsky et al., 2011). FAs elongate in response to external forces applied on the cell-ECM interface (Stricker et al., 2011). The assembly and maturation of FAs requires the sequential recruitment and phosphorylation of proteins such as talin, kindlin, paxillin,

vinculin, focal adhesion kinase (FAK) and Src-kinase at the cytoplasmic tail of integrin receptors (Figure 1.2C; Carisey et al., 2013; Lawson et al., 2012; Parsons and Parsons, 2004; Schaller, 2001; Tanentzapf and Brown, 2006). These core complex proteins undergo conformation change in response to external forces, which exposes cryptic site necessary for protein binding (Del Rio et al., 2009; Dumbauld et al., 2013; Yao et al., 2014). Mechanical linking of the actin cytoskeleton to the FAs is partially dependent on conformational changes in vinculin (Carisey et al., 2013; Humphries et al., 2007). Additionally, external forces are responsible for the changes in the enzymatic activity of core complex proteins such as FAK and Src-kinase. FAK activity is required for activation of Rho GTPase signaling at the FA sites; FAK also acts as a key mechanotransducer by regulating the turnover of FAs (Webb et al., 2004). Turnover or disassembly of FAs is important for persistent migration of cells. Cells that lack FAK are unable to respond to mechanical cues, show large FAs and have lower migration rates (Ilić et al., 1995). Tension across the FAs varies, with high tension noted at the assembling end and low tension at the disassembling end of FAs (Grashoff et al., 2010; Kumar et al., 2016). Since actin are linked to the FAs, actin filaments throughout FAs experience differential pulling forces. This variation of tension across FAs regulates the polymerization of actin filaments (Case and Waterman, 2015). Actin polymerization pushes the cellular membrane forward during migration and is necessary for cell shape changes. Thus, integrin receptors play crucial roles in mechanotransduction by connecting ECM and actin cytoskeletal network.

Intermediate Filament based integrin adhesions

All integrins except α6β4 bind to actin filaments to the cytoplasmic domain. α6β4 integrins that bind to basal lamina, however, associates with intermediate filaments (IFs) (Figure 1.2A; Dowling et al., 1996; Georges-Labouesse et al., 1996). Apart from α6β4 and IFs, hemidesmosomes comprise of protein from the plakin family like plectins and bullous pemphigoid antigen 230 (BP 230; Figure 1.2D; Borradori and Sonnenberg, 1999). Hemidesmosomes provide mechanical integrity to epithelial structure such as the skin. Loss of hemidesmosomes makes the tissue vulnerable to mechanical stress and causes blistering and rupturing of skin (Irwin McLean et al., 1996; Takahashi and Coulombe, 1996). Furthermore, keratinocytes lacking keratin IFs that are unable to form hemidesmosomes show disruption of plectin distribution and higher migration rates (Seltmann et al., 2013). Moreover, in *C. elegans,* hemidesmosomes are formed between epidermis and muscle walls and mechanical forces generated due to muscle contraction reinforce hemidesmosomes in the epidermis. This propagation of the mechanical cue is necessary for embryonic elongation (Zhang et al., 2011). Although, it has been established that hemidesmosomes are essential to maintain mechanical integrity, the mechanism by which hemidesmosomes do so needs further investigation.

Vimentin IFs are reported to localize at actin containing mature FAs. As described earlier, maturation of FAs is a forces dependent process (Chrzanowska-Wodnicka and Burridge, 1996). Vimentin IFs at FAs regulate signaling through FAK and formation of force bearing actin stress fibers (Gregor et al., 2014; Jiu et al., 2017). Thus, integrins adhesions linking IFs play an active important role in cellular mechanotransduction.

Mechanotransduction at cell-cell adhesions: Role of Cadherin in force transduction

Cells primarily establish contact with the neighboring cell by forming cadherin-based adhesions (Figure 1.3A). Force-induced changes in neighboring cells are communicated through these adhesions. Cadherins comprise a superfamily of calcium-dependent adhesion molecules. Cadherins typically consist of a globular extracellular domain, a single pass transmembrane domain and a cytoplasmic domain. Cadherins can be classified into two groups depending on the cytoskeletal proteins that are recruited to the cytoplasmic domain. These groups are "classical cadherins" that bind to actin filaments and "desmosomal cadherins" that bind to IFs (Figure 1.3A and C-D; discussed in the next section). The extracellular domain of classical cadherins like E-cadherin, N-cadherin, VE-cadherin and C-cadherin interact with homotypic cadherin molecules on the neighboring cell (also called trans interaction) to form adherens junctions (AJs). Ligation of cadherin molecules in trans promotes clustering of cadherin molecules (Figure 1.3B; Niessen et al., 2011). Magnetic twisting cytometry performed to manipulate forces at cadherin adhesions showed that cadherin adhesions respond to forces and that cadherins are involved in cellular mechanotransduction (Le Duc et al., 2010). Moreover, increasing tension at cadherin adhesions causes reinforcement of AJs (Borghi et al., 2012; Liu et al., 2010; Miyake et al., 2006). Following adhesion and clustering, cadherin molecules associate with proteins of the catenin family. Cadherins bind to α-catenin through direct interaction with either β-catenin or plakoglobin (PG/γ-catenin; Figure 1.3C). α-catenins play a central role in mechanotransduction at cadherin adhesions (Barry et al., 2014; Yonemura et al., 2010). α-catenin bound to cadherins undergoes a conformational change in response to force and

this conformational change is primarily responsible for mechanically linking actin cytoskeleton to the cadherin adhesions (Desai et al., 2013; Ladoux et al., 2015; Yonemura et al., 2010). Furthermore, actomyosin contractility and conformational change in α-catenin are required for binding of vinculin to these adhesions. Force-induced tension on vinculin stabilizes actin at the adhesions (Barry et al., 2014; Dufour et al., 2013; Thomas et al., 2013). Thus, vinculin also acts as a mechanosensor at cadherin adhesions. α-actinin and formins regulate mechanotransduction as cadherin adhesions by governing actin polymerization and bundling (Drees et al., 2005; Hansen et al., 2013; Le Duc et al., 2010).

Desmosomal junctions and mechanical resistance

Unlike classical cadherins, desmosomal cadherins bind to IFs (Figure 1.3A and D). Desmosomal cadherins consist of two subtypes protein, desmogleins and desmocollins. Desmosomal cadherins bind IFs through PG. PG interacts with IF linker proteins such plakophilin and desmoplakin (DP). DP directly binds IFs (Kowalczyk et al., 1999). Desmosomal junctions play an important function in maintaining tissue integrity and development of tissues that are constantly subjected to mechanical forces such as skin and heart. Epidermis lacking desmosomes are prone to blistering and rupturing (Allen et al., 1996; McGrath et al., 1997). Mutations in desmosomal junctional proteins, such as PG and DP, lead to defects in heart development (Gallicano et al., 2001; Grossmann et al., 2004; Ruiz et al., 1996).

IFs commonly bind to desmosomal cadherins but there have been reports that show IFs interacting with classical cadherins to form “desmosomal-like junctions”. A well-established example of these junctions is found in vascular endothelial cells where VE-

cadherins bind PG and recruit DP and vimentin IFs (Kowalczyk et al., 1998). Other studies have demonstrated the existence of desmosomal-like junction in migrating cells of developing embryos and that these junctions play important role in resisting tension that is generating at the cell-cell contacts during migration (Leonard et al., 2008; Weber et al., 2012).

Mechanical crosstalk between integrin and cadherin adhesions

The term crosstalk can be defined by interaction or integration of multiple signaling pathways (Weber et al., 2011). Although integrins and cadherin lack enzymatic activities (for example kinase or phosphatase), they are capable of activating various signaling pathways. These junctional proteins carry out signaling function by changing conformation in response to mechanical forces and recruiting proteins with enzymatic activities (Leckband and de Rooij, 2014; Webb et al., 2002). Integrins and cadherins are linked to similar cytoskeletal networks at the cytoplasmic domain and engage with or activate similar proteins (Weber et al., 2011). For example, regulation of RhoGTPase activity is essential for assembly and disassembly of both integrin and cadherin adhesions (Mayor and Carmona-Fontaine, 2010; Yamada and Nelson, 2007). Thus, cells within a tissue are able to propagate changes between cell-cell and cell-ECM contact and further facilitate long-range signal transduction.

The fact that both integrins and cadherin are linked cytoskeletal networks suggest that these molecules are mechanically linked to one another. Indeed, tension on cadherin adhesions helps to balance traction forces generated integrin-based adhesions during migration (Tambe et al., 2011; Trepat et al., 2009). Vascular endothelial cells are constantly

subjected to flow-induced shear stress. Tension exerted on VE-cadherins using magnetic cytometry causes remodeling of integrin adhesions to exert high traction forces (Andresen Eguiluz et al., 2017). In contrast, engaging integrin adhesion with FN coated bead leads to disassembly of VE-cadherin adhesion (Wang et al., 2006). Weakening of cadherin adhesion in keratinocytes by reducing Ca^{2+} levels in the media causes increases in traction forces exerted by FAs (Mertz et al., 2013). Similarly, modulation of cadherin adhesions in *Xenopus* mesendoderm tissue disrupts the distribution of traction forces generated by integrin adhesions in the mesendoderm tissue (Davidson et al., 2002; Weber et al., 2012). Furthermore, activation of integrins by adding soluble fibronectin (FN) caused an increase in cell-cell adhesion in *Xenopus* (Marsden and DeSimone, 2003).

This suggests a critical role of integrins and cadherins in sensing and responding to mechanical cues from the surrounding microenvironment. Even though integrins and cadherins are spatially separated and lack enzymatic activities, they utilize similar machinery to respond to forces and can influence each other's signaling. This suggests the existence of mechanical crosstalk between integrins and cadherin (Weber et al., 2011). Moreover, both integrin and cadherins adhesion require cytoplasmic connection to cytoskeletal networks to carry out mechanotransduction.

1.4 Role of cytoskeleton in mechanotransduction

Cell shape is primarily dictated by the organization of the cytoskeleton in cells. Within the cells, cytoskeletal networks like actin and microtubule undergo polymerization and depolymerization and this is required for changes in the organization of cytoskeleton

networks. These changes may occur as a response to external forces; however, these changes also generate sufficient forces to change cell shape and generate tension on cellular junctions.

The contractile nature of cells is mainly regulated by actin filaments. Most of our understanding of mechanosensation and mechanotransduction by actin filaments comes from studying cell migration. Actin differentially organizes within a migrating cell (Schwarz and Gardel, 2012). The branched network of actin in the lamellipodial region of the cell generates forces to push the cell membrane forward during migration (Machesky et al., 1999; Uruno et al., 2001). Towards the retracting end of a migrating cell, actin organizes into stress fibers. Actin stress fibers use the myosin II motor protein to generate contractile forces to pull the cells forward (Tojkander et al., 2012). The actomyosin contractility is also necessary for orientation of the mitotic spindle and formation of cytokinetic furrow during cell division (Cheffings et al., 2016; Pinheiro et al., 2017). Together, this actomyosin network is responsible for resisting mechanical forces acting on the cell. For example, in endothelial cell, actin stress fibers orient parallel to the direction of flow in response to shear stress (Girard and Nerem, 1995; Noria et al., 2004; Tzima et al., 2005). Actomyosin network is also important for the formation and maintenance of AJs. Furthermore, *in vitro* studies on actin filaments show that these filaments undergo conformational changes in response to compressive and stretching forces. Actin forms a catch bond with vinculin and thus tension exerted on actin filament increases its affinity to mechanosensitive proteins such as vinculin (Buckley et al., 2014; Huang et al., 2017).

Besides actin, other cytoskeletal protein networks such as microtubules and IFs also play important role in generating and resisting forces at cellular levels. Microtubule

filaments often times adopt bent architecture; some studies attribute this bent conformation to the load-bearing function of microtubules (Brangwynne et al., 2006). Microtubule polymerization and depolymerization generates force that is essential for chromatid separation during cell division (Elting et al., 2014; Forth and Kapoor, 2017). Microtubules are also known to regulate cell stiffness and signaling of FAK during migration (Palazzo et al., 2004). Moreover, post-translational modification of microtubules, detyrosination of α-tubulin, regulates mechanotransduction in skeletal muscle by controlling X-ROS signaling and maintaining the stiffness of cardiomyocytes (Kerr et al., 2015; Lyons et al., 2017; Robison et al., 2016). However, more studies need to be undertaken to fully understand the role of microtubules in mechanotransduction.

IFs are the largest group of cytoskeletal proteins containing ~65 highly conserved proteins. These are classified into five different families based on the structure and expression patterns. IFs are made up of a tripartite structure consisting of a central α-helical domain that is flanked with a non-helical head and tail domain. The IF network provides mechanical stability to cells because of the elastic, flexible, extendable nature of these filaments. IFs also have a high load-bearing potential. Unlike, actin or microtubule which have a growing and receding end, IFs can polymerize and depolymerize anywhere along the filaments. Most IFs polymerize by forming homodimers expect for keratin IFs, which are obligate heterodimers (Chung et al., 2013; Sanghvi-Shah and Weber, 2017). Even though IFs do not have any enzymatic activities, IFs have been demonstrated to play an active role in regulating mechanosensitive processes like migration. Vimentin IFs associate with integrins to form hemidesmosomal structures and regulate migration through FAK/Src kinase signaling (Gregor et al., 2014; Homan et al., 2002). Cells lacking vimentin

IFs show reduced mechanical resistance to external forces (Mendez et al., 2014). In addition, extrinsic mechanical forces result in stretching of IFs (Herrmann et al., 2007; Lowery et al., 2015). Solo kinase and keratin IFs together regulate the tension dependent formation of actin stress fibers (Fujiwara et al., 2016). Furthermore, loss of IFs leads to distant changes in actin organization ((Fujiwara et al., 2016; Jiu et al., 2017). IFs connect to cadherins to form desmosomes, where IFs act to resist tension across cell-cell adhesions. In migrating *Xenopus* mesendoderm cells, keratin IFs actively bind to the site of tension bearing classical cadherin adhesions to form desmosomal-like junctions. Loss of keratin IFs leads to failure of cells to respond to tension and drastically changes actin organization (Weber et al., 2012; Chapter 2). Keratin IFs are abundantly expressed in the skin where they function to provide mechanical rigidity to the cells. Loss of keratin IFs makes skin fragile and prone to rupture upon being subjected to mechanical stress (Coulombe and Lee, 2012; Takahashi and Coulombe, 1996). This evidence suggests IFs support the mechanical integrity of cells by actively responding to changing the mechanical environment.

Any force-induced changes in cell architecture are transmitted to the nucleus and influence nuclear morphology (Friedl et al., 2011). The nuclear response to changes in the mechanical microenvironment is mediated by nuclear envelope proteins. The nuclear envelope is made up of lamin proteins, member of IF family. Nesprins and SUN-Family proteins connect the nuclear lamins to cytoskeletal networks. Together, the molecular bridge between nucleus and cytoskeleton forms LINC (Linker of nucleoskeleton and cytoskeleton). Actomyosin contractility is necessary to stabilize the LINC complex and increase in tension on the LINC complex increases the rigidity of nucleus and affects cell differentiation. Loss of any of the LINC complex proteins result in defects in nuclear

rigidity, the positioning of nucleus and migration thus disrupting cell polarity during migration (Graham and Burridge, 2016; Guilluy et al., 2014).

1.5 Force driven global cellular changes during embryonic development.

Cells within a developing embryo are constantly subjected to mechanical forces such as stress, strain, shear and hydrostatic pressure from surrounding microenvironment (Figure 1.1A-E; Schwartz and DeSimone, 2008); the mechanisms by which cells resist these mechanical stimuli are just beginning to be understood. These mechanical forces also regulate cellular behavior like cell morphology, polarity and migration (Iskratsch et al., 2014). Furthermore, the geometry of the embryo plays a significant role in influencing the cellular response to mechanical forces. Processes such as cell division, differentiation and tissue movement are integral to embryonic development and generate forces at the molecular, cellular and tissue level. These forces, in turn have the potential to regulate the behavior of neighboring cells and tissues, which is essential to facilitate embryonic development. This section will cover well-characterized morphogenetic processes that are influenced by mechanical forces.

Mechanical forces and cell division.

Oriented cell division is an important feature of embryogenesis. Soon after fertilization, embryos of most species undergo a series of strictly regulated oriented mitotic divisions to form a blastula stage embryo. Cell division results in growth and increase in cell mass; this increase of cell mass within the confined space of the developing embryos

leads to geometric constraint and increases stress on the surrounding cells (Mao et al., 2013; Rupprecht et al., 2017). Cell division is altered by stretching or compressing cells in culture (Eder et al., 2017; LeGoff et al., 2013; Streichan et al., 2014). Similarly, in *Drosophila* wing disc, increased rates of cell division are observed in regions experiencing high pulling forces and lower rates of cell division are observed in regions under high compressive forces (Aegerter-Wilmsen et al., 2012; Chanet and Martin, 2014; Shraiman, 2005).

Alternatively, cells respond to external forces by aligning the axis of division to minimize tension (Nestor-Bergmann et al., 2014). Cell division results in easing of tension at cell-cell junctions as well cell-ECM junctions. The orientation of cell division and formation of the cleavage furrow is determined by assembly and alignment of the mitotic spindle (Rappaport, 1999; Rappaport and Rappaport, 1974). Cells plated on micropatterned substrates elongate in the direction of highest tension and this is sufficient to align the mitotic spindle parallel to the axis of tension resulting in oriented cell division (Fink et al., 2011; Lesman et al., 2014; Wyatt et al., 2015). Early experiments done by Hertwig in 1884 demonstrated that *Xenopus* embryos compressed using plates no longer divided randomly; instead, the orientation of division was orthogonal to the direction of compression. This further led to him to propose the Hertwig's law, which states cells divide along their long axis.

Studies undertaken in *Drosophila* wing disc have mapped strain levels across the wing disc and shown that strain correlates with the orientation of spindle formation and that cells divide parallel to the axis of strain (LeGoff et al., 2013). Furthermore, the tricellular junctions regulate the epithelial cell division by localizing force-generating

machinery at the site of spindle attachment in gastrulating *Drosophila* embryos (Bosveld et al., 2016). During lung development in mice, mechanical coupling of epithelial cells functions to coordinate cell geometry and spindle orientation to ensure the formation of airway tube (Tang et al., 2018).

In gastrulating zebrafish embryos, global tension anisotropy develops as the enveloping layer (EVL) cells undergo epiboly, a process of ventral-ward ectodermal spreading. The EVL cells reduce this anisotropy by orienting the spindle along the direction of tension (Campinho et al., 2013). Additionally, mechanical coupling of EVL cells has also been demonstrated to regulate oriented cell division (Xiong et al., 2014). During *Xenopus* gastrulation, the orientation of the spindle in the blastocoel roof (BCR) cells is controlled by opposing force from microtubule/myosin10 and actomyosin complex in the apicobasal direction. Furthermore, tension on the cellular junction arises due integrin dependent sorting exhibited by the BCR cells (Marsden and DeSimone, 2001; Marsden and DeSimone, 2003) and this tension is sufficient to drive FN assembly (Dzamba et al., 2009). The tension generated during FN assembly influences the orientation of spindle in BCR cells, which is required for proper epiboly and to prevent thickening of the tissue (Marsden and DeSimone, 2001; Rozario et al., 2009). FAK, a known regulator of mechanotransduction at cell-ECM junctions, regulates the orientation the spindle in BCR cells (Petridou and Skourides, 2014). Taken together, internal and external mechanical cues play a significant role regulating cell division during embryonic development.

Mechanical forces and cell differentiation

Early embryonic cells are pluripotent and differentiation of these cells is regulated by cell intrinsic and extrinsic factors such as morphogen gradients and mechanical signals. During the initial stage of development, cells primarily form cell-cell contacts. However, as development progresses, cells deposit ECM and begin to establish cell-ECM contact. The stiffness of the secreted ECM changes over time and cells adapt to this mechanical change in microenvironment by altering transcriptional programs and undergoing differentiation (Rozario and DeSimone, 2010). Nuclear localization of transcription factors is upregulated in response to increase mechanical stress (Olson and Nordheim, 2010). During avian skin development, force generated via actomyosin contractility spontaneously drives aggregation of progenitor cells and translocation of β-catenin to the nucleus to initiate the transcription machinery necessary for follicle formation (Shyer et al., 2017). Mesenchymal stem cells (MSCs) direct differentiation into specific lineages as a response to the force experienced at the cell-ECM due stiffness variation *in vivo*. MSCs differentiate into neuronal lineage on softer ECM whereas, on stiffer ECM, cells differentiate into the bone lineage. These changes occur due to forces-dependent differential gene expression (Engler et al., 2006). Furthermore, tensile stresses, shear forces and hydrostatic pressure from the surrounding microenvironment direct differentiation of MSCs into either osteogenic or chondrogenic lineages (Arnsdorf et al., 2009a; Arnsdorf et al., 2009b; Mauck et al., 2006; Panadero et al., 2016; Simmons et al., 2003).

Mechanical signals regulate signaling like Wnt, TGF-β and Notch during cardiac differentiation (Brand, 2003; Happe and Engler, 2016). Heart is one of the first organs to

develop and it facilitates circulation of blood to ensure proper embryonic growth (Boselli et al., 2015). In developing embryos constant laminar flow due to circulation of blood in vessels exerts shear stress on the endothelial cells, which is required for normal organization of these cells. Laminar flow increases cell-cell connectivity by upregulating transcription of PECAM1, VE-cadherin and catenin family members (Califano and Reinhart-King, 2010; DeMaio et al., 2004; Kondapalli et al., 2004; Noria et al., 1999; Ukropec et al., 2002). Disruption of flow causes down regulation of genes involved in endothelial differentiation (Hastings et al., 2007; Hove et al., 2003).

Normal lung development occurs in two phases; the initial phase of lung development involves branching morphogenesis and is followed by air sac development. Actomyosin contractility and stiffness of the surrounding ECM play important role in regulating migratory behavior and secretion of matrix metalloproteinases (MMPs) during branching morphogenesis (Beck et al., 2013; Ewald et al., 2008; Moore et al., 2002; Moore et al., 2005). Finally, stretching of lungs due to fetal breathing and fluid secretion is essential to proper differentiation of epithelial cells during the final phase of lung development (Przybyla et al., 2016).

Epithelial-Mesenchymal Transition (EMT) is a hallmark of metastatic cells but is also known to occur throughout embryonic development (Yang and Weinberg, 2008). During EMT, cells remodel cellular junctions and acquire migratory behavior; mechanical cues from the surrounding matrix influence these phenotypic changes in cells (Przybyla et al., 2016). Modulation of mechanical stress causes changes in the transcriptional regulation of cell adhesion molecules. Cells stiffen in response to externally applied forces on E-cadherin and VE-cadherin adhesions (Andresen Eguiluz et al., 2017; Le Duc et al., 2010)

and suppress transcription of E-cad (Kemler et al., 2004). Cadherin switch is observed during EMT in neural crest migration in response to the redistribution of force (Scarpa et al., 2015; Theveneau and Mayor, 2013). Cells, however, do not undergo a complete change in phenotype during EMT but exhibit overlapping features of epithelial and mesenchymal cell types (Campbell and Casanova, 2016). Cadherin-11 specifically promotes migratory behavior in leader cells by reducing cell stiffness without changing adhesion strength during neural crest migration (Blaue et al., 2018). Collectively, this suggests that mechanical forces greatly influence cell differentiation during embryonic development.

Forces and tissue movement

Gastrulation is the first morphogenetic process that requires large tissue-scale movement during embryonic development (Figure 1.4A). Similarly, tissue-scale movements are responsible for the shaping of organs later in development. The proper orchestration of gastrulation and organogenesis is highly regulated by spatiotemporal regulation of gene expression. Physical displacement of cell within embryonic generates sufficient force and as the cells are interconnected to one another, forces generated by one morphogenetic movement, in turn, affects movements of cell in other parts of the embryo (Keller et al., 2003; Rauzi et al., 2015). Furthermore, these tissue-scale movements are restricted to the confined spaces of the developing embryo and organs, thus geometrical constraint significantly influences the forces generated and exerted by the cell. Cellular rearrangements observed during embryogenesis involve dynamic remodeling of cell-cell junctions as well as cell-ECM junctions. Tension sensed and transmitted across these

junctions regulates cellular behaviors like shape change and migration by reorganizing cytoskeletal proteins within cells.

In *Drosophila* oogenesis, contractile actomyosin bundles on the basal surface of the epithelial follicle cells align with the collagen rich basement membrane and drive directional migration of the follicle cells. This causes rotation of the entire egg chamber as the follicle cells are connected to the germ cells at the apical junction. Together, oscillation of the follicle cells and the stiffness of the surrounding BM act as a "molecular corset" facilitating elongation of the egg chamber (Cetera et al., 2014; Crest et al., 2017; Gutzeit, 1990; Haigo and Bilder, 2011). During germ-band extension in *Drosophila*, cell shape changes necessary for intercalation are driven by the extrinsic tensile force generated due to mesoderm invagination (Butler et al., 2009; Dicko et al., 2017). Tension-dependent myosin recruitment is observed at E-cadherins based AJs in the intercalating cells. Contractile tension generated due to myosin activity leads to reorganization of cellular junctions essential for intercalation (Bertet et al., 2004; Bosveld et al., 2012; Fernandez-Gonzalez et al., 2009; Shindo and Wallingford, 2014; Yu and Fernandez-Gonzalez, 2016) *Drosophila* dorsal closure involves migration of epithelial cells over amnioserosa cells to close the opening at the dorsal side of the embryo. It has been demonstrated that actomyosin purse-string formation and force generation in the epithelial cells is critical for dorsal closure (Franke et al., 2005). Furthermore, pulsating action of the underlying amnioserosa cells generates forces long before the formation of actin purse-string in epithelial cells and is required for the dorsal ward movement of epithelial cells to initiate dorsal closure (Solon et al., 2009). Laser ablation experiments done to disrupt both epithelial and amnioserosa cells simultaneously demonstrated complete failure to close the dorsal opening; this

suggests that forces from both cell types are essential for dorsal closure (Kiehart et al., 2000).

More evidence of forces shaping embryos come from studies performed in *Xenopus* embryos. A series of dissection experiments done on early and late stage gastrula embryos demonstrated that tissue in the developing embryos either deformed or bent upon separation from the embryo (Beloussov et al., 1975). Thus, this suggests a possible relation of forces in maintaining tissue architecture and the presence of tension across cellular junctions. Increased tension on *Xenopus* C-cadherin (C-cad) junctions in BCR cells is essential for the assembly of FN. The assembly of FN begins at the site of cell-cell contact where high tension is observed (Figure 1.4B). Additionally, loss of hydrostatic pressure from the surrounding blastocoel cavity reduces FN fibrillogenesis (Dzamba et al., 2009). Proper assembly of FN is required for radial intercalation of BCR cells (Marsden and DeSimone, 2001; Rozario et al., 2009) and migration of mesendoderm tissue (Davidson et al., 2002; Winklbauer and Selchow, 1992). Anisotropic tension develops across the entire mesendoderm tissue during migration (Davidson et al., 2002). The tension is borne by C-cadherin based cell-cell contacts and is required for proper polarization of cell within in the tissue (Weber et al., 2012). The imbalance of forces across these cellular adhesions is balanced by the traction forces exerted by cells via integrin-based cell-ECM contact (Figure 1.4C; Davidson et al, 2002). The forces generated during the forward migration of mesendoderm tissue are essential for convergent-extension (CE) movements of mesoderm cells (Figure 1.4D; Hara et al., 2013). Similarly, mesoderm cells transmit myosin generated contractile tension across C-cad adhesions to undergo CE (Keller et al., 2000; Pfister et al., 2016; Skoglund et al., 2008). CE movement that initiates at gastrulation causes stiffening

of mesoderm cell and this stiffening is critical to promote EMT during neural crest migration (Barriga et al., 2018).

Cell sorting is essential for the formation of germ layers during gastrulation. Differential cortical tension and adhesion strength in the progenitor cells facilitates sorting behavior (Maître et al., 2012). Experiments performed using atomic force microscopy (AFM) have demonstrated differences in adhesion strength and cell cortex tension in progenitor cells. This difference in mechanical properties of the cells was observed to be due to differential actomyosin contractility within the progenitor cells (Krieg et al., 2008) and the interstitial fluid osmolarity (Krens et al., 2017). Over the course of gastrulation, cells continue to modulate cortical tension in order to achieve proper morphogenesis. In zebrafish, EVL cell spreading occurs by reducing cell cortical tension and this results in a build-up of anisotropic tension. This anisotropic tension causes doming of yolk and facilitates radial intercalation of underlying mesenchymal cells (Morita et al., 2017). Furthermore, frictional forces arise during migration of mesendodermal and neural ectodermal cells. Frictional forces are generated due to transient coupling via E-cad based adhesion between the two different cell types and are necessary for proper specification of neural anlage (Smutny et al., 2017). Based on this we can conclude that embryonic development is a mechanosensitive process and cells in the embryos are constantly subjected to a combination of pulling and compressive forces; these forces are resisted by cell intrinsic forces and in turn help in shaping the developing embryos.

Mechanical forces are not only required for early embryonic development but also function in the formation and maintenance of organs; abnormal mechanical forces result in malfunctioning organs (Mammoto and Ingber, 2010; Mammoto et al., 2013). During

oogenesis in *Drosophila*, mechanical coupling of border cell and nurse cells via E-cad guides proper polarization and directed migration of border cells (Cai et al., 2014). Tension stabilizes integrin based myotendinous junction that connects muscle and tendons during muscle development in *Drosophila* (Pines et al., 2012). Collective cell migration is observed during trachea formation in Drosophila and zebrafish posterior lateral line primordia (pLLP). Tension generated on cell junctions is necessary for forward migration of these collectively migrating cells (Caussinus et al., 2008; Knutsdottir et al., 2017). Actomyosin contractile forces at VE-cad AJs are necessary for proper vascular development (Huveneers et al., 2012; Lagendijk et al., 2017). Shear forces generated due to blood flow are required for heart development (Boselli et al., 2015). Fluid forces are also responsible for collective migration of epithelial cells during kidney development (Vasilyev et al., 2009) and pressure due to fetal breathing is important for air sac formation in mice (Li et al., 2018). Fluid flow generated due to the beating of cilia is required for symmetry breaking and formation of visceral organs (Grimes and Burdine, 2017; Nonaka et al., 2002).

Mechanical stimuli from ECM also play instructive roles in organogenesis. For example, during branching morphogenesis, epithelial cells undergo division to extend the growing bud in a matrix dependent manner. Epithelial cells respond to growth factor cues from the surrounding ECM such as FGF, VEGF and BMP signaling as well as to mechanical stiffness (Sakai et al., 2003). The stiffness of ECM is a function of matrix deposition and crosslinking. During salivary gland morphogenesis, spontaneous cleft forms between epithelial cells. The cleft is stabilized by deposition of ECM and leads to the formation cell-ECM junction enriched with FAK, which acts as a mechanotransducer

to further stabilize the cleft and cause additional deposition of ECM (Moore et al., 2005). The cleft grows as result of actomyosin contractility regulated by FAK (Daley et al., 2011) and inhibiting myosin contractility leads to disruption in clefting (Schnatwinkel and Niswander, 2013; Wang et al., 2017). Furthermore, the mechanical stress exerted by the ECM is critical for mammary gland branching. Epithelial cells experience a compressive force from the surrounding matrix. Arborization is initiated at the site of highest mechanical tension and also requires FAK signaling. Formation of new branches in lung, kidney and salivary gland also requires remodeling of the ECM, which is facilitated by secretion of MMPs. Thinning of ECM is observed at the growing tip of the bud possibly due to degradation by MMPs (Fata et al., 2003; Lu et al., 2011; Moore et al., 2005). Thus, these evidence suggest ECM guides organogenesis by regulating morphogen as well as mechanical signaling.

1.6 Conclusion

Much of our knowledge about how mechanical forces influences cell behavior has expanded a great deal with the development and application of sophisticated biophysical and biochemical tool. However, a lot still remains to be understood. Based on the evidence presented above, it is becoming clear that mechanotransduction and mechanosensation is a two-way process and relies on input and output from the cells. These processes heavily influence embryonic development and the embryo is a result of equilibrium achieved by balancing of deforming and resisting forces.

1.7 Summary and outline of the dissertation.

In gastrulating *Xenopus* embryos large-scale force generating tissue movements occur and thus it is a powerful system to study the importance of forces that are essential for shaping a developing embryo. Gastrulation in *Xenopus* begins at the dorsal side with apical constriction of bottle cells and involution of mesoderm cells. Endothelial cells undergo vegetal rotational and contributes to the mesoderm involution. Endoderm and mesoderm together form a annular ring of migrating cells called mesendoderm. Mesendoderm migration begins at the dorsal side of the embryo. As gastrulation progresses, mesendoderm cells at the ventral side also begin to migrate. Additionally, mesoderm cells, adjacent to migrating mesendoderm cells, undergo CE movement in the mediolateral direction. Simultaneously, BCR cells that assemble FN undergo radial intercalation, which leads to thinning of the BCR and spreading, in a process called epiboly. Although all of these movements require precise mechanical regulation of cell-cell and cell-ECM contact, migration of mesendoderm provides with an excellent experimental model to study the forces that regulate morphogenesis as well as migration. *Ex vivo* explants of mesendoderm tissue faithfully recapitulate *in vivo* movement and can be easy target for gene manipulation.

Mesendoderm cells migrate on the FN matrix secreted by the BCR by forming integrin $\alpha5\beta1$ adhesions (Davidson et al., 2002). Mesendoderm tissue migrates collectively and maintains cohesion by forming C-cadherin adhesions with neighboring cells. Anisotropic tension develops on the rear C-cadherin adhesion as the tissue migrates towards the animal pole. This tension is required for formation of directed protrusion in mesendoderm cell (Weber et al., 2012). Loss of adhesions in mesendoderm tissue causes

cells to protrude randomly (Winklbauer et al., 1992). This suggests that maintenance of adhesion is necessary for directed migration. Furthermore, blocking of integrin adhesions with a functional blocking antibody results in rearward movement of the mesendoderm tissue (Davidson et al., 2002). Thus, we hypothesize that a balance of forces is required between integrin and cadherin adhesions for forward migration of mesendoderm tissue. This hypothesis is directly tested in chapter 2. Keratin IFs and PG are recruited to stress bearing C-cadherin adhesions and are essential for the formation of directed protrusions in mesendoderm cells (Weber et al., 2012). However, the mechanism by which keratin IFs and PG regulate cell polarity during migration requires further experiments. In chapter 2, we show that the traction forces exerted by integrin adhesions during mesendoderm migration balance tension on C-cadherin adhesion. We have also characterized the role of keratin IFs in regulating proper assembly and migration of mesendoderm during gastrulation. In chapter 3, I focus on understanding the role of PG, component of the cadherin complex, in the migration of mesendoderm and have identified a potential interaction between PG and integrin adhesions. Thus, the overall goal of this study was to understand the role of forces that are required for self-organization of tissue during morphogenesis and more specifically during embryonic development.

Figure 1.1: Cell deformation in response to mechanical forces.

Cells maintain tissue cohesion by forming cadherin adhesions (purple with red outline) with neighboring cells and integrin adhesions (brown) with the ECM (green). Cells in the tissue are constantly subjected to different mechanical forces such as (A) Stretch, (B) Compression, (C) Shear flow, (D) Osmotic Stress and (E) Hydrostatic pressure from the surrounding microenvironment. Cellular mechanotransduction results in deformation or shape change due to cytoskeletal rearrangement. Blue arrows indicate the direction in which different forces are acting on the tissue. (F) ECM (green) crosslinking regulates stiffness; ECM stiffness increases with increasing crosslinking. Cells on a stiffer substrate (left) are able to exert high traction forces through integrin adhesion (brown), form larger FAs (brown) and spread efficiently on the matrix. Cells on a soft substrate (right) fail to exert traction forces through integrin adhesions, form smaller FAs (brown) and are unable to spread on the underlying matrix. Orange circle indicates nuclear deformation associated with cells spreading.

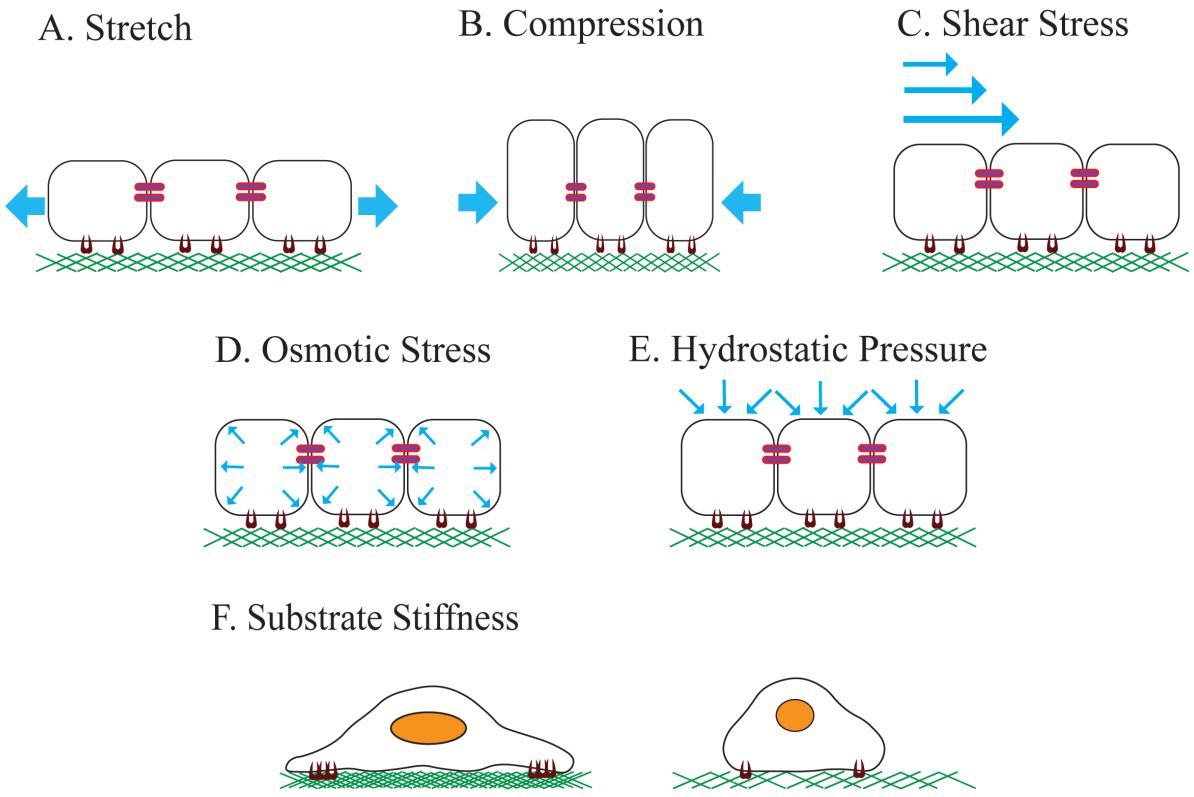
A. Stretch
B. Compression
C. Shear Stress
D. Osmotic Stress
E. Hydrostatic Pressure
F. Substrate Stiffness

Figure 1.2: Integrin adhesions and activation.

(A) Cells forming different kinds of integrin-based adhesions (alpha subunit in red and beta subunit in blue). Integrin adhesion can be classified into two types depending on the cytoskeletal network linked to integrins. Focal adhesions (FAs) are actin (purple) based integrin adhesion whereas hemidesmosomes are intermediate filament (IFs; orange) containing adhesions. (B) Bidirectional integrin signaling. Integrins exist in an inactive form on the surface of the cells (center). Activation causes conformational changes in integrin subunits. Conformation change can cause by binding of talin (orange rod) and kindlin (yellow) to the cytoplasmic domain of integrin beta subunit. This is the inside-out signaling (left). Binding of ligand (green) causes change in conformation and clustering of integrins. This is the outside-in signaling (right). (C) Cartoon of FAs showing representative FAs complex protein. (D) Cartoon of hemidesmosome showing key hemidesmosomal proteins.

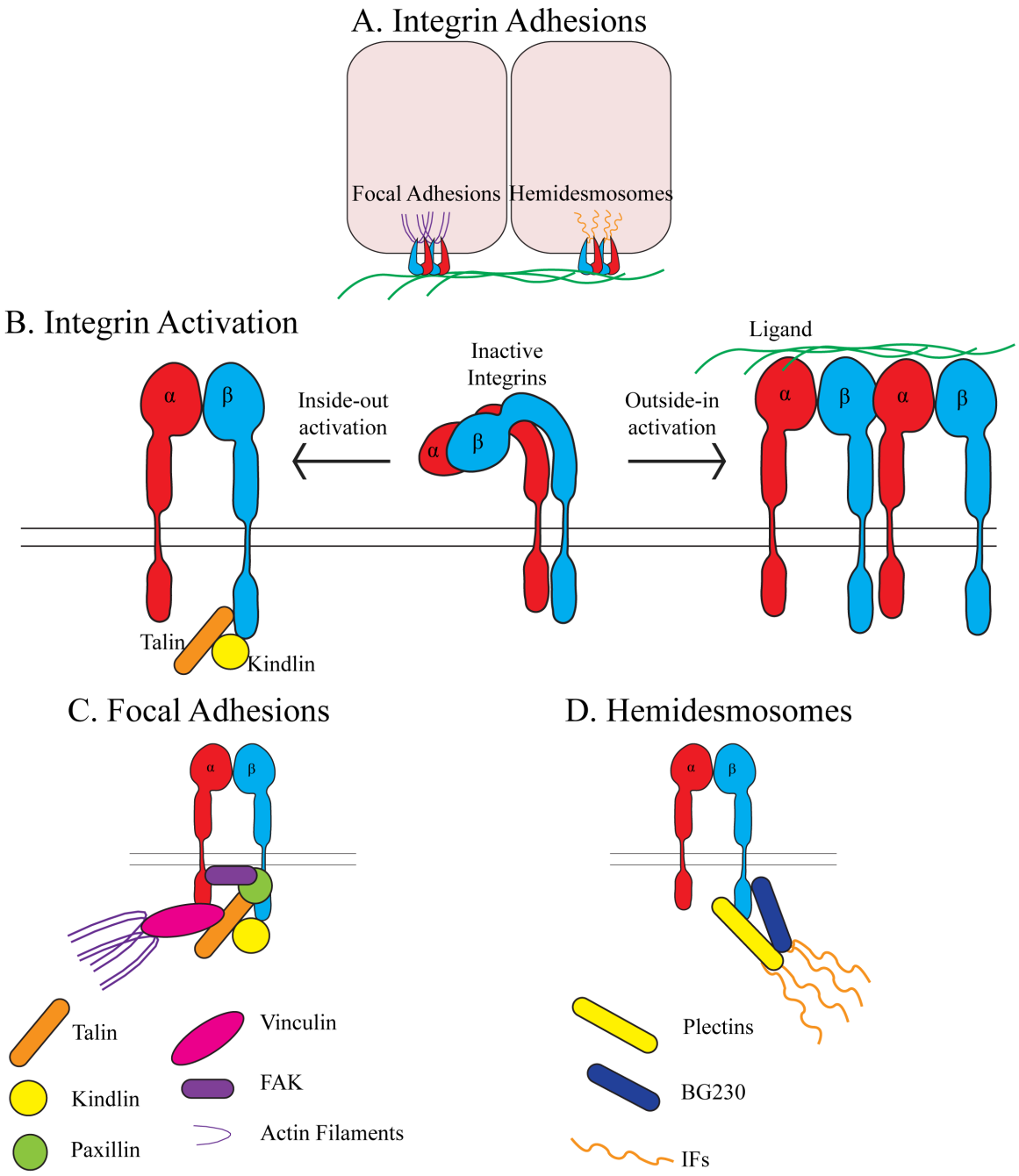
A. Integrin Adhesions
Focal Adhesions
Hemidesmosomes
B. Integrin Activation
Inactive Integrins
Inside-out activation
Outside-in activation
Ligand
α
β
Talin
Kindlin
C. Focal Adhesions
D. Hemidesmosomes
Talin
Kindlin
Paxillin
Vinculin
FAK
Actin Filaments
Plectins
BG230
IFs

Figure 1.3: Cadherin adhesions and clustering.

(A) Cells form adherens junctions (AJs) by utilizing classical cadherins (red) and desmosomes with desmosomal cadherins (blue) with the neighboring cells. AJs contain actin (purple) whereas desomosomes contain IFs (orange). (B) Cadherin clustering: Classical cadherins form homophilic adhesions with the extracellular domain. This event is called ligation (left). Cadherin clustering occurs after initial ligation and is important for binding to actin network (purple; right). (C) Cartoon of AJ showing representative AJ protein. (D) Cartoon of hemidesmosome showing key desmosomal proteins.

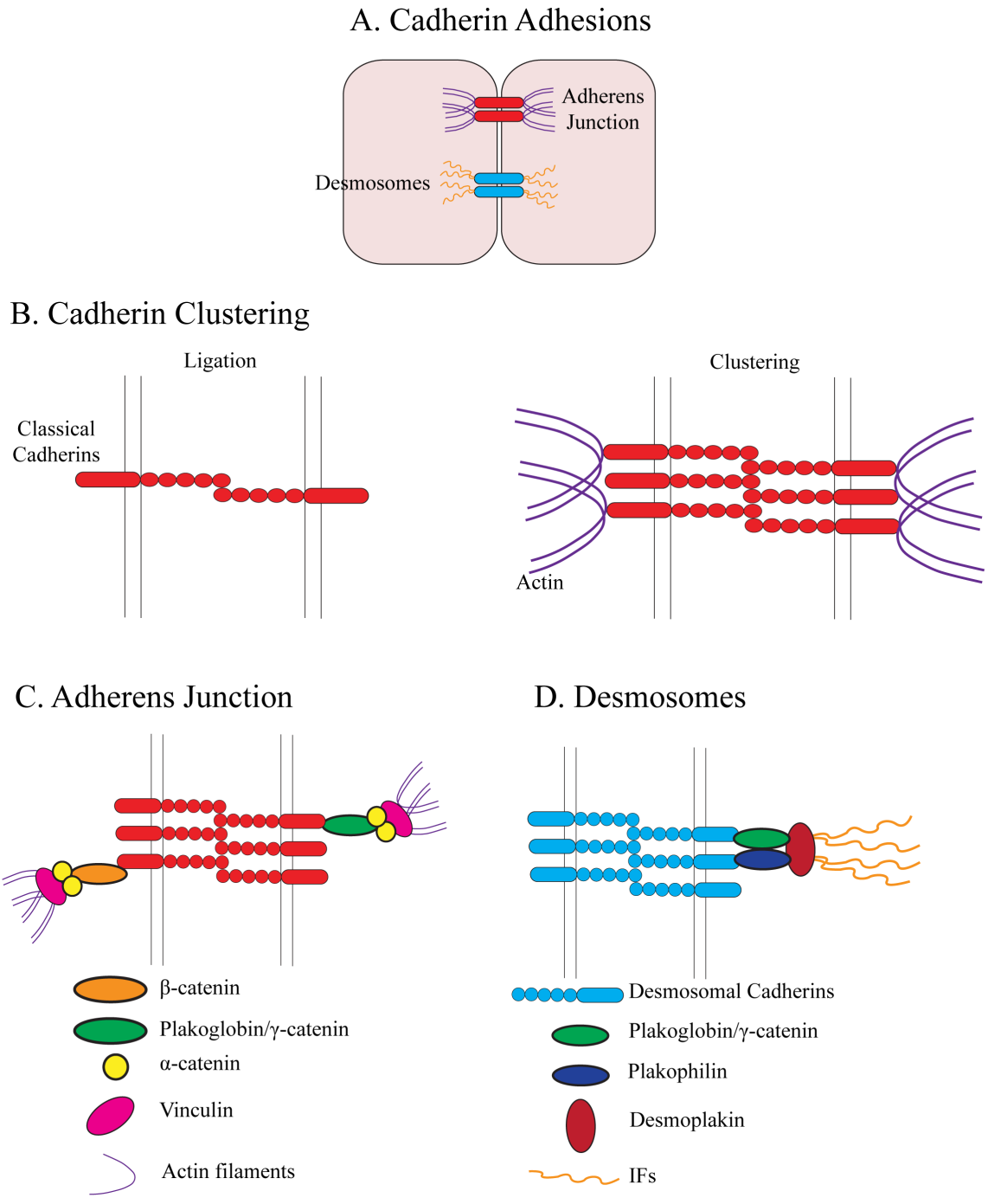
A. Cadherin Adhesions
Adherens Junction
Desmosomes
B. Cadherin Clustering
Ligation
Classical Cadherins
Clustering
Actin
C. Adherens Junction
β-catenin
Plakoglobin/γ-catenin
α-catenin
Vinculin
Actin filaments
D. Desmosomes
Desmosomal Cadherins
Plakoglobin/γ-catenin
Plakophilin
Desmoplakin
IFs

Figure 1.4: Tissue movement occurring during *Xenopus* gastrulation.

(A) Cartoon of gastrulating *Xenopus* embryo. Arrows indicate the direction of cell movement in different tissue during gastrulation. (B) FN assembly at the blastocoel roof. Blue arc represents animal cap and the green line indicates FN matrix (top). Blue cells represent BCR cells expressing C-cadherin (dark blue). Mechanical tension across C-cadherin adhesions is transmitted to centrally moving integrin adhesion (brown) bound to FN (green). Cryptic sites on FN necessary for fibrillogenesis are exposed due to the movement on integrins toward the center of the cells. Arrows indicate the tension generated during FN assembly. (C) Collective migration of mesendoderm. Mesendoderm tissue migrates collectively on the FN matrix assembled by BCR cells (top). Adhesion between cells in maintained by C-cadherin (dark blue). Integrins (brown) in the leading row exert force necessary for forward migration and this force is necessary to balance anisotropic tension on rear C-cadherin adhesion. Keratin IFs (red) are recruited to the rear C-cadherin adhesion in a tension-dependent manner and are necessary to a maintain balance between traction forces generated by integrin and anisotropic tension on C-cadherin. Integrin adhesion in leading row results in a Rac1 activity gradient with the high activity observed in the protrusions and low activity in the cell body (Orange-yellow gradient represent Rac1 activity). (D) CE movement of mesoderm cells. Mesoderm cells undergo mediolateral intercalation movement by extending protrusion and pulling neighboring cell toward one another. Mesoderm cells constantly have to reorganize C-cadherin adhesion (dark blue) to undergo CE movement. CE movement is necessary to elongate embryo in the anterior-posterior direction. Arrows indicate the direction of CE.

A. Xenopus Gastrulation

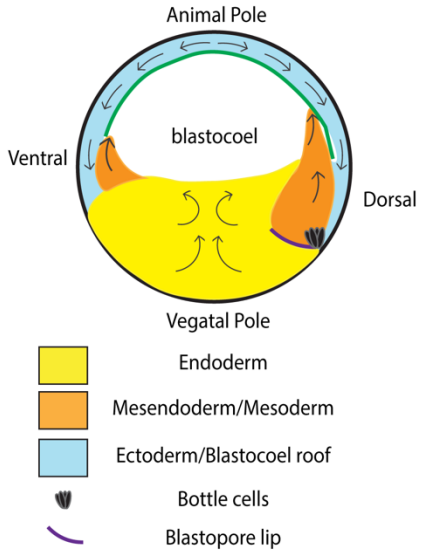

B. FN Assembly

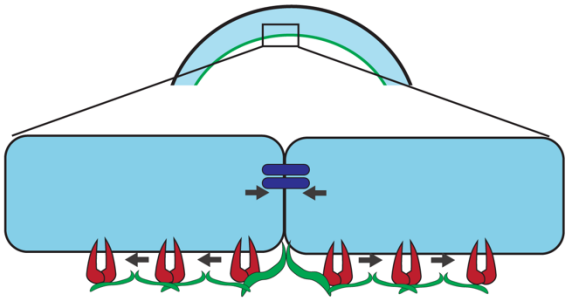

C. Mesendoderm Migration

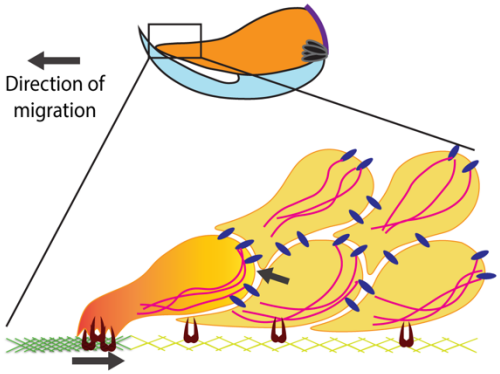

D. Convergence and Extension

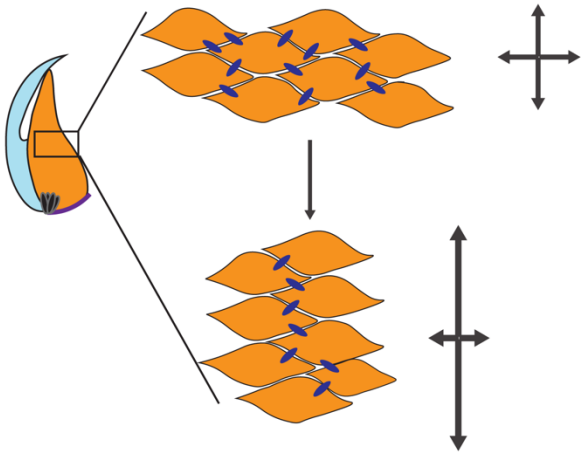

Chapter 2

Keratin IFs are required for proper assembly and morphogenesis of mesendoderm tissue during gastrulation.

This chapter is based in part on previously published work: Sonavane et al., 2017. Mechanical and signaling roles for keratin intermediate filaments in the assembly and morphogenesis of *Xenopus* mesendoderm tissue at gastrulation.

Development (2017) 144, 4363-4376 doi:10.1242/dev.155200

2.1 Introduction

Coordinated cellular movements are a key feature of many morphogenetic processes that occur in metazoan development. The cell and tissue rearrangements responsible for these movements often play out within the confined spaces of embryos where forces generated are sensed by other proximal cells and tissues (Heisenberg and Bellaïche, 2013). These forces can also be transduced into chemical signals within cells to regulate cell behaviors that promote morphogenesis or influence gene expression (Mammoto et al., 2013; Miller and Davidson, 2013; Wozniak and Chen, 2009).

Collective cell migration is a fundamental process important in embryogenesis, wound-healing and cancer cell metastasis (Friedl and Gilmour, 2009; Mayor and Etienne-Manneville, 2016). Formation and maintenance of adhesive and mechanical linkages, and the coordinated changes in cell polarity that result from these cell-cell contacts, are defining features of collectively migrating cells (Collins and Nelson, 2015). For example, in Drosophila border cells a tension gradient across E-cadherin containing junctions has been proposed to contribute to polarization of protrusive activity at the front of the cluster where cell-cell forces are highest (Cai et al., 2014). Forces generated during collective migration of MDCK cells result in redistribution of the Hippo pathway molecule Merlin, from cell-cell junctions to the cytoplasm where it leads to polarized Rac1 activation (Das et al., 2015). Collectively migrating cells also respond to chemotactic cues and in many instances a robust response to these signals requires cell-cell contact (Dumortier et al., 2012; Malet-engra et al., 2015; Theveneau et al., 2010; Winklbauer and Selchow, 1992). How mechanical and chemical inputs are combined and processed to direct specific migration behaviors remains an important question.

Rho family GTPases are regulators of cell polarity in migrating single cells and are integral to the relay of chemical and mechanical information from the ECM to the cell interior (Ridley, 2015). Rac1 activation promotes actin polymerization, lamellipodial protrusion and integrin engagement with the ECM (Del Pozo et al., 2002). Cells that migrate collectively typically organize into leader and follower cells and Rac1 activity is often increased in leader cells. In the case of Drosophila border cell migration, Rac1 activation is necessary and sufficient for leader cell behavior (Inaki et al., 2012; Wang et al., 2010; Yamaguchi et al., 2015). The importance of leader cells in generating traction forces necessary to direct migrating cohorts forward varies among tissue types. For example, specialized protrusive tip cells that lead narrow arrays of collectively migrating cells during Drosophila tracheal morphogenesis, and emergent migratory MDCK cells can provide the traction forces sufficient to propel both themselves and follower cells forward (Caussinus et al., 2008; Reffay et al., 2014). In contrast, both leader and follower cells in some epithelial cell sheets and in zebrafish lateral line primordia are protrusive (Farooqui and Fenteany, 2005; Haas and Gilmour, 2006). While traction forces are typically highest along the free edges of epithelial sheets and clusters, internal cells also generate traction forces (Tambe et al., 2011; Trepat et al., 2009). Both leader and follower cells extend monopolar protrusions in *Xenopus* mesendoderm (Weber et al., 2012; Winklbauer et al., 1996), however, the spatial arrangement of traction stresses in this tissue have yet to be reported. In this study we report the spatial distribution of traction stresses applied to the substrate by migrating mesendoderm.

Xenopus mesendoderm cells migrate across the BCR during gastrulation as a collective mass and this basic organization is maintained when mesendoderm is removed

from the embryo and cultured intact on a FN substrate. C-cad adhesions are required to maintain cell cohesiveness and the extension of monopolar protrusions, which contact and adhere to FN (Winklbauer and Nagel, 1991) using α5β1 integrins (Davidson et al., 2002). These cells become multipolar protrusive on

FN when cell-cell adhesive contacts are disrupted following tissue dissociation in low Ca^{2+} (Winklbauer and Selchow, 1992). Local "tugging" forces on C-cad adhesions at the rear of a single mesendoderm cell are sufficient to recruit keratin(8) IF and PG to sites of stressed adhesions and restore monopolar protrusive activity (Weber et al., 2012). Expression of keratin 14 in leader cells is also been reported to be essential for the collective dissemination of tumor cell clusters in a mouse model of breast cancer (Cheung et al., 2013; Cheung et al., 2016). These data suggest that keratin IFs may be integral players in a range of collective cell migration events.

In serum starved non-motile cells vimentin IFs extend throughout the cell (Helfand et al., 2011; Valgeirsdóttir et al., 1998). Upon serum addition or activation of the small GTPase Rac1, vimentin IFs disassemble and protrusive lamellipodia form. Specific disruption of the vimentin IF network also promotes the formation of lamellipodia around the cell suggesting that Rac1 and vimentin are functionally antagonistic (Helfand et al., 2011). Whether keratin IFs display a similar antagonism with Rac1 is unknown. In this study, we report that keratin IFs maintain mechanical linkages between cells that are required for normal collective cell migration behaviors including the regulation of cell-cell and cell-ECM adhesion, cytoskeletal organization and cell contractility. The integrity of these mechanical connections is critical for the higher-order assembly and morphogenesis of mesendoderm tissue at gastrulation as well as the spatial regulation of Rac1 GTPase

activity.

2.2 Materials and Methods

Xenopus embryos and explant preparation

Xenopus embryos were obtained using standard methods and staged according to (Nieuwkoop P., 1994). Dorsal marginal zone (DMZ) and donut explants were prepared as described previously (Davidson et al., 2002) with the modification that Stage 11 embryos were used (Figure 2.1A). Glass coverslips for explant imaging were washed with alkaline ethanol solution, flamed and then glued, using Norland optical adhesive 68, to openings drilled with a lathe into the bottom of 35 mm petri dishes. Coverslips were then coated with 300ul of 5.0µg/ml bovine plasma FN overnight at 4C. Coverslips were blocked with 5% bovine serum albumin (BSA), washed and dishes filled with 1X Modified Barth's Saline (MBS). DMZ explants were plated for one hour prior to imaging.

Morpholino oligodeoxynucleotides and knockdown efficiency

Antisense morpholino oligodeoxynucleotides (MO) to inhibit keratin (8) expression were purchased from GeneTools and injected into the animal pole of embryos immediately after fertilization at a concentration of 40ng/embryo. The keratin MO (5'-TCGATCTGACGGACATGGTGGAGCT-3) was designed using *Xenopus* krt8 sequence NCBI accession number NM_00108756.1 (Weber et al., 2012). Control injections used the standard GeneTools Control MO (5_'-CCTCTTACCTCAGTTACAATTTATA-3'). To test MO knockdown efficiency, embryos injected with control and keratin(8) (krt8) MO

were lysed in SOL buffer (140mM KCl, 2mM $MgCl_2$, 5mM EGTA, 10mM NaPO, 5mM NaF, 0.5% Triton, pH7.0 with NaOH) and centrifuged for 15 mins at 14,000rpm at 4^0C. The supernatant was transferred to a fresh tube and the insoluble pellet was washed in XEX buffer (1.5M KCl, 300mM Sucrose, 50mM NaF, 10mM Tris-base, 0.5% NP-40, 10mM EGTA, pH 7.4). 6X lamellae buffer was added to the remaining insoluble pellet and analyzed on 10% SDS-PAGE. C-11 antibody (pan keratin antibody, Sigma, SAB3701450 at 1:20,000 dilution) was used to blot for keratin IFs. Anti-GAPDH antibody (Proteintech Group, Inc., PTG10494-1-AP at 1:5000 dilution) was used to blot for GAPDH from the supernatant and was used as a loading control. Intensity of the krt8 and GAPDH was quantified using ImageJ. Paired T-test was used to determine statistical significance.

RNA constructs

RNA encoding fluorescently tagged proteins was transcribed in vitro from linearized plasmids. Transcripts were injected into the dorsal marginal zone region of two blastomeres at the 2 or 4-cell stage with a final concentration of 200-2000 pg of RNA per embryo (See Table 2.1). The following constructs were used in this study: pCS2+ LifeAct-mCherry (Pfister et al., 2016), pCS2+ α5-EGFP (construct was made by cloning EGFP in frame with the cytoplasmic tail of *Xenopus* α5 integrin using Stu1 and Not1), pCS2+ GAP43-EGFP (E DeRobertis, University of California), pTriEX Rac1 Biosensor, Turquoise-Rac1 and Ypet-PBD (K. Hahn University of North Carolina, Chapel Hill) pCS2+ EGFP-Paxillin (subcloned by cold fusion into pCS2+ using Xba1 and SnaB1 from a construct obtained from R Horwitz, University of Virginia), pCS2+ EGFP-krt8 (V. Allan, University of Manchester; Clarke and Allan, 2003), pTriEx-mCherry-PA-Rac1Q61L and

pTriEx mCherry-PA-Rac1C450A (K. Hahn University of North Carolina, Chapel Hill).

Traction Force Microscopy (TFM): Preparation of Polyacrylamide Gels with NHS ester

Polyacrylamide gels with NHS ester were prepared using the method described in (Rajagopalan et al., 2004) with a few modifications. In brief, a mixture containing 6% acrylamide (Fisher Scientific, Pittsburg, PA), 0.36% bis-acrylamide (Fisher Scientific), 15 μmol/ml acrylic acid NHS ester (Fisher Scientific), 20% 0.25 M HEPES (4-(2-hydroxyethyl)-1-piperazineethanesulfonic acid; Fisher Scientific) was made and the pH of the solution was adjusted to 5.9-6.0 by careful addition of 1M HCL. To 250ul of this solution, approximately 50ul of 1μm-diameter fluorescent beads (Sphero carboxyl fluorescent particles; yellow; 1% w/v; Spherotech Inc., Lake Forest, IL) were added immediately followed by addition of ammonium persulfate (1% final volume) to initate polymerization. Before polymerization, the solution was cast on coverslips, which were already activated with 3-3-aminopropyltrimethoxysilane and glutaraldehyde. To ensure the beads were packed properly, dishes with unpolymerized gel were centrifuged at 900 rpm for 20 mins. The elastic modulus of the gel was determined to be 18.4 ± 1.9 kPa by the ball indentation method (Dimitriadis et al., 2002). DMZ or donut explants from embryos injected with Alexa-555 10,000 kDa dextran (Invitrogen #D34679) were plated on polyacrylamide gels embedded with beads. Time-lapse images of fluorescent dextran-filled cells (to visualizecell positions) and fluorescent beads were taken beginning one hour after explants were plated. Following imaging, trypsin was added to the dish, explants were allowed to detach and images of the beads were again acquired as a starting position reference to calculate traction stresses.

Traction Force Microscopy: Traction stress calculations using Matlab

Gel deformations were calculated by quantifying bead displacements using a Particle Image Velocimetry (PIV) ImageJ plugin (Tseng et al., 2012). Measurement noises were subsequently attenuated through a self-adaptive filtering scheme (Huang et al., 2012), and then traction forces were calculated from the magnitude and direction of the substrate deformation utilizing Fourier transform traction cytometry (FTTC; Butler et al., 2002). Both types of calculations were accomplished using Matlab. The location of leading edges of DMZ and donut explants were determined manually by imaging fluorescent dextran-filled cells, then equally distanced (10 micron) contours were drawn parallel to the leading-edge curvature. The area between adjacent contours was used to create 10 um wide bins spanning the width of the explant. All of the calculated stress value points (stress values were calculated in 8 microns by 8 microns grids) within a bin were averaged to obtain the values represented in each bar of the kymograph as a function of distance from the DMZ leading edge. To calculate vector values the traction stress vector was resolved into a horizontal component that is propelling the DMZ from left to right when this horizontal component is positive (pointing towards left), and a vertical component that is perpendicular to it. The vector sums take the directionality of stress into account and represent only the traction stresses contributing to forward movement of the explant. Absolute values represent the total magnitude of the stress regardless of whether it contributes to or resists the forward movement of the explant.

Microscopy and Image Analysis

Confocal z-stacks images were taken on a Nikon C1 confocal microscope at 0.5-1μm intervals. For time lapse movies, images were collected every two mins for 10-15 mins. Total internal reflection fluorescence (TIRF) Microscopy was done using an Olympus 1X70 inverted TIRF microscope with an Olympus 60X/1.45 TIRF objective. Images for time lapse were collected 15 or 30 seconds apart for 5 mins. Areas of FAs and number of FAs per cell were calculated by thresholding the image such that only FAs were saturated and the area of saturated pixels was counted. DMZ explants expressing pCS2+ GAP43-EGFP were used to analyze length of specialized filopodia and persistence of protrusion. Lengths were measured manually by tracing individual filopodia. Four randomly selected filopodia were measured per cell. Persistence of protrusion was calculated by tracking the number of times an individual protrusion retracts or newly appears over the course of 5 mins. Mann-Whitney test was used to determine statistical significance among FA areas, length of specialized filopodia under different conditions and persistence of protrusion.

FRET Microscopy

DMZ explants expressing Rac1 Biosensor, Turquoise-Rac1 and Ypet-PBD were imaged using a Leica Confocal. While imaging, microscope settings such as laser power and gain were kept constant. FRET efficiency was calculated using the PFRET ImageJ plugin (Chen and Periasamy, 2006) obtained from UVA Keck Center for Cellular Imaging. Line scan profiles of single cells were obtained from FRET efficiency images and an average of the FRET efficiency was plotted over distance from the front of the cell.

Photoactivation of Rac1

Mesendoderm tissue expressing mCherry-PA-Rac1 constructs (i.e., mcherry-PA Rac1C450A; mcherry-PA Rac1Q61L) and EGFP-keratin was excised at stage 11 and incubated in 1X$Ca^{2+/}Mg^{2+}$ free MBS (CMF-MBS) to dissociate the cells. Cells were then plated subconfluently onto coverslips coated with FN (10µg/ml). Cells were allowed to adhere for one hour and then imaged using a Zeiss Cell Observer SD (spinning disk confocal microscope) with Plan-Apochromat/63X or 100X objectives. A small region of the cells was irradiated with 457nm laser using a Zeiss Direct FRAP manipulation add-on hardware module. Statistical significance was determined using T-test at each time point conditions. Independent confirmation of these results was obtained in a separate set of experiments using an Olympus FV1000 with UPlanSApo/60X/1.35 objective. Data obtained with the Zeiss system are included in Figure A.1 and A.2.

Explant treatment, fixation and Actin Staining

DMZ explants on FN were treated with DMSO or 10µM Y27632, 5mM or 1mM Acrylamide for one hour. DMZ were fixed in 0.25% Glutaraldehyde, 3.7% Formaldehyde and 0.1% Tween20 for 10 mins at room temperature, stained with 488-ActiStain (Cytoskeleton) and imaged with the Nikon C1 confocal microscope.

Removal of leading edge cells from DMZ explants

DMZ explants expressing EGFP-paxillin and LifeAct-mCherry were plated on coverslips coated with FN (5µg/ml). Explants were allowed to adhere for one hour and imaged on an Olympus 1X70 inverted TIRF microscope with an Olympus 60X/1.45 TIRF

objective. The leading edge of the explant was carefully excised using an eyebrow knife and allowed to heal for one hour before images of the explants were taken again on the same microscope.

Scanning electron microscopy

Stage 11.5 *Xenopus* gastrula were fixed overnight with 4% formaldehyde/2.5% glutaraldehyde in 0.1X MBS. The BCR was removed from fixed embryos to expose the basal side of the mesendoderm tissue. Samples were postfixed in 1% OsO4, critical point dried, and gold-palladium sputtercoated. Specimens were imaged using a Zeiss Sigma VP HD Field Scanning Electron Microscope.

Cell Stretching and pMLC Western Blot analysis

Whole mesendoderm tissue from control and krt8 MO injected embryos was d issected and dissociated in 1X CMF MBS. Dissociated cells were then plated in a silicone well plate (Cell Scale, Waterloo, Canada) previously coated overnight at 4 C with 200ul of 10µg/ml FN or Ccad-Fc. Wells were blocked with 5% BSA, then washed, and filled with 100ul of 1X MBS. Cells were allowed to adhere for one hour before the membranes were cyclically stretched (10% stretch) using a MechanoCulture FX stretching device (Cell Scale, Waterloo, Canada). Fifteen cycles of: 10 seconds stretch, 10 seconds hold, 10 seconds relax and 10 sec hold were performed. Some cells were kept in 1X CMF MBS in suspension for the duration of the stretch cycles to serve as non-adherent controls. Cells were lysed with 100µl of lysis buffer: 100mM NaCl, 25mM Tris pH7.4, 1mM EDTA, 1mM EGTA, 1mM beta-glycerophosphate, 2.5mM Na4P2O7, 1% NP40, protease inhibitor cocktail (Sigma

P2714), and 1mM PMSF. Cell lysates were centrifuged for 10 mins at 14,000 rpm at 4˚C to remove yolk. The supernatants were transferred to new tubes, diluted with 6X reducing Laemmli buffer, and separated by SDS-PAGE (10 or 12%) and transferred onto nitrocellulose membranes. Blots were probed with antibodies directed against phospho-Myosin Light Chain (S19; Cell Signaling, 3671 at 1:1000 dilution) and beta-actin (Sigma, A3854 at 1:25,000 dilution). Signal intensity for each band was quantified using ImageJ and ratios of pMLC to beta-actin were calculated in Microsoft Excel. A Paired-t test was used to evaluate statistical differences in pMLC levels under different conditions.

2.3 Results

Keratin IFs are obligate heteropolymers of type I acid and type II basic subunits, and krt8 is the only type II basic keratin expressed at gastrulation (Franz and Franke, 1986; Franz et al., 1983). I used a previously reported antisense morpholino directed against the 5'-UTR of krt8 to knockdown expression (Weber et al., 2012). Knockdown efficiency was determined using western blot analysis and observing whole embryo phenotypes. Krt8 MO reduced the expression of soluble krt8 by approximately 50% compared to control MO at gastrulation stages (Figure 2.2A). Tailbud stage krt8 morphant embryos had shorter axes compared to control embryos and showed skin blistering (Figure 2.2B arrows).

A role for keratin IFs in the spatial regulation of traction forces in migrating mesendoderm.

The protrusive and motile behaviors of individual cells in intact *Xenopus* mesendoderm suggest that traction stresses are distributed throughout the tissue and

required for collective movement (Davidson et al., 2002). Based on these observations and analyses of collectively migrating MDCK cells (Trepat et al., 2009), we hypothesized that traction stresses are likely greatest at the leading edge of the mesendoderm and progressively decrease in subsequent rows of cells, where cumulative traction stresses would be balanced by increasing cell-cell stresses (Weber et al., 2012). In order to test this model directly, we adapted TFM methods to map the distribution of traction stresses generated by individual cells within explants migrating on deformable FN substrates. In this approach, a polyacrylamide substrate of known elastic modulus is prepared with embedded fluorescent beads, which serve as fiducial marks. The TFM substrate is coated with fibronectin and mesendoderm explants allowed to attach. Explant cells deform the substrate as they migrate and the resulting displacements of the embedded beads are recorded using a confocal microscope. Traction forces are derived from these data utilizing Fourier transform traction cytometry (Butler et al., 2002). Additional details are provided in Methods. The explant preparations used in this study (i.e., DMZ, dorsal marginal zone, and "donut" explants) are described in Davidson et al. (2002) and summarized in Figure 2.1.

Average radial traction stresses (vector values) within DMZ explants are concentrated along the leading row (green highlighted area between panels A and B in Figure 2.3, and Figure 2.3G) and are reduced significantly in the second row (yellow highlighted area between panels A and B in Figure 2.3, and Figure 2.3G) and beyond. "Stress maps" were further binned into 10μm strips starting with, and outlined by, the leading edge of the explant (Figure 2.3; white dotted lines are separated by 50μm, the approximate width of 1 row of cells). Averages of vector (Figure 2.3B, G) and absolute

(Figure 2.3C, H) values of traction stresses were calculated for each 10μm binned region. The leading protrusive edge of the tissue generates the highest traction stresses (absolute traction stresses; Figure 2.3C) contributing to directional migration (positive vector values indicate net traction stresses that contribute to forward migration, i.e., ~180Pa, Figure 2.3B). Following rows exert 3-fold lower traction stresses (average absolute traction stresses; Figure 2.3C, H), and the vectors of these traction stresses are randomized and cancel as reflected in the preponderance of zero to negative values for the binned vector traction stresses (Figure 2.3B, G). These data suggest that cells in following rows migrate randomly or are being "dragged" along by leading-edge cells. This confirms that directional traction stresses responsible for forward migration originate at the leading-edge and are not distributed throughout the tissue.

The geometry of the mesendoderm and its substrate, the BCR, differs markedly from a DMZ explant on a plastic or glass surface. In the embryo, mesendoderm is comprised of a circumferential ring of tissue, separated from the BCR by the cleft of Brachet as it begins to migrate along the dorsal side of the embryo, spreading laterally to the ventral margin of the tissue as gastrulation progresses. This "donut" of tissue can be removed and placed on a FN substrate for further analysis (Figure 2.1B). We next addressed whether the traction stresses generated by mesendoderm in the donut configuration are comparable to that of the DMZ (Figure 2.4). Like the DMZ, highest traction stresses are generated by leading-row cells, however, the distribution of these stresses is not symmetrical. Traction stresses are greatest on the anterior-dorsal side and weakest on the posterior-ventral (Figure 2.4A). In addition, the magnitudes of these stresses vary depending on the extent of closure. Average radial traction stresses are approximately

30% of those observed in DMZ explants as migration begins and increase as closure proceeds, ultimately matching that of DMZ explants just prior to closure when traction stresses again decrease (Figure 2.4B). These data suggest that donut explants do not require large radial traction forces to close.

Reduced expression of newly synthesized keratin IFs results in misdirected cell protrusions in intact mesendoderm and failure of individual cells to repolarize in response to local tugging forces on C-cadherins (Weber et al., 2012). To investigate whether these changes in protrusive behaviors are reflected in the magnitude and/or direction of traction stresses, we performed krt8 knockdown experiments. High traction stresses are not limited to the leading-row in krt8 morphants (green highlighted areas between Figure 2.3 panels D, E, F). Although reduced relative to the first row, traction stresses in the second row of these explants (e.g., yellow highlighted area between Figure 2.3 panels D, E, F), remain significantly higher than follower rows in control morphants (Figure 2.3C, F, H). However, average vector traction stresses reveal many randomly directed forces (high negative and positive values of vector sums; Figure 2.3E, G) that in some cases are cancelled out by balancing forces in opposing directions. This likely contributes to the observed decrease in the overall rate of tissue migration in krt8 morphants (Figure 2.5). Average traction stresses from two time points of three separate explants are expressed as vector (Figure 2.3B, E, G) and absolute (Figure 2.3C, F, H) values. Based on these results, we conclude that keratin IFs are important for maintaining the normal spatial distribution of cellular traction stresses across a collectively migrating mesendoderm explant.

Leading edge and following row cells display differences in protrusive behavior and

Rac1 activity.

We next addressed whether protrusion morphology of cells in the leading edge and following rows correlates with the distribution of traction stresses obtained by TFM. Transcripts encoding GFP-tagged α5integrin (α5-GFP) were injected along with LifeAct-mCherry (Riedl et al., 2008) into early cleavage stage blastomeres. At stage 11, DMZ explants were prepared and plated on FN; both cell-substrate adhesions and actin were then visualized using TIRF microscopy. Leading edge cells in controls extend broad lamellipodia containing an actin meshwork and α5-GFP in focal adhesions (Figure 2.6A-C). Occasional filopodia are also seen in the leading-edge cells of the mesendoderm during migration. However, following row cells have smaller lamellipodia and extend long filopodial protrusions enriched with both integrin α5-GFP and actin (Figure 2.6D-F). Following row cells extend more filopodial processes per cell and the average length of these processes is significantly greater than the filopodia of leading edge cells (leading edge: 6.96 ± 0.3 μm; following row: 11.06 ± 0.5 μm) with some extending up to 30 μm in length (Figure 2.6G). Scanning electron microscopy of fixed and fractured embryos confirms the presence of comparable length filopodia in vivo (Figure 2.6H) in following row cells (e.g., compare Figure 2.6I, J). These structures extend and make contact with neighboring cells (Figure 2.6J). Time lapse TIRF imaging of mesendoderm cells expressing membrane-EGFP revealed that these filopodia are highly dynamic and in following row cells were observed to curve and spiral frequently as they grow in length. Overall, lamellipodial protrusions in following row cells are less persistent than in leading edge cells and undergo frequent direction changes (Figure 2.6K). In addition, physical removal of leading edge cells caused following row cells to lose filopodia, repolarize and

adopt the behavior of a new leading edge with lamellipodia and few filopodia (Figure 2.7).

Because Rac1 is a known regulator of actin polymerization and lamellipodia (Ridley et al., 1992), we next addressed whether observed differences in protrusive behaviors between leading edge and following row cells correlate with differences in Rac1 activity. To resolve spatial differences in Rac1 activity, FRET microscopy was performed on mesendoderm cells expressing a Rac1 Biosensor (Hodgson et al., 2010). In leading edge cells of the mesendoderm, Rac1 is widely distributed throughout the cell (Figure 2.6L). However, a gradient of Rac1 activity is observed in these cells with highest FRET efficiency noted in lamellipodia at the leading edge (Figure 2.6M, P). The Rac1 biosensor is also distributed throughout following row cells but we failed to observe a polarized gradient of Rac1 activity in these cells (Figure 2.6N, O, P).

Spatial regulation of focal adhesion dynamics is altered in keratin IF-depleted mesendoderm.

These results reveal significant differences between leader and follower row cells with respect to the distribution of traction stresses generated, and the protrusions observed. We next explored whether differences in focal adhesion (FA) dynamics between normal leader and follower cells, and cells with reduced keratin IF expression, could help explain these behaviors. Mesendoderm explants expressing EGFP-paxillin, a marker of FAs (Turner, 2000), and LifeAct-mCherry, were imaged using TIRF microscope. Mature persistent FAs were evident in forward protrusions with few FAs noted in the cell body away from the leading edge (Figure 2.8A, K). Actin in these cells forms a branched network that co-localizes with paxillin at sites of FAs (Figure 2.8B, B’ and B’’). Both FA area

(Figure 2.8I, leading edge CoMO=0.3874 ± 0.02μm^2) and numbers (Figure 2.8J, leading edge CoMO=111.9 ± 8.9 FAs per cell) are greatest in forward protrusions of leading edge cells, coincident with highest traction forces (Figure 2.1A-C). In contrast, following row cells have fewer FAs (Figure 2.8J, following row CoMO = 43.42 ± 4.3 FAs per cell), are reduced in area (Figure 2.8I, following row CoMO = 0.2374 ± 0.01μm^2) and more dispersed throughout the cell body (Fig 1.8C). Similar to leading edge cells, branched actin in following row cells co-localizes with paxillin at FAs (Fig 1.8D, D' and D''). FAs in following row cells are highly dynamic with smaller, nascent contacts assembling and disassembling rapidly, suggesting lower overall adhesion to the substrate. This is consistent with reduced traction stresses noted in following row cells (Figure 2.3A-C and G).

Krt8 morphant cells have misdirected protrusions (Weber et al., 2012) with both leader and follower cells exerting high traction stresses (Figure 2.3D-F and G). These changes in behavior relative to controls are also reflected in both the formation and dynamics of FAs. TIRF images and time-lapse movies reveal that leading edge cells in krt8 morphants form fewer FAs relative to controls (Figure 2.8J, 77.63 ± 8.1 vs. 111.9 ± 8.9) but FA area is significantly increased (Figure 2.8I, 0.517 ± 0.04 μm^2 vs. 0.3874 ± 0.02μm^2). These large mature FAs are present in both forward-facing and misdirected protrusions, and at the cell rear in both leading (Figure 2.8E, F, F" and K) and following (Figure 2.8G, H and H") rows. Prominent actin stress-fibers anchored in FAs extend across the long axes of these cells (Figure 2.8E-F' and G-H', see also Figure 2.9). FA area and number are little changed between leading and following row cells of krt8 morphants (Figure 2.8I and J) unlike in controls. These data indicate the importance of keratin IFs in maintaining the "row-specific" differences in cell behaviors and overall organization of mesendoderm.

Prominent actin stress fibers are observed upon depletion of keratin IFs.

Because TIRF limits visualization to within 100nm of the FN-coated glass surface, we used confocal microcopy to investigate the deeper organization of actin filaments in both fixed and live mesendoderm explants. As reported previously (Bjerke et al., 2014) a dense meshwork of actin is present within the large monopolar, lamellipodia that form along the leading edge of control explants in the direction of travel (Figure 2.9A-B). These actin-filled processes protrude persistently in the forward direction with fine cortical actin filaments evident throughout the cell body. Protrusions in following row cells (Figure 2.9A and C; arrows) are smaller, highly dynamic and less persistent than those in the leading row; long filopodia noted in Figure 2.6 (D-F) are also evident in these cells (Figure 2.9A and C; arrowheads). Knockdown of keratin IFs (Figure 2.8E-H, krt8MO) results in dramatic changes in cell shape and actin organization. Parallel stress fibers extending throughout the cell body are noted in both leading and following row cells (Figure 2.9E-G). Protrusions are often misdirected in these cells, particularly in the leading row (Figure 2.9E, F; see also Weber et al., 2012). Cell protrusions are typically smaller than those observed in control explants but they are highly dynamic and appear to apply tugging forces on neighboring cells. Acrylamide (non-polymerized) can also be used to disrupt intermediate filaments acutely in cells (Eckert and Yeagle, 1988). Mesendoderm explants exposed to increasing concentrations of acrylamide underwent a rapid reorganization of the actin cytoskeleton, from dense actin meshwork in protrusions and fine cortical filaments in the cell body, to long stress fibers (Figure 2.10). Overall, the appearance of acrylamide-treated cells closely matches that of keratin morphant explants and supports the

specificity of the krt8MO phenotype. Maintenance of cell cohesion is essential for collective migration and in *Xenopus* mesendoderm, this involves maintenance of C-cad based adhesion complexes linked to both actin and keratin IFs (Weber et al., 2012). Fine cortical actin filaments are apparent at cell-cell junctions in controls, however, in krt8 morphant cells the morphology of these junctions is altered (Figure 2.9D, H); actin stress fibers now span the cells and appear continuous with their neighbors (Figure 2.9H).

Phosphomyosin II levels are upregulated in krt8 morphant explants.

The appearance of streak-like focal adhesions (Figure 2.8E-H") and actin stress fibers (Figure 2.9E-H) in krt8 morphants suggests that contractility is increased in these cells (Even-Ram et al., 2007). Actin association with myosin and phosphorylation of myosin light chain II (pMLC) are essential for regulating cell contractility during migration (Vicente-Manzanares et al., 2009) and in response to changes in ECM stiffness (Clark et al., 2007). To address whether actomyosin contractility was increased in krt8 morphants, pMLC levels were quantified by Western blot (Figure 2.11A-D). Because mesendoderm explants also contain non-migrating ectodermal tissue, mesendoderm from control and krt8 morpholino-injected embryos was specifically dissected, dissociated and plated at sub-confluent densities on stretchable silicone membranes coated with either FN (to mimic cell-ECM interaction) or C-cadherin (C-CadFc, to mimic cell-cell interaction). Cells attach and spread on both FN and C-cadFc substrates but appear more symmetrical on C-CadFC than on FN (Figure 2.12). After one hour, half the cultures were subject to cyclical rounds of uniaxial stretch and the remainder were left "unstretched". Stretching was performed to simulate the tension experienced by adhesions (cell-matrix or cell-cell) during migration.

pMLC increased 2-3 fold in control cells stretched on FN (Figure 2.11A, B). No increase in pMLC was detected when cells were instead stretched on C-CadFc (Figure 2.11C, D). In contrast, pMLC was increased in krt8 morphant cells adherent to either FN or C-cad-FC substrates in the absence of stretch. Unlike the situation for CoMO cells on FN, stretching krt8 morphant cells did not further increase pMLC levels. The "stretch-independent" enhancement of pMLC in krt8 morphant cells required specific adhesion to either cadherin or FN substrates; no significant increase in pMLC was observed when krt8 morphant cells were kept in suspension (Figure 2.11A-D). Thus, mesendoderm cells respond specifically to mechanical deformations of the FN substrate by becoming more contractile. Notably, however, knockdown of keratin IFs can result in a similar increase in MLC phosphorylation levels and contractility in the absence of applied stretch, consistent with observed changes in traction stresses, actin filament organization and focal adhesion dynamics (Figures 1.1, 1.6, 1.9).

Inhibition of myosin II activity inhibits formation of actin stress fibers in krt8 morphants.

Keratin-depleted cells are more contractile, exert higher traction stresses and form larger, more mature focal adhesions than controls. pMLC is known to be essential for FA maturation and inhibition of myosin II activity reduces FA area (Pasapera et al., 2010). We next asked, therefore, whether inhibiting pMLC would reverse some of the features of keratin knockdown including stress fiber formation. Mesendoderm explants were treated with the ROCK inhibitor Y27632 to inhibit MLC phosphorylation and then fixed and stained with phalloidin. Leading edge cells from control (CoMO) explants revealed the

typical arrangement of actin meshwork in lamellipodia and fine cortical actin filaments throughout cell bodies (Figure 2.11E). The addition of Y-27632 had no appreciable effect on overall morphology or actin organization in these cells (Figure 2.11F), which maintained actin-rich, broad lamellipodial protrusions along the leading-edge and smaller protrusions in following-row cells. In contrast, the cell bodies of krt8 morphant cells contained abundant actin stress fibers in both leading and following-row cells (Figure 2.11G, I). Treatment of krt8 morphant explants with ROCK inhibitor suppressed stress fiber formation, increased cortical actin filaments, and leading-edge cells regained actin-dense lamellipodia (Figure 2.11H, I). These data indicate that inhibition of myosin II is sufficient to block actin stress fiber formation and the increased cell contractility that accompanies keratin IF knockdown (Figure 2.1, 2.6 and 2.9).

Functional antagonism of keratin IFs and Rac1.

As described previously, a "basket-like" arrangement of keratin IFs forms at the rear of mesendoderm cells undergoing collective cell migration (Weber et al., 2012) and this arrangement is most pronounced in the leading-row cells, which are also notable for the broad monopolar-directed lamellipodial protrusions they extend in the direction of travel. Rac1 GTPase activity is highest in these forward protrusions and decreases toward the cell rear (Figure 2.6L, M, P). Helfand et al. (2011) have reported that Rac1 and vimentin IFs are functionally antagonistic. Given the spatial arrangement of keratin IFs and Rac1 GTPase activity in the mesendoderm, we asked whether similar opposing functions might be operating in these cells. The Rac1 FRET biosensor was expressed in control and krt8 morphants and Rac1 GTPase activity imaged (Figure 2.13A-D). As described in Figure 2,

Rac1 activity in controls is highest in lamellipodial protrusions at the cell front and lowest at the cell rear (Figure 2.13A, B, E). In krt8 morphant explants, the gradient of Rac1 GTPase activity evident in controls is lost (Figure 2.13C, D, E). Thus, absence of a Rac1 activity gradient in these cells is correlated with keratin 8 knockdown and consistent with the possible functional suppression of Rac1 activity by the keratin cytoskeleton.

We performed the converse experiment by expressing a photoactivatable, constitutively active form of Rac1 (mCherry-PA-Rac1Q61L; Wu et al., 2009) along with EGFP-krt8 to visualize keratin filaments. A region of interest (ROI) was selected for irradiation at 456nm with a confocal microscope. Activation of mCherry-PA-Rac1 leads to the local formation of a membrane ruffle and lamellipodia within 3 minutes of irradiation (Figure 2.13F-H, arrowheads). In addition, activation of PA-Rac1 is accompanied by the loss of EGFPkeratin IFs within the ROI in proximity to the newly formed protrusions (Figure 2.13G, H, L). A nonphotoactivatable Rac1 construct (mCherry-PA-Rac1C450A) was co-expressed along with EGFP-krt8 as a control and irradiated as described. No protrusions were induced within the ROI of control cells following irradiation (Figure 2.13I-K). Moreover, EGFP-keratin filaments were maintained in the irradiated ROI (Figure 2.13I-L) confirming that loss of EGFP-keratin filaments in Figure 6F-H was not the result of photobleaching or photodamage. These data support the conclusion that keratin IFs and active Rac1 have opposing roles in the mesendoderm.

2.4 Discussion

Traction stresses are generated primarily by leading edge cells in the mesendoderm.

A primary goal of this study was to establish the importance of cell-ECM traction forces in the assembly, organization and collective progression of mesendoderm cells across the BCR at gastrulation. It is well established from mammalian cell culture studies that both the leading and trailing edges of migrating single cells exert traction on the ECM (du Roure et al., 2005; Lauffenburger and Horwitz, 1996). In collective modes of cell migration, the generation of traction forces by cells at the free or leading edge, are typically balanced by cell-cell adhesions at the rear (e.g., Weber et al., 2012) and in some instances, at lateral contacts between cells. The extent to which directed cohesive migration involves the active "tugging" of one cell upon another vs. the coordinated "crawling" of independent cells (Farooqui and Fenteany, 2005; Tambe et al., 2011; Trepat et al., 2009) is not always clear, and likely varies with cell and tissue type and the presence or absence of directional cues arising from chemokine signaling (Dalle Nogare et al., 2014). Based on earlier observations (Davidson et al., 2002) we proposed a distributed traction model to explain mesendoderm collective migration (Weber et al., 2012). This model predicts that highest traction stresses are generated by cells at the leading edge with following rows of cells displaying progressively lower tractions. Correspondingly, cell-cell stresses are progressively increased in succeeding rows, reflecting the balancing of accumulated traction stresses at any given position away from the leading edge (Trepat et al., 2009). Other collectively migrating cells and tissues are known to rely on leader cells that pull follower cells forward (Brugués et al., 2014; Rausch et al., 2013; Tse et al., 2012).

TFM experiments (Figure 2.3 and 2.4) revealed traction stresses are being generated along the leading edge of the first row of cells but are largely absent in the second row and beyond, in contrast to what is predicted by a distributed traction mechanism. This

indicates that leading row traction forces are being balanced by cell-cell adhesive contacts with the follower rows. Thus, leader cells are actively pulling the following row cells a long, and follower-row substrate tractions are not a major contributor to the forward migration of the mesendoderm. It is not yet possible to measure traction forces in the embryo but there are two pieces of evidence depicted in Figure 2.14 that support the conclusions arising from the explant studies. First, bisection of live embryos at gastrula stages reveals the presence of a clear, expanded "space" (i.e., the cleft of Brachet) between the mesendoderm tissue and the BCR in agreement with the lack of detectable traction stresses in following row cells of explants on FN (Figure 2.3). However, the leading-edge of the mesendoderm, which defines the forward boundary of the cleft, is tightly adherent to the BCR and resists physical separation (unpublished observations). Second, (Moosmann et al., 2013) used x-ray microtomography to image internal tissue movements of intact living gastrula stage embryos; these data confirm the separation of follower rows of mesendoderm cells from the BCR but also the tight association of the leader row cells. Moreover, inward deformation of the BCR at the site of contact with the leading row suggests not only strong adhesion but also that the mesendoderm is under considerable anisotropic tension oriented in the direction of travel, in agreement with explant studies (Davidson et al., 2002). Taken together, these data suggest that high traction stresses in the leading edge are borne by cell-cell stresses in the follower rows and, moreover, that this distribution of forces is required for overall organization of the tissue.

The high traction stresses resolved at the leading-edge correlate with the presence of large, mature FAs. Cells exert traction stresses on the ECM through their integrin-based FAs (Lauffenburger and Horwitz, 1996) and transmission of forces to the ECM via these

adhesions is essential for FA maturation (Chrzanowska-Wodnicka and Burridge, 1996; Pasapera et al., 2010; Plotnikov et al., 2012; Roca-Cusachs et al., 2013) and forward cell migration (Beningo et al., 2001). Follower row cells form smaller and fewer FAs, which is consistent with the inability of these cells to generate significant traction stresses. However, if the leading row is physically removed from a migrating DMZ explant, the following row cells quickly transform their morphology to become indistinguishable from the cells they replaced in terms of protrusive activity and the appearance of larger, mature FAs (Figure 2.7). This suggests that follower row cells are normally unable to exert substrate tractions forces sufficient for FA maturation due to the high cell-cell stresses they experience as a consequence of their position behind the leading row. Cadherin adhesion is also reported to antagonize cell-matrix adhesions (Borghi et al., 2010; Mertz et al., 2013). Together, this may explain why the following row cells do not adhere strongly to the BCR in the embryo.

Following row cells also extend long, highly-dynamic filopodia (Figure 2.6). Their function in the mesendoderm is not known but, based on evidence from other systems, may be involved in morphogen signaling (Bischoff et al., 2013; Roy et al., 2014; Stanganello and Scholpp, 2016). In *Xenopus* embryos, these structures have been reported to align with FN matrix assembled by BCR cells (Boucaut et al., 1990) and to promote cytoplasmic exchange (Danilchik et al., 2013). It is perhaps interesting to note that these specialized-filopodia extend into the cleft of Brachet where they may participate in receptor-mediated signaling important in mesendoderm development. Brachet's cleft is a fluid filled compartment defined by the space between the BCR and the involuting mesoderm. It is bounded and possibly "sealed-off" from the blastocoel cavity by the tightly adherent advancing forward edge of the mesendodermal mantle (Figure 2.14). Plouhinec et al.,

(2013) report that chordin secreted by the dorsal Spemann organizer region of the ectoderm diffuses within the cleft to form a morphogen signaling gradient. This raises the intriguing possibility that the observed remodeling of the FN fibrillar matrix by the advancing mesendoderm (Davidson et al., 2004) represents the release of fragments of FN and any associated chemokines (e.g., PDGF; Smith et al., 2009) into the cleft, where they are then sampled by these filopodia. Leader cells involved in collective cell invasion have been shown to upregulate MMP and degrade ECM (Gaggioli et al., 2007; Wolf et al., 2007). It will be of interest to establish in future studies if leading edge cells proteolytically modify the FN matrix or, as a result of applied cell traction stresses, cause the force-induced unfolding of FN to expose cryptic binding sites with biological activity (Smith et al., 2007).

A role for the keratin intermediate filament cytoskeleton in mesendoderm tissue organization?

Knockdown of keratin IF's dramatically alters follower-row cell behaviors indicating the likely importance of maintaining strong cell-cell adhesions in the tissue to balance leading-edge tractions. The functional consequences of reduced keratin levels include increased traction stresses (Figure 2.3D) and maturation of FAs (Figure 2.8), altered cell protrusions (Figure 2.6), and a reorganization of the actin cytoskeleton from fine cortical filaments in the cell body to stress fibers (Figure 2.9). The overall migration rate of krt8 morphants is also lower (Figure 2.5) possibly due to lack of FA turnover (Webb et al., 2004). Previously, we reported that local tugging forces on C-cadherins in single mesendoderm cells on FN results in recruitment of keratin IFs, cell repolarization and directed migration (Weber et al., 2012). Keratin IFs are known to provide mechanical

integrity to cells (Coulombe et al., 1991; Ramms et al., 2013) and are involved in maintaining strong cellular adhesions (Huen et al., 2002; Kröger et al., 2013). It is likely keratin IFs are playing a similar role in the mesendoderm.

Thus, we hypothesize that in krt8 morphants high traction stresses generated at the leading edge are unable to be resisted by weakened cell-cell adhesions in the following rows. This results in increases in cell-ECM adhesion, traction stresses, and FA maturation, but because these cells are no longer able to balance the directional forces generated by leading row cells, they become randomly protrusive and misoriented. Similar modulation of cell-ECM traction stresses in response to disruptions in cadherin-based adhesions have been reported for clusters of cultured keratinocytes (Mertz et al., 2013).

Knockdown of krt8 results in a striking reorganization of the actin cytoskeleton and presence of mature FAs in both leading and following rows of cells. In cultured cells depletion of plectin, which functions as a linker of actin and intermediate filaments and microtubules, results in increased MAP kinase signaling and enhanced stress fiber formation (Osmanagic-Myers et al., 2006). While the mechanisms responsible for increased stress fiber formation and contractility in keratin depleted mesendoderm are not known, it is possible that loss of keratin IFs alters plectin function resulting in global changes in cytoskeletal organization. Significant increases in actin stress fibers noted at mesendoderm cell junctions in keratin morphant cells (Figure 2.9H) may also be compensating for the loss of mechanical integrity associated with reduced keratin IFs. Disruptions of desmosomal junctions are associated with increased myosin II levels at adherens junctions, which promotes contractility (Sumigray et al., 2014; Yonemura et al., 1995) and junctional stability (Cavey and Lecuit, 2016).

Cells are able to sense and respond to changes in matrix rigidity during migration and myosin II is recruited to reinforce integrin adhesions as substrate forces increase (Choi et al., 2008; Galbraith and Sheetz, 1999). We observed a similar, integrin-dependent increase in myosin II activity (i.e., pMLC levels) in control mesendoderm cells subjected to stretch on FN (Figure 2.11). Stretching control cells on C-cad-Fc substrates had no effect on myosin II activity. This might reflect resistance to stretch being borne by keratin IF based cadherin adhesions. Interestingly, myosin II activity is elevated in krt8 morphant cells plated on either FN or C-CadFc, further suggesting that myosin II phosphorylation is upregulated to compensate for loss of mechanical integrity in keratin IF depleted cells.

Rho GTPases are important regulators of cell adhesions and cytoskeletal networks (Nobes and Hall, 1999), and are subject to tight spatiotemporal regulation in migratory cells (MacHacek et al., 2009; Yamada and Nelson, 2007). As reported in other systems Rac1 activity is highest in lamellipodia where it spatially coincides with FAs at the leading edge of mesendoderm explants. Disruption of the Rac1 activity gradient in krt8 morphants and the disassembly of keratin IFs resulting from photoactivation of Rac1 (Figure 2.13), suggest that keratin IFs may normally antagonize Rac1 activity. For example, at the cell rear where keratin IFs are assembled in a basket-like arrangement (Weber et al., 2012); (Figure 2.14). Similar mechanisms have been reported for vimentin (Helfand et al., 2011; Jiu et al., 2017) and keratin 18 (Fujiwara et al., 2016). The presence of actin stress fibers and increased cell contractility in krt8 morphant cells may reflect an upregulation of RhoA signaling (Chrzanowska-Wodnicka and Burridge, 1996). Inhibiting myosin II activity in krt8 morphant explants with ROCK kinase inhibitor blocks the formation of actin stress fibers and leads to the formation of lamellipodia similar to those of control cells. Taken

together, we conclude that keratin IFs play an important role in cell migration possibly by regulating the activities of Rho-GTPase family member proteins.

The geometry of mesendoderm closure.

Most of the data reported in this study were obtained using the DMZ explant (Figure 2.2). This explant also allows migration movements to be followed for longer periods of time than in the donut (Figure 2.2), which ultimately "closes" coincident with the cessation of cell migration. While the overall features of mesendoderm migration and organization are shared in both preparations there are some differences. These include a higher velocity of cell migration in donuts that more closely matches the rate in embryos (Davidson et al., 2002) and a more dynamic, complex pattern of traction stresses along the leading-edge (Figure 2.4). Average radial traction stresses are not only lower overall but also reveal a dorsal-ventral asymmetry. Mesendoderm migration begins on the dorsal side of the embryo and extends laterally to the ventral side with time. The ventral margins of donut explants fail to generate strong radial tractions, even though the cells continue to move at a rate comparable to cells on the dorsal side of the donut. In the absence of significant ventral radial traction stresses how does closure occur? Donut explants may also generate tangential forces that likely originate in follower row cells that are located above the leader and follower-rows that face the BCR (Figure 2.14 and Figure 2.15A-C). Many of these upper follower row (UFR) cells have their long axes oriented perpendicular to the forward directed leading-row cells attached firmly to the BCR FN. Actin stress fibers run the length of these UFR cells terminating at cell junctions where they appear continuous with stress fibers in neighboring cells (Figure 2.15C). We propose that these

circumferentially arranged cells are the source of tangential stresses helping to drive closure of the mesendoderm in donut explants and in embryos (Figure 2.14) even in the absence of significant radial traction stresses. Future studies will be needed to establish the contribution of UFR cell contractility to closure. The presence of these cells suggests another morphogenetic machine working in concert with leading-row traction stresses to shape the mesendoderm and guide its collective movement at gastrulation.

The importance of the keratin IF system as an integrator of mechanical forces required for the multiple morphogenetic movements of *Xenopus* gastrulation was first proposed by Klymkowsky et al., (1992). The current study provides direct evidence for keratin IF involvement in coordinating single cell behaviors to affect a tissue level movement. We conclude that even a delicate rebalancing of traction forces and intercellular stresses may have profound consequences for cell polarity, cytoskeletal organization, and the individual motile behaviors of cells involved in directing the collective movements of a tissue.

Table 2.1: RNA transcripts injected per embryo.

RNA transcript	Picograms injected per embryo
LifeAct-mCherry	250
α5-GFP	250
GAP43-EGFP	200
Rac1 Biosensor	1600-2000
Turquoise Rac1	800-1000
yPet PBD	800-1000
EGFP-Paxillin	250
EGFP-krt8	500
mCherry-PA-Rac1Q61L	2000
mCherry-PA-Rac1C450A	2000

Figure 2.1: Preparation of *ex vivo* explants from live embryos.

(A) Cartoon of a bisected stage 11 embryo and steps involved in preparing a Dorsal Marginal Zone (DMZ explants). Red dashed lines indicate the region of excisions. After excision, endoderm tissue adjoining the mesendoderm/mesoderm tissue is removed. The explant is then jackknifed open so that the region normally adjacent to the BCR is placed in contact with a FN coated coverslip. (B) Cartoon of a late stage 11 embryo with blastocoel roof removed to reveal mesendoderm cup. Red dashed line indicates the region of excision. In order to maintain proper orientation with respect to BCR and assemble FN, the donut explant is inverted and placed in contact with a FN coated coverslip. 'd' and 'v' indicate the dorsal and ventral sides of the donut respectively. Images of the DMZ and donut explants were provided by Bette Dzambe.

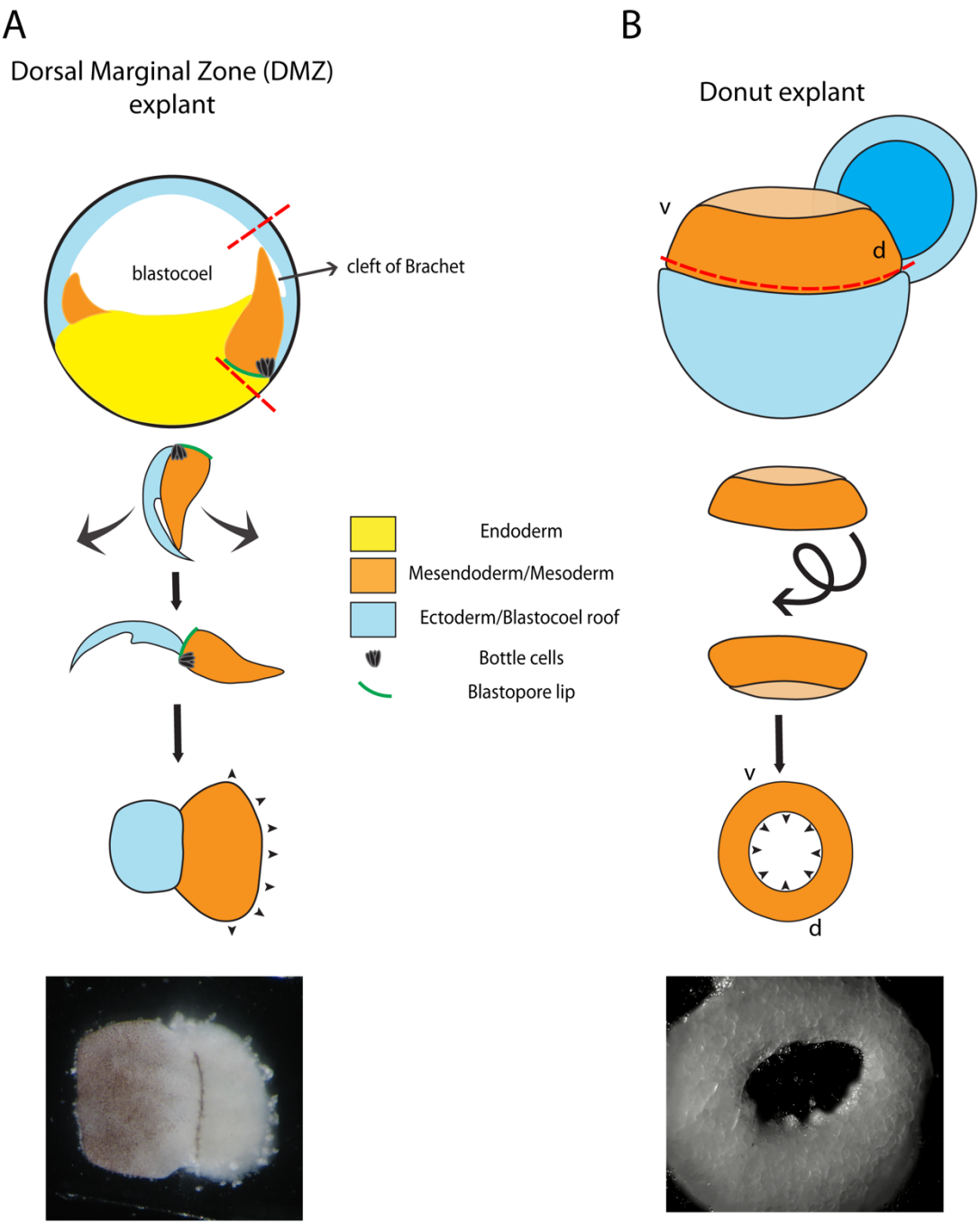
A
Dorsal Marginal Zone (DMZ) explant
blastocoel
cleft of Brachet
Endoderm
Mesendoderm/Mesoderm
Ectoderm/Blastocoel roof
Bottle cells
Blastopore lip
B
Donut explant
v
d
v
d

Figure 2.2: Krt8 morpholino efficiency.

(A) Representative Western blot of Krt8 expression levels in stage 11 embryos injected with Control and Krt8 morpholino, GAPDH was used as a loading control. Quantification shows Krt8 expression at stage 11 normalized to GAPDH relative to control embryos (N = 4). Data: Mean ± SEM, ** $p<0.01$. (B) Representative images of time matched tailbud stage embryos injected with control and krt8 morpholino. Arrows show development defects such as blistering and loosely attached cells due to reduced krt8 expression.

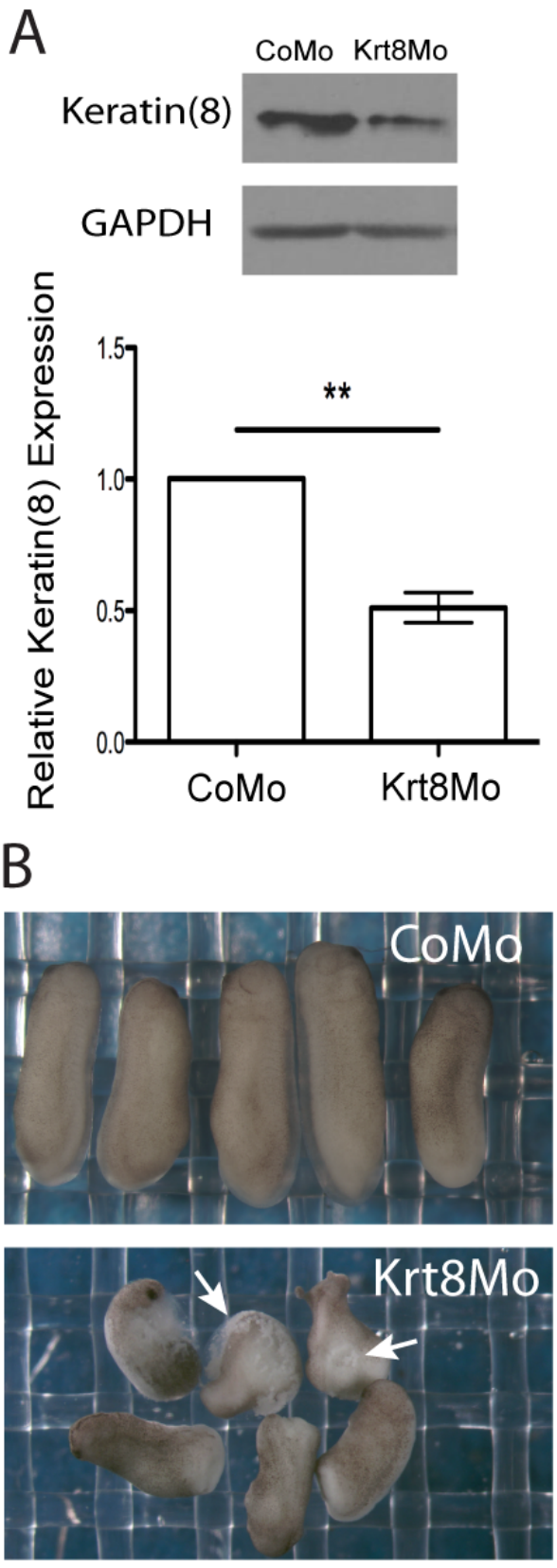
A
CoMo
Krt8Mo
Keratin(8)
GAPDH
Relative Keratin(8) Expression
1.5
1.0
0.5
0.0
**
CoMo
Krt8Mo
B
CoMo
Krt8Mo

Figure 2.3: Distribution of traction stresses in control and keratin morphant explants on FN substrates.

Representative traction stress maps for (A) control and (D) krt8 morphant mesendoderm explants. Arrows indicate the magnitudes and directions of traction stresses. Distance between white dotted lines (A, D) approximates 50μm width of one cell row. Green and yellow highlighted areas between vertical panels correspond to leading and second rows of cells, respectively. Heat maps were binned into 10μm slices starting from the leading edge. Average (B, E) vector and (C, F) absolute values of traction stresses for each 10μm slice, plotted as kymographs (B, C, E, F). Kymographs of average vector values of traction stresses correspond to the heat maps of (B) control and (E) krt8 morphants. Kymographs of average absolute values of traction stresses corresponding to the heat map of (C) control and (F) krt8 morphants. Comparisons of average (G) vector and (H) absolute values of traction stresses for two time points from three separate control and krt8 morphant explants. Data: mean ± SEM, * $p<0.05$. Scale bar = 50μm (A, D). These data were generated in collaboration Chong Wang and Bette Dzamba.

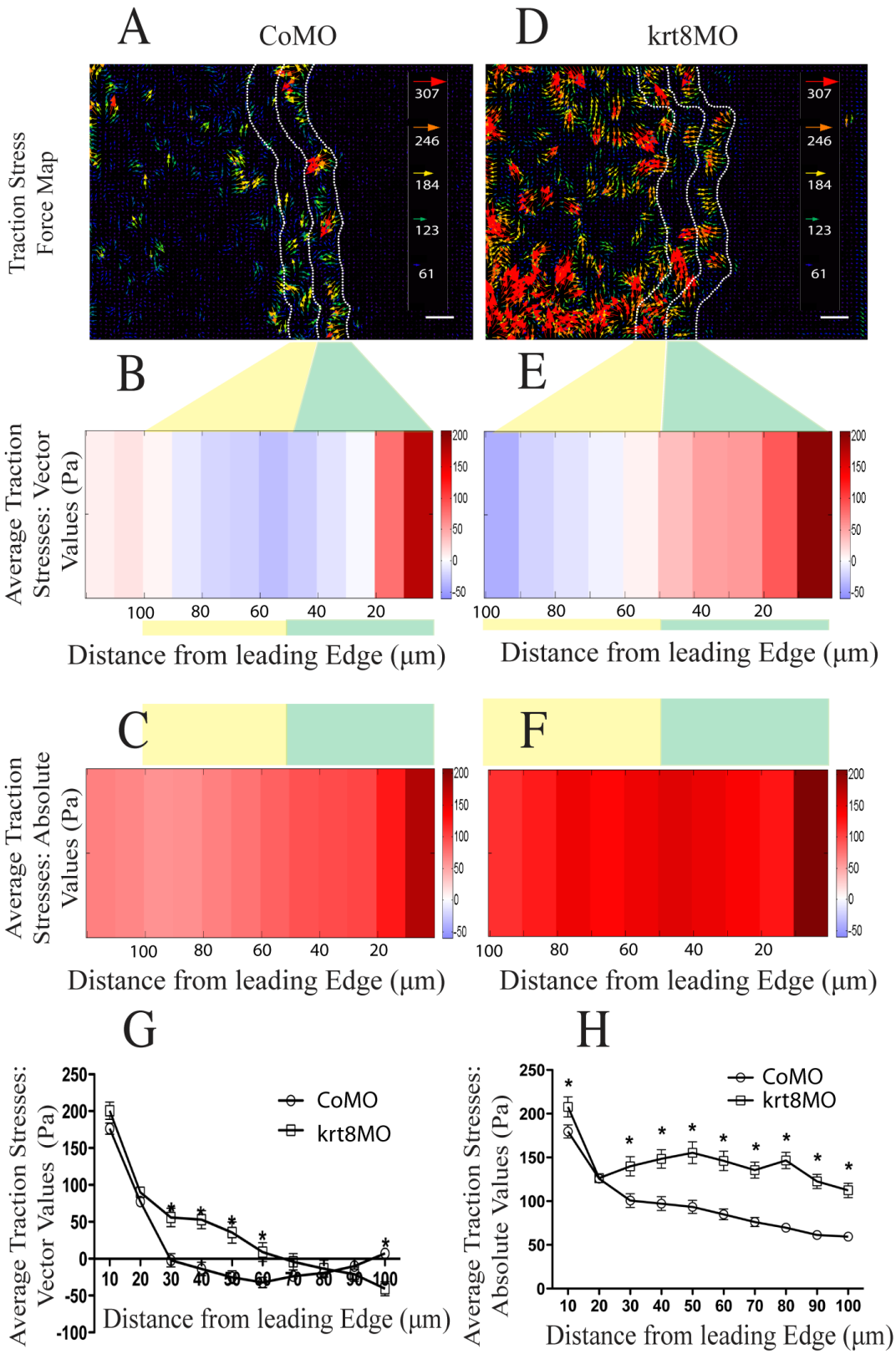
A
CoMO
D
krt8MO
Traction Stress Force Map
307
246
184
123
61
B
E
Average Traction Stresses: Vector Values (Pa)
200
150
100
50
0
-50
100 80 60 40 20
Distance from leading Edge (μm)
C
F
Average Traction Stresses: Absolute Values (Pa)
G
H
CoMO
krt8MO
Average Traction Stresses: Vector Values (Pa)
250
200
150
100
50
0
-50
-100
10 20 30 40 50 60 70 80 90 100
Distance from leading Edge (μm)
Average Traction Stresses: Absolute Values (Pa)

Figure 2.4: Traction stresses concentrated at the leading edge of a donut explant gradually increase as the donut closes.

(A) Representative traction stress maps of a control donut explant at four stages of closure. Arrows in the heat map indicate directions of force and are scaled and pseudocolored to indicate force magnitude. White lines on the maps correspond to the leading edge of the donut and show the progression of donut closure over time. Numbers on each panel indicate the equivalent radii of open area in center of the donut. Equivalent radii were derived from the area of the open center (Area = Πr2). 'd' and 'v' indicate the dorsal and ventral sides of the donut respectively. Scale bar = 25μm. (B) Kymographs of average traction stress generated by mesendoderm cells during donut closure. The donut explant was divided into 10μm wide concentric contours from the leading edge and mean traction stresses within each 10μm region were calculated. The X-axis of the kymograph represents the distance from the donut center and the Y-axis represents equivalent radii of the donut explant. (C) Cartoon showing resolution of traction stresses in a donut and DMZ explant. For a donut explant, traction stresses perpendicular to the leading edge and opposite to the direction of migration were considered positive radial traction stresses. For a DMZ explant, traction stresses opposite to the direction of migration (left to right) were considered positive radial traction stresses. These data were generated by Chong Wang and Bette Dzamba.

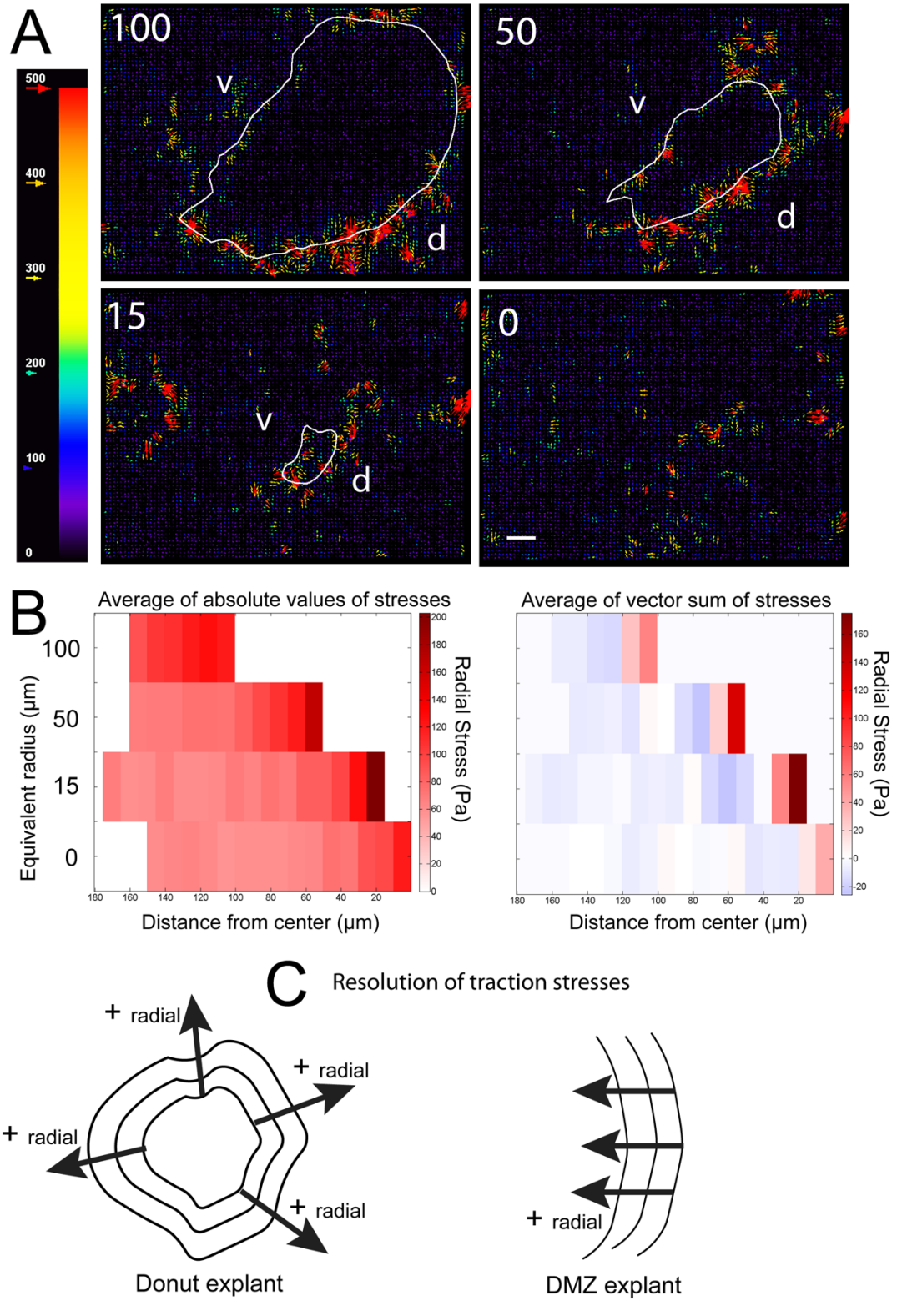
A
500
400
300
200
100
0
100
v
d
50
v
d
15
v
d
0
B
Average of absolute values of stresses
Equivalent radius (μm)
100
50
15
0
Distance from center (μm)
Radial Stress (Pa)
Average of vector sum of stresses
Distance from center (μm)
Radial Stress (Pa)
C
Resolution of traction stresses
+ radial
+ radial
+ radial
+ radial
Donut explant
+ radial
DMZ explant

Figure 2.5: Migration rates of mesendoderm tissue from control and krt8 morphant embryos.

Positive values denote forward migration and negative values indicate leading edge retractions during the course of migration. Average rate of forward migration for Control Mo: 44.67±5.077μm/hr and Xck Mo: 19.73±7.561μm/hr, * $p<0.05$. Velocities were calculated from two time points from three separate control and krt8 morphant explants. This data was generated by Chong Wang.

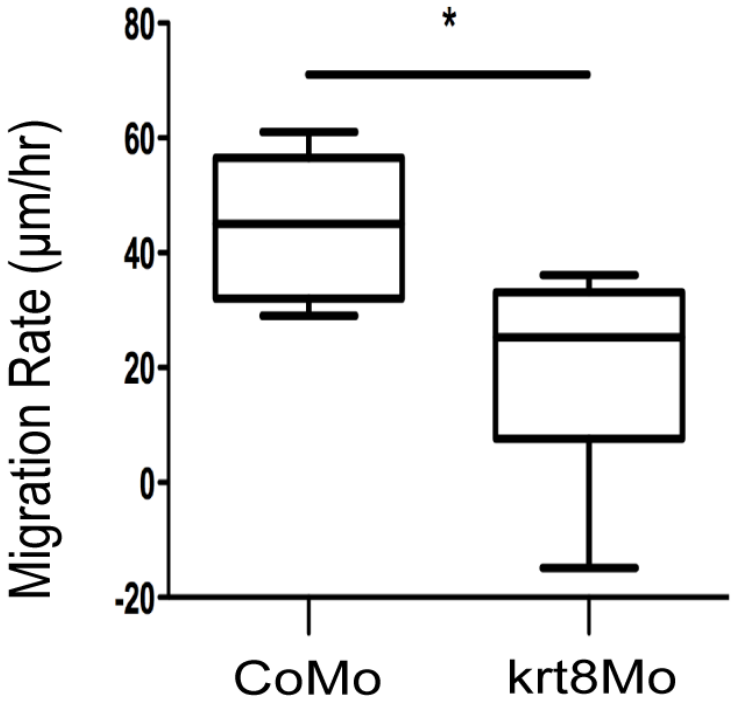
*
80
60
40
20
0
-20
Migration Rate (µm/hr)
CoMo
krt8Mo

Figure 2.6: Mesendoderm cells organize into leader and follower cells with distinct protrusive morphologies.

(A-F) Representative TIRF images of (A-C) leading edge and (D-F) following row cells. (A and D) Integrin α5-EGFP, (B and E) mCherry-LifeAct, (C and F) merged images. (G) Quantification of filopodial lengths in leading edge and following row cells. Lengths were calculated from nine TIRF movies. Data: mean ± SEM, ***, $p<0.001$, expressed as dot plots. (H) Scanning electron micrograph of *Xenopus* mesendoderm, blastocoel roof-facing side; leading edge (le), following row (fr). Boxes in (H), lamellipodia of leading edge (I), specialized filopodia in following row (J). (K) Graph shows number of times a protrusion of a cell changes direction over the course of 5 mins. TIRF images of cells expression mem-EGFP were used to track individual protrusion. Data: mean ± SEM, *** $p<0.001$ (6-9 individual explants imaged from 2-3 separate experiments). (L-O) FRET microscopy of Rac1 activity in leading edge (L and M) and following row (N and O) cells on FN. Confocal images taken one hour following plating of explants on FN. (L and M) Turquoise-Rac1 (L), Rac1-PBD FRET efficiency (M) in leading edge cells. (N and O) Turquoise-Rac1 (N), Rac1-PBD FRET efficiency (O) in following row cells (15 individual explants imaged explants from 5 separate experiments). (P) Graph showing distribution of FRET efficiency within individual cells. Data: mean ± SEM (Numbers of cells analyzed: Leading edge = 77 cells and Following row = 37 cells). Scale bar = 25μm (C, F, H, L and N) or 10μm (I and J). EM images were provided by Bette Dzamba.

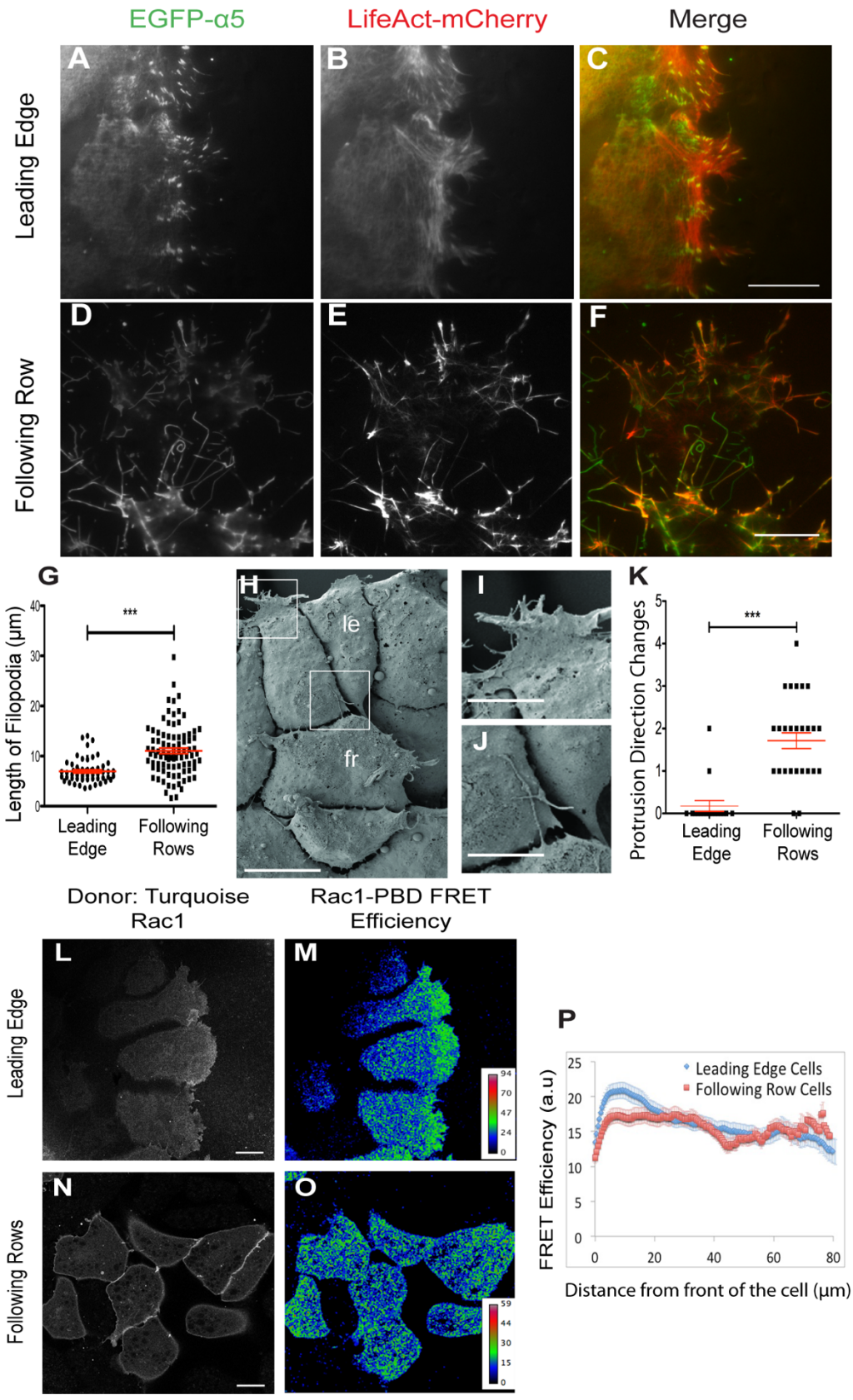
EGFP-α5
LifeAct-mCherry
Merge
Leading Edge
Following Row
A
B
C
D
E
F
G
Length of Filopodia (μm)
***
Leading Edge
Following Rows
H
le
fr
I
J
K
Protrusion Direction Changes
***
Leading Edge
Following Rows
Donor: Turquoise Rac1
Rac1-PBD FRET Efficiency
L
M
N
O
Leading Edge
Following Rows
P
FRET Efficiency (a.u)
Leading Edge Cells
Following Row Cells
Distance from front of the cell (μm)

Figure 2.7: Following row cells can reorganize to form leading edge cells.

(A) Mesendoderm explant expressing EGFP-paxillin (Green) and LifeAct-mCherry (Red) was plated on FN and imaged after one hour using TIRF microscopy. The leading edges of the explants were excised with an eyebrow knife and the explant was allowed to heal for one hour. (B) Following healing, explants were further imaged (4 individual explants imaged from 2 separate experiments). Scale bar = 25um (A and B).

Original Leading Edge

Newly Formed Leading Edge

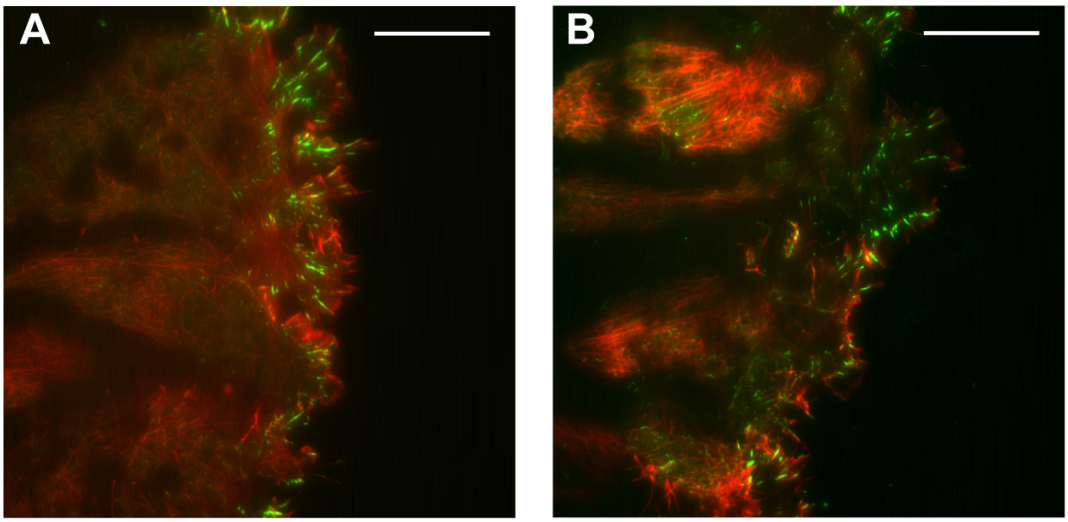

Figure 2.8: Focal adhesion dynamics and actin cytoskeleton are altered in krt8 morphant explants.

(A, C, E and G) Representative TIRF images of mesendoderm explants expressing LifeAct-mCherry (Red) and EGFP-Paxillin (Green). Boxes (A, C, E and G) indicate magnified areas in panels (B-B", D-D", F-F" and H-H"), corresponding to merged (B, D, F and H) and separate LifeAct-mCherry (B', D', F' and K') and EGFP-Paxillin (B'', D'', F'' and K'') channels. Quantification of FA area (I), FAs per cell (J) and percent distribution of FAs within cells (K) were calculated from the first frames of nine movies for each condition (Movies 3-6) (9 individual explants per condition imaged from 3 separate experiments). Data: mean ± SEM *, $p<0.05$; **, $p<0.01$; ***, $p<0.001$; ns, not significant. Scale bar = 25um (A, C, E and G) or 10um (B, D, F and H).

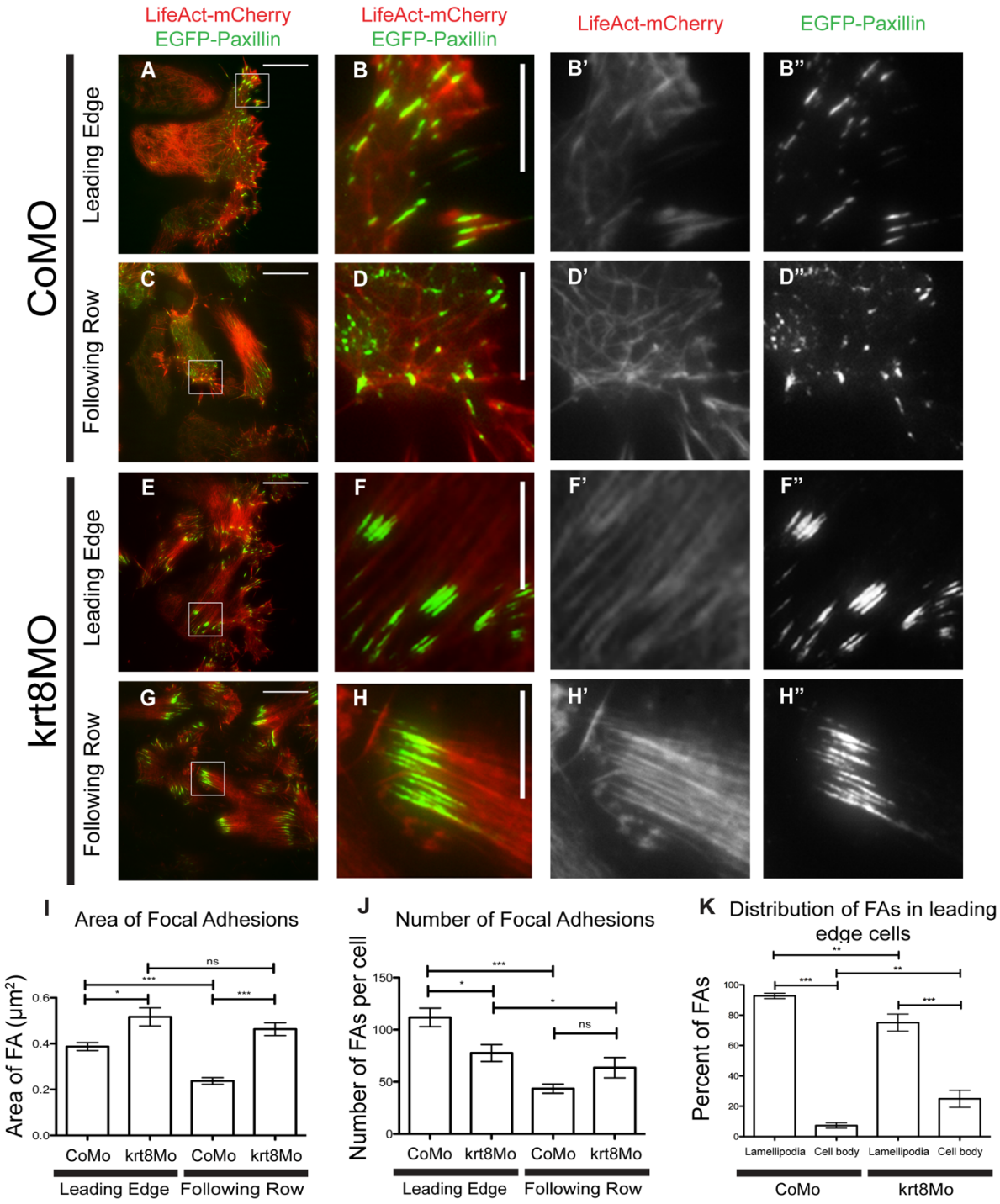
LifeAct-mCherry
EGFP-Paxillin
LifeAct-mCherry
EGFP-Paxillin
LifeAct-mCherry
EGFP-Paxillin
CoMO
krt8MO
Leading Edge
Following Row
A
B
B'
B''
C
D
D'
D''
E
F
F'
F''
G
H
H'
H''
I
Area of Focal Adhesions
Area of FA (μm²)
0.6
0.4
0.2
0.0
ns
***
*
***
CoMo
krt8Mo
CoMo
krt8Mo
Leading Edge
Following Row
J
Number of Focal Adhesions
Number of FAs per cell
150
100
50
0
***
*
*
ns
CoMo
krt8Mo
CoMo
krt8Mo
Leading Edge
Following Row
K
Distribution of FAs in leading edge cells
Percent of FAs
100
80
60
40
20
0
**
***
**
***
Lamellipodia
Cell body
Lamellipodia
Cell body
CoMo
krt8Mo

Figure 2.9: Actin stress fibers predominate in mesendoderm explants from keratin morphant embryos.

(A-H) Confocal projections, phalloidin-stained (A-D) control and (E-F) krt8 morphant explants on FN. Pseudocolors correspond to fluorescence intensity heat map. Collapsed Z-stack images of representative (A and E) explants at low magnification, (B and F) leading row lamellipodia, (C and G) following row protrusions, and (D and H) cell-cell junctions. Arrowheads in (A and C) indicate specialized filopodia, arrows in (A and C) indicate small protrusions. Dotted lines in (D and H), borders between two cells (6 individual explants per condition imaged from 2 separate experiments). Scale bars = 25um (A, B, E and F) or 10um (C, D, G and H).

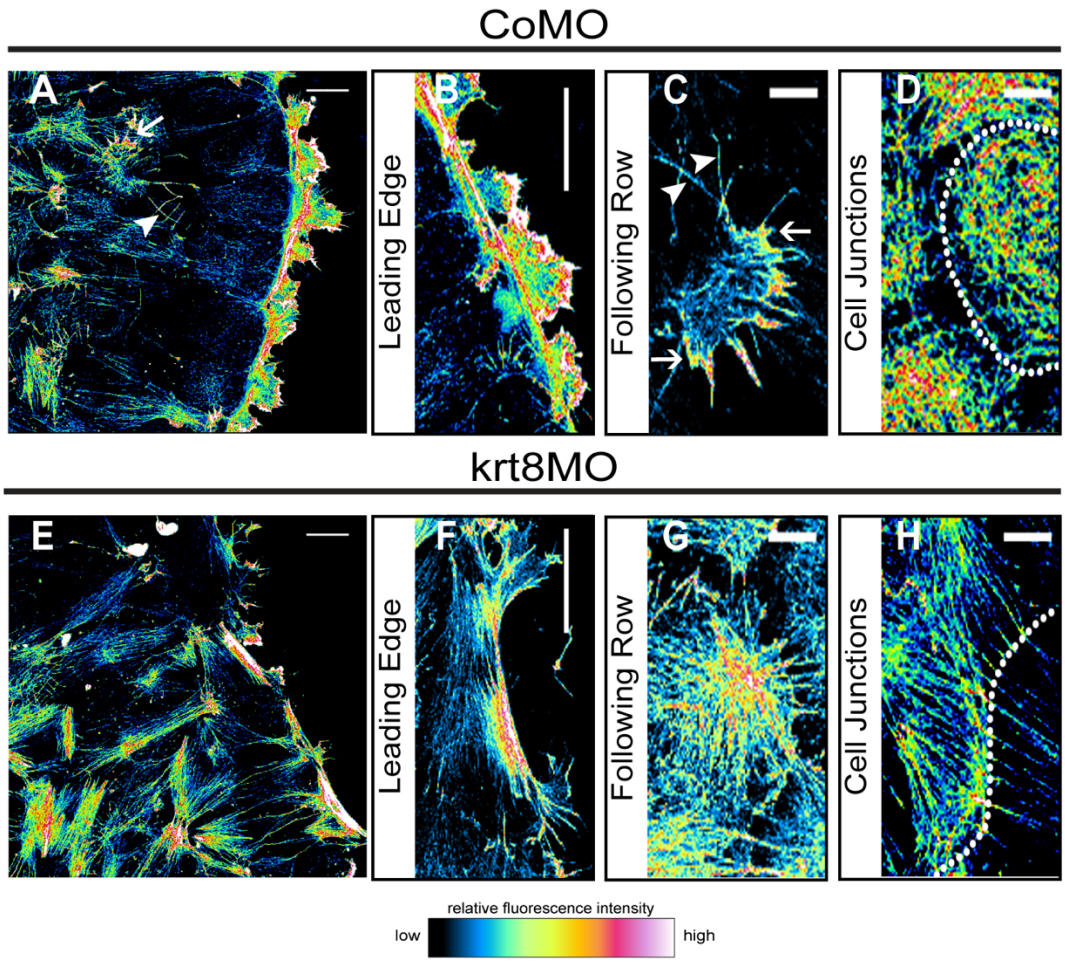
CoMO
A
B
Leading Edge
C
Following Row
D
Cell Junctions
krt8MO
E
F
Leading Edge
G
Following Row
H
Cell Junctions
relative fluorescence intensity
low
high

Figure 2.10: Acrylamide treatment of mesendoderm explants leads to rearrangement of actin cytoskeleton.

(A-C) Confocal projections of fixed and phalloidin stained mesendoderm explants on FN substrates after treatment with acrylamide at the concentrations indicated (B and C). Pseudocolors correspond to the fluorescence intensity heat map (9 individual explants per condition imaged from 3 separate experiments). Scale bar = 25um (A-C).

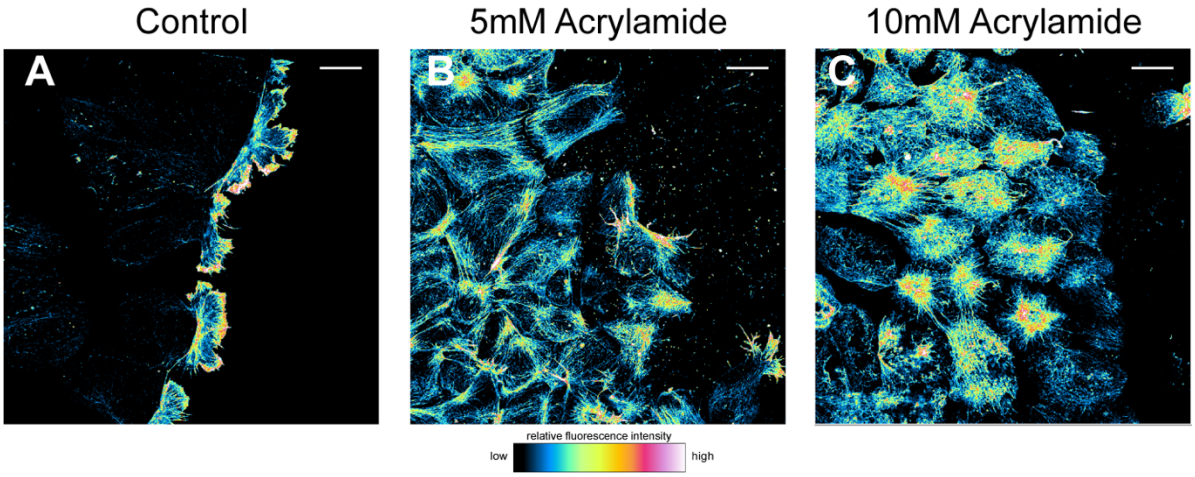
Control
5mM Acrylamide
10mM Acrylamide
A
B
C
relative fluorescence intensity
low
high

Figure 2.11: Myosin light chain II phosphorylation is upregulated in keratin morphant mesendoderm.

(A and C) Representative Western blots of phosphomyosin II levels from control and krt8 morphant dissociated mesendoderm cells. Silicone stretchers coated with either (A) FN or (C) C-Cad. Following one hour attachment, cells were subjected to 15 rounds of 10% cyclical stretch. Cell lysates were made immediately following stretch. Blots were probed with antibodies against phosphorylated myosin II-light chain (S19) and actin (N = 5 for FN and N=4 for C-Cad). (B and D) Quantification of pMLC levels normalized to actin. Data: mean±SEM. *, $p< 0.05$; **, $p<0.01$; ns, not significant. (E-H) Confocal projections of phalloidin-stained explants on FN after one hour treatment with Y27632 (10μM) or DMSO. Pseudocolors correspond to the fluorescence intensity heat map. Control explant treated with (E) DMSO or (F) 10μM Y27632. krt8 morphant explant treated with (G) DMSO or (H) 10μM Y27632 (9 individual explants per condition imaged from 3 separate experiments). Scale bar = 25um (E-H).

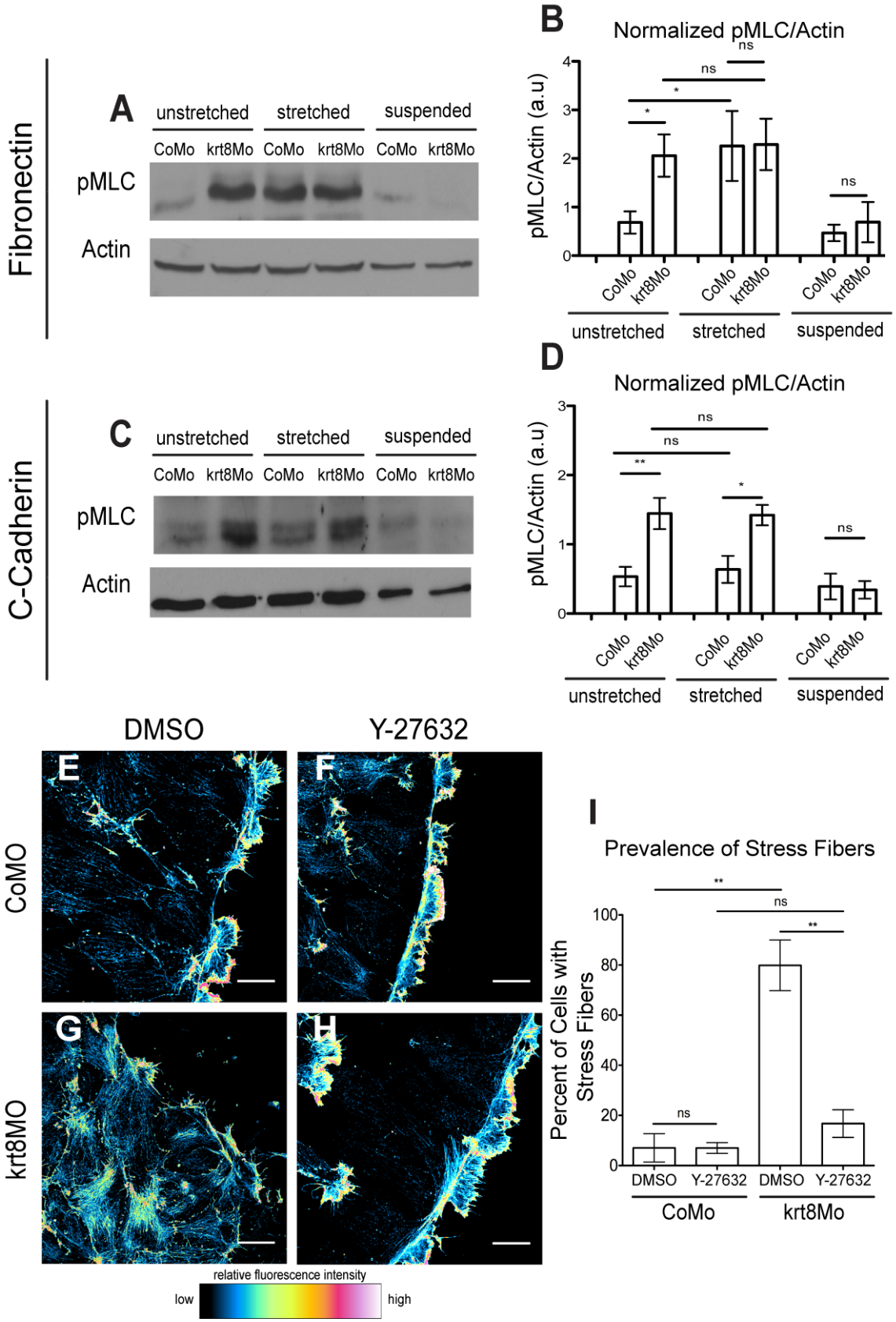
Fibronectin
A
unstretched
stretched
suspended
CoMo
krt8Mo
pMLC
Actin
B
Normalized pMLC/Actin
pMLC/Actin (a.u)
ns
*
unstretched
stretched
suspended
C-Cadherin
C
D
Normalized pMLC/Actin
**
DMSO
Y-27632
CoMO
krt8MO
E
F
G
H
relative fluorescence intensity
low
high
I
Prevalence of Stress Fibers
Percent of Cells with Stress Fibers

Figure 2.12: Mesendoderm cell morphology on FN and C-cad-FC substrates.

(A-B) Representative images of dissociated mesendoderm cells plated on plastic dishes coated with (A) 10μg/ml FN and (B) 5μg/ml C-Cad- FC. After 1 hour, many of these cells have made contact and form small clusters. The morphology of these cells is similar to that observed on stretchable silicon substrates (e.g., Figure 5A-D) but images of cells on coated plastic substrates are shown here because of the better optical quality. Arrows indicate protrusions. Scale bar = 50um (A and B). These images were provided by Bette Dzamba.

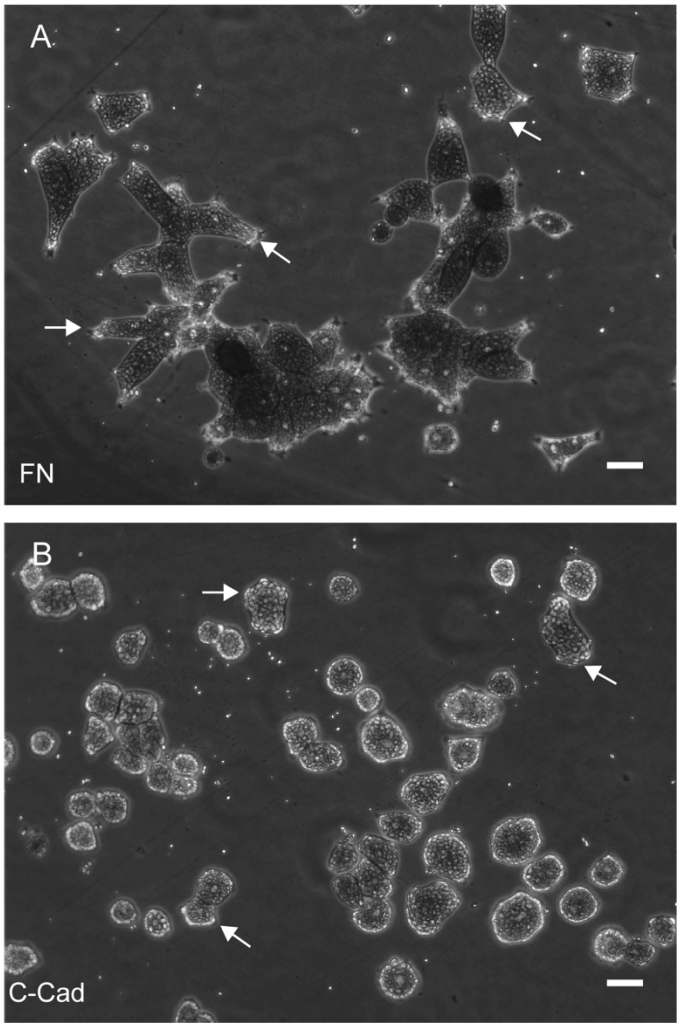
A
FN
B
C-Cad

Figure 2.13. Mutual antagonism of Rac1 GTPase activity and Keratin IFs in leading edge mesendoderm.

(A-D) FRET analysis of Rac1 activation in control and keratin morphant mesendoderm. Confocal FRET imaging one hour after plating DMZ explants on FN. (A and B) control and (C and D) keratin morphant explants showing distribution of (A and C) donor Turquoise-Rac1 and (B and D) Rac1-PBD FRET efficiency (9 individual explants per condition imaged across 4 separate experiments). (E) Graph showing distribution of FRET efficiency within leading edge cells in control and krt8 morphant explants. Data: Mean ± SEM (Total number of cells analyzed: CoMo = 24; krt8Mo = 29). (F-H) Confocal images of photoactivation of Rac1 in dissociated mesendoderm cells expressing mCherry-PA-Rac1Q61L (Red) and EGFP-krt8 (Green) or (I-K) nonphotoactivatable mCherry-PA-Rac1C450A (Red) and EGFP-krt8 (Green). Regions irradiated with a 456nm wavelength laser are indicated; box in (F-H) and circle in (I-K). Times following irradiation: t = 1 min (F, I), t = 2 mins. (G, J), t = 3 min (H and K). (M) Graph comparing intensity of EGFP-krt8 after activation of photoinducible Rac1 constracts (Number of cells analyzed: 3 per condition; mean ± SEM *, $p<0.05$; **, $p<0.01$) Scale bars = 25 um (A, C and F-K). Photoactivation data was generated in collaboration with Gregory Weber.

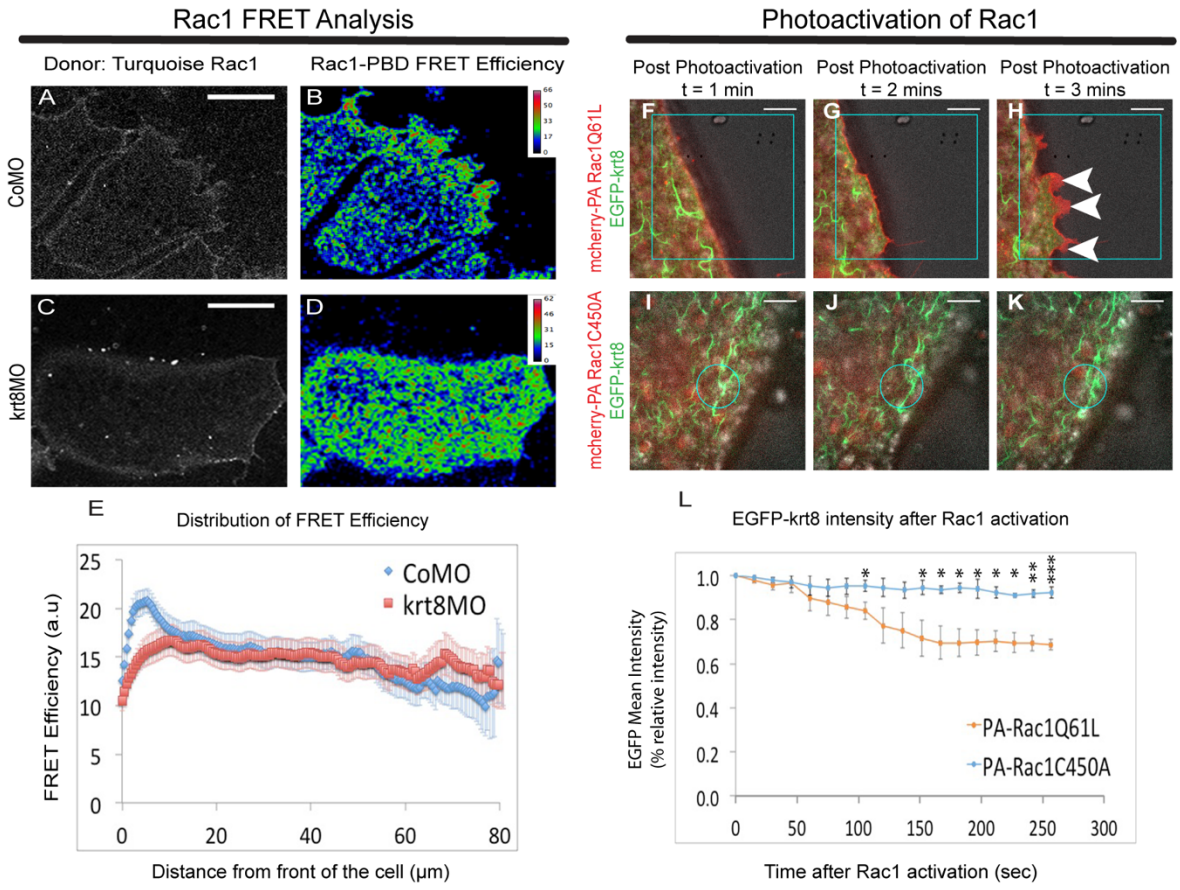
Rac1 FRET Analysis
Donor: Turquoise Rac1
Rac1-PBD FRET Efficiency
A
B
C
D
CoMO
krt8MO
Photoactivation of Rac1
Post Photoactivation t = 1 min
Post Photoactivation t = 2 mins
Post Photoactivation t = 3 mins
F
G
H
I
J
K
mcherry-PA Rac1Q61L
EGFP-krt8
mcherry-PA Rac1C450A
EGFP-krt8
E
Distribution of FRET Efficiency
CoMO
krt8MO
FRET Efficiency (a.u)
Distance from front of the cell (μm)
L
EGFP-krt8 intensity after Rac1 activation
EGFP Mean Intensity (% relative intensity)
PA-Rac1Q61L
PA-Rac1C450A
Time after Rac1 activation (sec)

Figure 2.13: Cartoon summary of mesendoderm morphogenesis in a mid-gastrula stage *Xenopus* embryo.

(Center) Cut-away profile view of the boxed region from bisected embryo (Upper Left) showing the anterior progression of the mesendoderm and its spatial relationship to the bcr, fibrillar FN matrix, and the trailing mesoderm and endoderm. (Lower Left Box) Higher magnification view highlighting the leading edge mesendoderm cell with large forward protrusion "pulling" on the overlying blastocoel roof. The FN matrix is remodeled as the leading-edge passes over it. The rear of the leading-edge cell is attached to follower row cells via a cadherin containing adhesion complex that includes basket-like arrangement of keratin filaments. Arrows indicate the balancing of forward traction stresses with intercellular stresses at the rear. Follower cells extend long specialized-filopodia (cytonemes) into the cleft of Brachet, which is widened at this location by the failure of following row cells to adhere to the bcr. (Lower Right Box) *En face* view of mesendoderm highlighting the relationship of leading-edge cells with their broad lamellipodia in contact with the bcr, to circumferentially arranged upper row cells with their stress fiber-like organization of actin filaments (see also Figure 2.15). Upper row cells likely contribute to closure of the mesendoderm mantle by applying tangential stresses (black arrows) perpendicular to the radial stresses of the underlying leading row cells. Rac1 activity gradient (green shading) in leading-edge cells is highest in the protrusions.

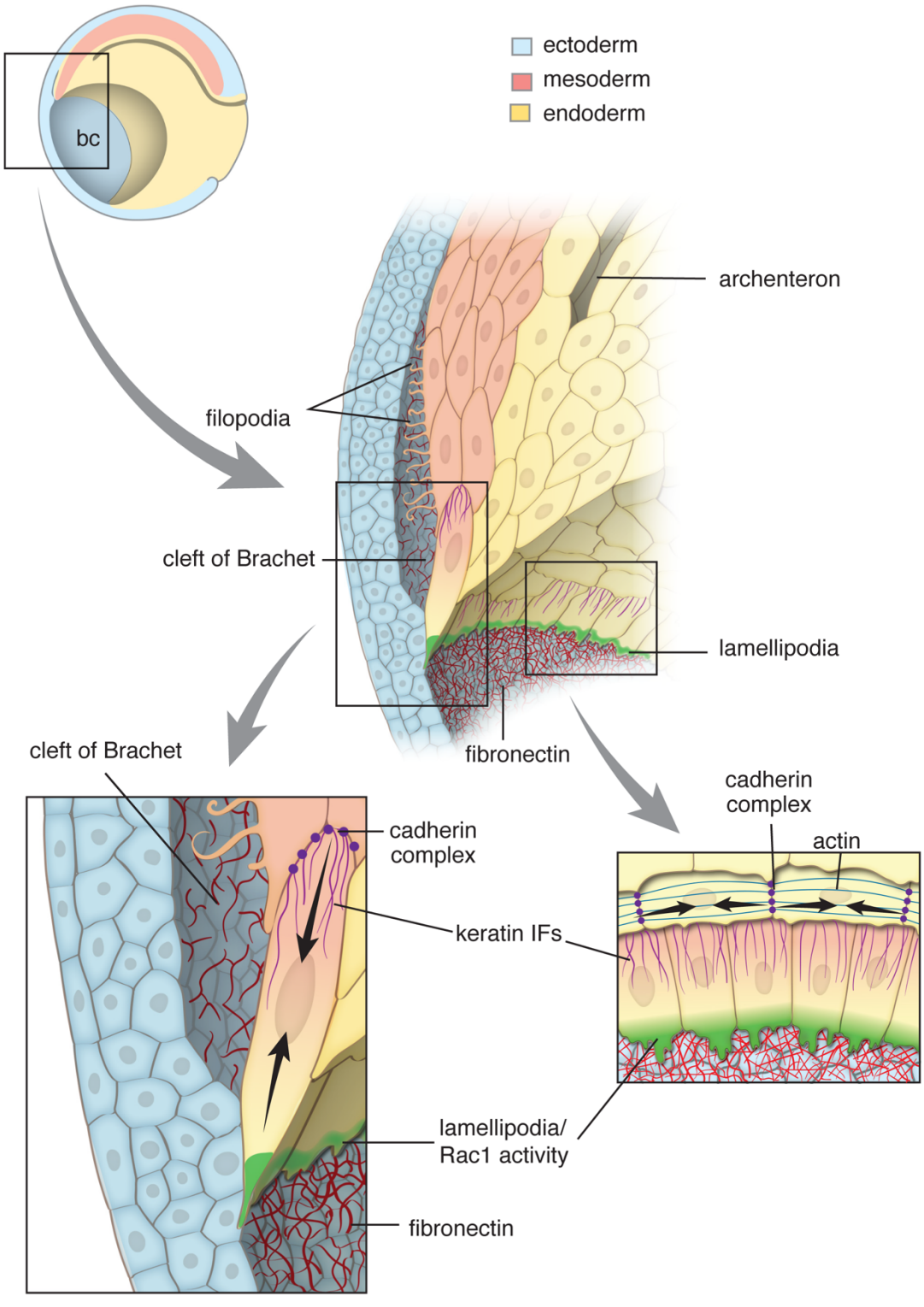
ectoderm
mesoderm
endoderm
bc
archenteron
filopodia
cleft of Brachet
lamellipodia
fibronectin
cleft of Brachet
cadherin complex
keratin IFs
lamellipodia/ Rac1 activity
fibronectin
cadherin complex
actin

Figure 2.15: Organization of mesendoderm in intact embryos.

(A) Cartoon of the organization of mesendoderm cell rows during gastrulation. Perspective of panels B and C are indicated by the eye. The leading row (lr) and following row (fr) cells are in contact with the BCR and fibronectin matrix whereas the upper following rows (UFR) of cells are only in contact with one another. Cells are numbered with respect to their position away from the free edge. (e.g. fr1, ufr2). (B) Scanning electron micrograph of mesendoderm and blastocoel roof tissue excised from a fixed stage 12 embryo. Upper following row cells (yellow) extend protrusions onto the leading row (orange) cells beneath. Scale bar = 10μm. (C) Projection of confocal z-sections of stage 12 mesendoderm and blastocoel roof tissue immunostained with antibodies to FN (green) and beta-catenin (magenta). Actin (white) was visualized using phalloidin. Green arrows indicate circumferential forces. UFR, upper following row; lr, leading row; bcr, blastocoel roof. Scale bar = 20 μm. This data was provided by Bette Dzamba

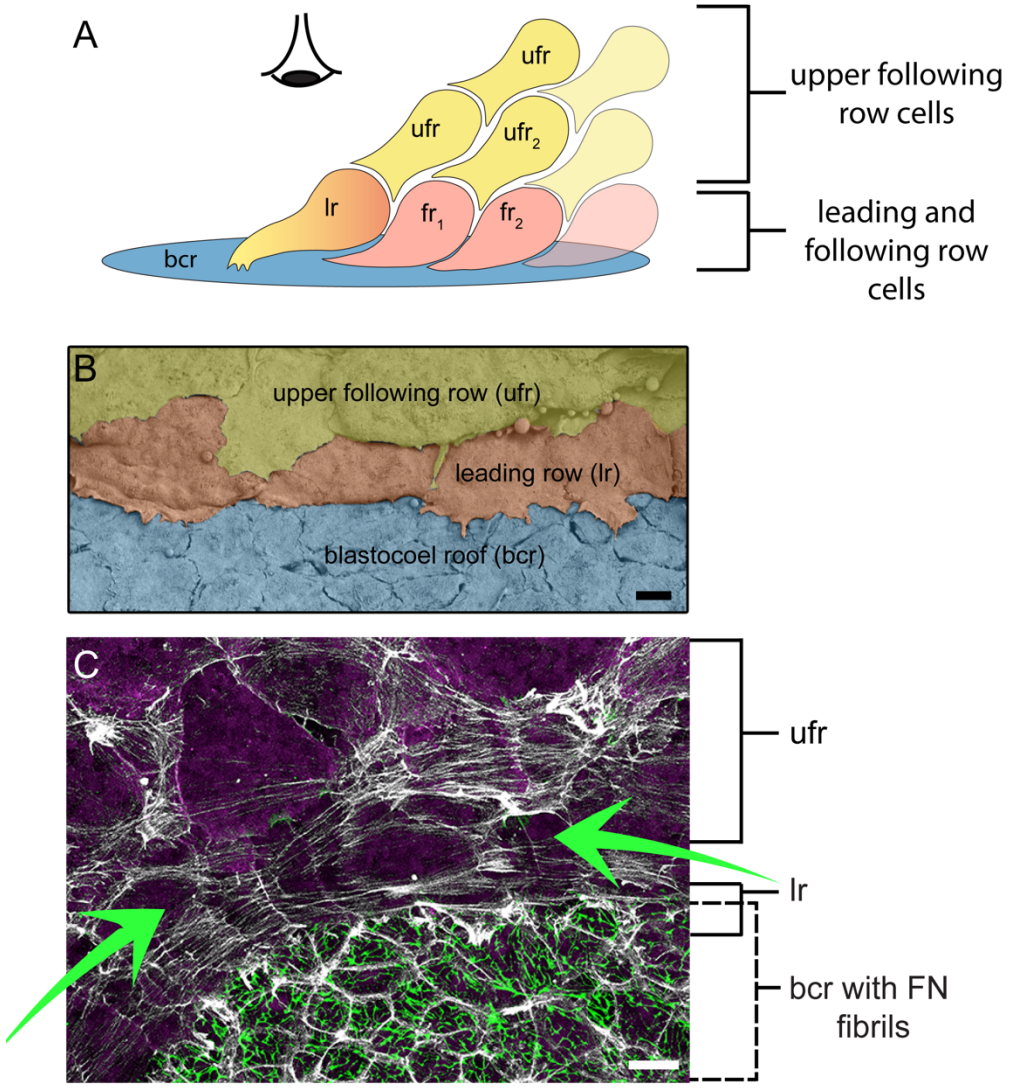
A
ufr
ufr
ufr2
lr
fr1
fr2
bcr
upper following row cells
leading and following row cells
B
upper following row (ufr)
leading row (lr)
blastocoel roof (bcr)
C
ufr
lr
bcr with FN fibrils

Chapter 3

A novel interaction between plakoglobin and integrins in collective migration of mesendoderm tissue.

This chapter is composed of unpublished data.

3.1 Introduction

Plakoglobin, a member of the catenin family, plays important roles in signaling and the formation and maintenance of cellular adhesions. Similar to its homolog β-catenin, PG contains 13 sequential armadillo repeats that mediates interaction with classical cadherins at adherens junctions (AJ). β-catenin and PG that are not bound to cadherins are subjected to degradation by axin and the adenomatous polyposis coli destruction complex (Stamos and Weis, 2013). Additionally, PG is also found at desmosomal junctions where it links the cytoplasmic tail of the desmosomal cadherins to desmoplakin (DP) which in turn associates with IFs. Loss of PG causes a reduction in adhesion strength as well as loss of mechanical integrity of tissues. These effects are underscored by defects in heart function and blistering of skin (Bierkamp et al., 1996; Li et al., 2012).

Signaling roles of PG and other catenins

β-catenin is well known to regulate the formation of the dorsoventral axis during early embryonic development in *Xenopus* embryos (Fagotto et al., 1996; Fagotto et al., 1997; Guger and Gumbiner, 1995; Heasman et al., 2000; Wylie et al., 1996). It functions as a component of the canonical Wnt signaling cascade. Signals from Wnt ligand prevent the destruction of β-catenin and causes its transport to the nucleus where it binds to transcription factors such as T cell factor and Lymphocyte enhancer factor and regulates expression of proteins essential for axis specification (Guger and Gumbiner, 1995). Overexpression of β-catenin on the ventral side of the embryo causes duplication of axis. Similarly, PG can be targeted to the nucleus where it can bind and activate transcription. Overexpression of PG on the ventral side of the embryos causes axis duplication

(Karnovsky and Klymkowsky, 1995). These data hint to a possible redundancy in function of PG and β-catenin during axis specification in *Xenopus* embryos.

PG function in cell migration

Collective cell migration plays a critical role during embryonic development and requires maintenance of cell-cell contacts (Collins and Nelson, 2015). In addition to providing mechanical stability to the migrating tissue, the cellular contacts and especially their adhesion molecules like cadherins and catenins serve as signaling centers. Communication and coordination of cell-cell and cell-ECM adhesions is important for collective migration. Traction forces exerted by integrin-based cell-ECM junctions are balanced by tension across cadherin-based cell-cell junctions (Maruthamuthu et al., 2011; Trepat et al., 2009). Loss of cadherin adhesions disrupts collective migration by changing the distribution and directionality of traction forces and altering cell polarity (Mertz et al., 2013; Chapter 2). PG is a key component at cellular junctions, but its role in regulating the interaction between cell-cell and cell-ECM adhesions has not be explored in detail. Because my studies have shown that interference with cellular adhesion disrupts collective migration, it seems likely that PG may play a role in maintaining crosstalk between cadherin and integrin-based cellular adhesions.

In other contexts, PG is known to play an important role in cell motility (Todorović et al., 2010; Yin et al., 2005). In keratinocytes, PG suppresses cell migration by increasing cell-cell adhesion strength in a Ca^{2+} dependent manner (Yin et al., 2005). Keratinocytes lacking PG show increased RhoA and Rac1 activity and have higher numbers of lamellipodial protrusions (Todorović et al., 2010). Moreover, PG null keratinocytes also

display increased Src and FAK activities. All of these features support a role of PG in maintaining the balance of cell-cell and cell-ECM adhesion. Furthermore, PG can also regulate migration by stabilizing FN mRNA and subsequent expression and deposition of FN in these keratinocytes (Todorović et al., 2010). Formation of lamellipodial protrusions, activation of Rho GTPases and deposition of FN converge to integrin signaling. Thus, these results suggest that PG may play a more direct role in regulating integrin-based cell-ECM adhesions in addition to its role in regulating the interaction between cadherin-based cell-cell adhesions and integrin-based cell-ECM adhesions.

Desmosomal-like junctions: Junction dependent role of PG in migration.

PG can bind to both classical and desmosomal cadherins with similar affinity (Choi et al., 2009; Gumbiner and McCrea, 1993; Zhurinsky et al., 2000). At desmosomes, PG binds to desmosomal cadherins and recruits IFs to these junctions. However, PG doesn't directly interact with IFs; instead, PG interacts with IF-linker proteins like plakophilin and DP. DPs directly interact with IFs and localize IFs to the desmosomes. (Kowalczyk et al., 1997; Kowalczyk et al., 1999). As described in chapter 1, desmosomal junctions enable tissues to resist intrinsic and extrinsic mechanical forces and disruption of these adhesions results in loss of mechanical integrity of the tissue (Leckband and de Rooij, 2014).

Although IFs primarily localize to desmosomal cadherins, there are instances where IFs associate with classical cadherins through interaction with PG to form "desmosomal-like junctions" (Kowalczyk et al., 1998; Leonard et al., 2008; Weber et al., 2012). For example, in vascular endothelial cells, VE-cadherins interact with PG to recruit DP and

vimentin IFs (Kowalczyk et al., 1998). During lens development in chicken embryos, epithelial cells at the lens equator differentiate to form migratory fiber cells. These migratory fibers cells exhibit desmosomal-like junctions and recruit vimentin IFs to N-cadherin-containing junctions with the help of PG, plakophilin and DP (Leonard et al., 2008).

In *Xenopus,* mesendoderm cells migrate collectively by forming C-cadherin adhesions with neighboring cells and integrin α5β1 adhesions with the underlying FN matrix. Anisotropic tension on C-cadherin is generated during migration, which is balanced by the traction forces exerted by the integrin adhesions (Davidson et al. 2002; Weber et al., 2012; Chapter 2). PG is recruited to the C-cadherins in a tension-dependent manner to form desmosomal-like junctions. This recruitment is necessary for assembly of the keratin-cadherin mechanosensitive complex. Loss of PG leads to mislocalization of keratin IFs and reduction in their binding to C-cad. These cells also form misdirected protrusions. Importantly, since integrin adhesions are necessary for the formation of lamellipodial protrusions, their misdirection in the absence of PG suggests that PG regulates integrin signaling. Thus, I hypothesize that during mesendoderm migration that PG is a key regulator of force balance between integrin and cadherin adhesions.

Does PG associate with IFs at integrin adhesions?

As mentioned above, PG may play a more direct role in regulating integrin-based cell-ECM adhesions in addition to its prospective role in balancing forces between integrin and cadherin adhesions. Integrins typically link ECM with the actin cytoskeleton (See Chapter 1). However, not all integrins bind to actin; α6β4, which binds to the basal lamina,

associates with IFs to form hemidesmosomes. In general, plectins are the key cytoskeletal linkers that recruit IFs to hemidesmosomal junctions (Borradori and Sonnenberg, 1999). While PG binding to IFs at desmosomes is clearly established, the possibility that PG may directly regulate integrin-based cell-ECM adhesions raises the question of whether PG and IFs also interact at hemidesmosomes? Although initial studies of hemidesmosomes showed that PG is absent from these junctions (Cowin et al., 1986), it could be the case that the prospective role of PG might be cell-type or integrin-specific. Thus, further investigation seems warranted. In our experimental system, photoactivation of dominant negative Rac1 (dnRac1) in mesendoderm cells shows that keratin IFs are anchored to the FN matrix as the cells repolarize (Figure A.4). This hints to a possibility that keratin IFs are linked to FN matrix via integrin adhesions to form hemidesmosomes. Since keratin IFs form a complex with PG at cadherin adhesions, I hypothesize that keratin IFs and PG also form a complex at integrin.

PG in morphogenesis

During gastrulation, assembly of FN matrix by BCR cells requires tension on C-cadherin. Overexpression of cadherin in BCR cells results in precocious FN assembly (Dzamba et al., 2009). Interestingly, overexpression of PG also results in precocious FN assembly and loss of PG causes inhibition of FN fibrillogenesis. However, unlike what was observed in keratinocytes (Todorović et al., 2010), PG does not regulate FN secretion through changes in mRNA stability or transcription in *Xenopus* gastrulae (Hirsh et al., in preparation). Additionally, although surface levels of integrins and cadherins are unaltered in PG morphant embryos, there is a decrease in the adhesion strength of integrin and

cadherin-based adhesion measured using AFM (Hirsh et al., in preparation). Integrin and cadherin adhesions maintain tissue integrity and transduction of mechanical signals during embryonic development. Because adhesion strength is reduced in PG morphants, PG could be playing an active role in mechanotransduction during embryonic development. Additionally, these observations indicate that PG might play an important role in facilitating mechanical crosstalk between cadherins and integrin during mesendoderm migration.

The data reported in chapter 2 emphasize that balance of mechanical forces between integrin and cadherin adhesions is critically for the assembly of mesendoderm tissue. While there is evidence that demonstrates the role of PG in signaling during *Xenopus* development, it remains unclear, whether PG regulates mechanical crosstalk between integrins and cadherins during mesendoderm migration. In this section, I report changes in the organization of actin morphology and keratin IF at the cadherin adhesions in PG morphant mesendoderm explants. Thus, I confirm the role of PG as an adhesion molecule that is necessary for linking cytoskeletal networks to cellular adhesions. Notably, I report a novel interaction between integrins and PG to form hemidesmosomal-like junctions and also make the case that PG actively and directly regulates integrin-based FAs in mesendoderm migration.

3.2 Materials and methods

Xenopus embryos and explant preparation

Xenopus embryos were obtained using standard methods and staged according to (Nieuwkoop and Faber, 1994). Mesendoderm explants (DMZ) were prepared according to Davidson et al., 2002 with the modification that Stage 11 embryos were used. Glass coverslips required for explant imaging were washed with alkaline ethanol solution, flamed and then glued, using Norland optical adhesive 68, to openings drilled with a lathe into the bottom of 35 mm petri dishes. Coverslips were then coated with 300ul of 5.0µg/ml bovine plasma FN overnight at 4 °C. Coverslips were blocked with 5% bovine serum albumin (BSA), washed and dishes filled with 1X MBS. DMZ explants were plated on glass coverslips for one hour prior to imaging.

Morpholino oligodeoxynucleotides and knockdown efficiency

Antisense morpholino oligodeoxynucleotides (MO) to inhibit keratin (8) expression were purchased from GeneTools and injected into the animal pole of embryos immediately after fertilization at a concentration of 40ng/embryo. The antisense PG MO (5'-TTTCCACTACGTCTCCCAAATCCAT-3) was designed using *Xenopus* PG sequence NCBI accession number NM_001090582.1 (Weber et al., 2012). Control injections used the standard GeneTools Control MO (5_'-CCTCTTACCTCAGTTACAATTTATA-3'). To test MO knockdown efficiency, embryos injected with control and PG MO were lysed in modified RIPA buffer and separated on 8 or 10% SDS PAGE gels as described in Bjerke et al., (2014). PG antibody (BD Biosciences #610253 at 1:1000 dilution) and beta-actin antibody (Sigma, A3854 at 1:25,000 dilution) were used to analyze the relative expression of PG in control versus PG morphant embryos.

Dissociation of Mesendoderm Cells

Mesendoderm from stage 11 embryos was dissected and cells dissociated in 1X CMF MBS. Dissociated cells were then plated on glass coverslip coated with 10ug/ml of C-cad-Fc/FN or equivalent amounts of recombinant FN fragment (9.11/9.11a/HepII; Ramos and DeSimone, 1996) overnight and blocked with 5% BSA for 30 mins before cells were plated.

TIRF microscopy

TIRF Microscopy was done using an Olympus 1X70 inverted TIRF microscope with an Olympus 60X/1.45 TIRF objective. Time-lapse images were collected 15 seconds apart for 5 mins. The area of FAs was calculated by thresholding the image such that only FAs were saturated and the area of saturated pixels was counted**.** A Mann-Whitney test was used to determine statistical significance among FA areas.

RNA constructs

RNA encoding fluorescently tagged proteins were transcribed in vitro from linearized plasmids. Transcripts were injected into the dorsal marginal zone region of two blastomeres at the 2 or 4-cell stage with a final concentration of 250pg of RNA per embryo The following constructs were used in this study: pCS2+ LifeAct-mCherry (Pfister et al., 2016), pCS2+ EGFP-Paxillin (subcloned by cold fusion into pCS2+ using Xba1 and SnaB1 from a construct obtained from R Horwitz, University of Virginia), pCS2+ EGFP-krt8 and pCS2+ mCherry-krt8 (V. Allan, University of Manchester; Clarke and Allan, 2003) and pCS2+ myc-PG-EGFP.

Explant fixation and Actin Staining

DMZs were fixed in 0.25% Glutaraldehyde, 3.7% Formaldehyde and 0.1% Tween20 for 10 mins at room temperature one hour after dissection, stained with 488-ActiStain (Cytoskeleton) and imaged with a Nikon C1 confocal microscope.

3.3 Results

PG expression during embryonic development was knocked down using the antisense MO described in Weber et al., (2012). Knockdown efficiency was determined by western blot analysis and observing whole embryo phenotypes. Knockdown resulted in >60% reduction in endogenous levels of PG compared to control MO at gastrulation stages (Figure 3.1A). Tailbud PG morphant embryos had shorter axes compared to control embryos due to defects in CE (Figure 3.1B; Hirsh et al., in preparation).

PG alters FA dynamics in migrating mesendoderm cells.

Mesendoderm cells migrate collectively by organizing into leader and follower cells. The leader cells are primarily responsible for generating traction forces necessary for forward migration by forming FAs in the lamellipodial regions (Chapter 2). PG morphants form misdirected protrusions (Weber et al., 2012) and integrin adhesions are weaker (Hirsh et al., in preparation). Thus, I tested whether this difference in adhesion strength would be reflected in the dynamics of FAs and thus might contribute to the migration defects in the mesendoderm tissue in PG morphants. I visualized control and PG morphant mesendoderm

explants expressing EGFP-paxillin, a definitive marker of FAs (Turner, 2000), and LifeAct-mCherry (Riedl et al., 2008) using TIRF microscopy. Time-lapse movies of control mesendoderm explants show that leading edge cells form mature and persistent FAs (Figure 3.2A, B, B', B"). FAs in the leading-edge cells are restricted to the forward protrusions and few FAs are observed in the cell body (Figure 3.2A). A branched actin network colocalizes with FAs (Figure 3.2B, B', B") and the area of these FAs (Figure 3.2I, leading edge CoMO = 0.3738±0.016μm^2) is highest in the forward lamellipodial protrusions. In following rows, cells form fewer FAs that are smaller in area (Figure 3.2I, following row CoMO = 0.2368 ± 0.01μm^2). As described in chapter 2, these FAs are not restricted to protrusions and are highly dynamic in nature and form nascent contacts with the underlying matrix unlike what is seen in FAs in leading edge cells. (Figure 3.2C, D, D' and D"). Taken together, these data confirm that mesendoderm explants organize into leader and follower cells (Chapter 2).

PG morphant explants displayed similar organization of FAs as the control mesendoderm explants. Moreover, leader cells in PG morphant explants formed FAs in the lamellipodial protrusions with few observed in the cell body. However, the area of these FAs (Figure 3.2J, 0.2802 ± 0.01μm^2) was smaller than those in control leading edge cells. The FAs were enriched with actin filaments (Figure 3.2E, F, F' F" and Fig 3.3). Following row cells in PG morphants formed FAs that were more dynamic and smaller in area (Figure 3.2I 0.2238 ± 0.01μm^2) compared to the PG-deficient leading row cells (Figure 3.2G, H, H', H"). Thus, there is a difference in FA dynamics in the control and PG morphants. This suggests that PG actively governs focal adhesion dynamics and thus the rate of migration of mesendoderm explants.

A disrupted actin network is observed in PG morphant mesendoderm explants.

PG is reported to localize at AJ as well as at desmosomal junctions (Nelson, 2008). I next asked whether loss of PG affects actin organization in collectively migrating mesendoderm cells. Fixed mesendoderm explants stained with phalloidin were examined using a confocal microscope. In leading edge cells, a dense network of actin is present in the broad lamellipodial protrusion of the cells, whereas a cortical actin network is observed in the cell body (Figure 3.3A). In the following rows, cells form smaller protrusions and cortical actin is observed in the cell body (Figure 3.3B). Following rows also show actin-rich filopodial-like structures (Figure 3.3B arrows).

Loss of PG results in dramatic changes in actin organization in mesendoderm explants. Leading edge cells show disruption of the actin network with few actin filaments evident in these cells. However, lamellipodial protrusions are enriched with actin (Figure 3.3C arrowheads). Organization of actin in the following row cells is perturbed in the PG morphants (Figure 3.3D) compared to the control explants. Actin appears to be concentrated at the center of the cell body of these following row cells (Figure 3.3D red arrowheads). This observation, along with an earlier report (Kofron et al., 2002), suggests a critical role for PG in organizing actin and is consistent with the idea that PG is required for actin attachment at AJ.

Localization of Keratin IFs to C-Cadherin adhesions is partially dependent on PG.

Keratin IFs are recruited to C-cad adhesions bearing stress via PG in migrating mesendoderm cells. However, loss of PG does not completely disrupt organization of

keratin IF in mesendoderm cells (Weber et al., 2012). To further identify the role of PG in the recruitment of keratin IFs, dissociated mesendoderm cells expressing EGFP-krt8 and plated on C-CadFc were examined using a TIRF microscopy. TIRF microscopy allows for visualization of a 100nm region from the coverslip. Since cells on glass coverslips form adhesions close to the membrane, TIRF microscopy was performed to visualize adhesion dynamics. Cells from control MO injected embryos formed long keratin filaments (Figure 3.4A-C). Keratin IFs in these cells showed few movements in the Z-plane and stayed in the cortical region over the course of 5 minutes. Interestingly, in PG morphant cells keratin IFs also localized to the cortical region (Figure 3.4D-F). Surprisingly, their organization appeared fragmented (Figure 3.4D-F, arrow). This could be due to increase in movement of keratin IFs in the Z-plane (data not quantified). Arrowheads in Figure 3.4D-F track the movement of keratin IFs over time and shows that keratin IFs moved in and out from the cortical region. In summary, keratin IFs are recruited to desmsomal-like junctions at the cell cortex that contain classical rather than desmosomal cadherin. Keratin IFs can localize to these sites in absence of PG; however, their increased movement in PG morphant cells suggests that PG is required for proper organization and anchoring of keratin IFs. Thus, we can conclude that PG is only partially responsible for this recruitment.

Keratin IFs and PG co-localize on both C-Cad and FN substrates.

TIRF microscopy was used to visualize adhesion dynamics of mesendoderm cells on C-CadFc and FN. Mesendoderm cells expressing myc-PG-EGFP and mCherry-krt8 were imaged to study desmosomal-like junctions and hemidesmosomes. Initial observation of mCherry-krt8 in dissociated cells plated on C-CadFc substrate (as a surrogate for a

classical cadherin adhesion) showed that keratin IFs were extensively localized at the cortex of the cells (Fig 3.5A and A'), whereas myc-PG-EGFP localized in a punctate manner (Figure 3.5A-C, arrowheads). Strikingly, the small PG punctae co-localize with keratin IFs (Figure 3.5A-C). Time-lapse movies of wildtype mesendoderm cells showed that keratin IFs move in the X-Y plane but this movement was restricted where keratin IFs co-localize with PG. Surprisingly, cells on FN substrate also showed co-localization of keratin IF and PG in small punctate regions (Figure 3.5D-F) similar to cells on C-CadFc (Figure 3.5A' and D'). However, time-lapse movies showed that the entire keratin IF network is highly mobile in cells on FN compared to C-cad. This difference may reflect the fact that cells are highly migratory on FN substrate whereas, on C-CadFc, cells spread but not migrate. Mesendoderm cells plated on poly-L-lysine showed no co-localization of keratin IFs and PG (Figure 3.5G-I). In fact, keratin IFs adopt a wagon wheel organization on PLL substrate because the cells are unable to exert forces on the substrate and thus fail to polarize properly (Weber et al., 2012). Cells on PLL did not move and thus the organization of keratin IFs did not change over time. Taken together, these findings suggest that cell spreading and generation of traction forces on the substrate is required for the formation of the keratin IFs and PG complex. Moreover, these results also suggest that PG may associate with integrins in the mesendoderm cells.

Activation of Integrins is necessary for keratin IF to associate with PG on FN substrate.

The results above demonstrate that keratin IFs can co-localize with PG in cells plated on FN substrate (Figure 3.5D, 3.6B and B'). FN is a large multifunctional protein containing several domains and can bind to integrins as well as syndecan receptors. Thus,

I next investigated whether the co-localization of keratin IFs and PG on FN is dependent on integrin or syndecan receptors. Cells expressing mCherry-krt8 and myc-PG-EGFP and plated on different FN fragments with more restricted capabilities for engaging integrins (Fig 6A; bacterial GST fusion peptides; Ramos and DeSimone, 1996) were visualized using a TIRF microscope. The behavior was compared to cells plated on intact FN substrate, which as mentioned earlier showed punctae of co-localization of PG with keratin IFs (Figure 3.6B and B'). The recombinant FN fragment 9.11 contains integrin binding RGD and synergy sites required for integrin activation whereas 9.11a fragment contains a point mutation in the synergy site (Ramos and DeSimone, 1996). Hence cells plated on the 9.11 substrate can engage and activate alpha5beta1 integrins and cells on 9.11a can engage integrins but fail to activate them. Cells plated on the 9.11 substrate showed punctae of keratin IFs and PG co-localization similar to those observed on intact FN (Figure 3.6C and C'). When plated on 9.11a substrate, however, cells failed to show any co-localization of keratin IFs and PG (Figure 3.6D and D'). To further test for a specific requirement of integrin and FN interaction, I plated mesendoderm cells on a HepII substrate and looked for co-localization of keratin IFs and PG. The HepII domain in FN molecules specifically interacts with syndecans. Mesendoderm cells on HepII domain do not show any co-localization of keratin IFs and PG (Figure 3.6E and E'). Thus, these results indicate that engagement and activation of integrins is necessary for the co-localization of keratin IFs and PG complex on FN substrate to form these novel hemidesmosomal-like junctions.

3.4 Discussion

PG plays an important role in axis specification during embryonic development and may function in the WNT signaling network (Merriam et al., 1997). However, these studies focused on stages that precede gastrulation, and the role of PG in regulating cellular movement during gastrulation has received little attention. PG morphant embryos have short axes (Hirsh et al., in preparation; Weber et al., 2012). This suggests that PG might be involved in regulating the CE movements necessary for proper axis elongation. Indeed, the loss of PG caused polarity defects in mesoderm undergoing CE movements. These defects were not due to defects in cell differentiation (Hirsh et al., in preparation) but possibly instead of changes in cytoskeletal networks or cellular adhesions. Because PG is found at both AJ and desmosomal-like junctions, it was recognized as a prospective link to the cytoskeletal networks. Thus, PG has been of interest as a potential key component in regulating changes in cytoskeletal and junctional morphology and thereby controlling migratory behaviors of mesendoderm cells.

In the experiments described above, I investigated the role of PG in mesendoderm migration during gastrulation in *Xenopus* embryos, and I have made a number of novel observations using both PG depletion and overexpression approaches. My findings indicate that lack of PG results in the disruption of cytoskeletal linkages at the C-Cadherin-containing desmosomal-like junctions and also the formation of smaller FAs in the leading edge mesendoderm cells. Interestingly, overexpression of myc-PG-EGFP showed that PG links keratin IFs not only to classical cadherins but also to integrin adhesions to form novel hemidesmosomal-like junctions.

FAs exert traction force on the ECM and this traction force is necessary for migration of individual cells (Beningo et al., 2001). In mesendoderm tissue, FAs in the leading edge exert forces on the underlying matrix that are necessary for persistent forward migration of mesendoderm cells (Chapter 2). Tension generated at FAs is required for FA growth and persistent cell migration (Beningo et al., 2001; Balaban et al., 2001; Rape et al., 2011). Failure of PG morphant cells to form large FAs as shown in my studies suggests that PG morphants are unable to exert traction forces necessary for forward migration. Furthermore, keratin IFs and PG co-localize on FN matrix in dissociated mesendoderm cells to form integrin-based hemidesmosomal-like junctions. In the absence of PG, it seems likely that these hemidesmosomal-like junctions might not form and keratin IFs would not be able to adhere to integrin. Consequently, in mesendoderm tissue, FA dynamics and collective migration would be disrupted. Thus, PG very likely actively regulates a balance between traction forces generated at integrin and tension across cadherin adhesions necessary for forward migration of the mesendoderm tissue (Figure 3.7; Chapter 2).

Initial study suggested that keratin IF recruitment to the C-cad is a force dependent process and relies on PG (Weber et al., 2012). However, keratin morphant mesendoderm showed severe defects in the organization of the tissue and migration compared to PG morphants (Weber et al., 2012). In order to understand how this difference arises, I decided to investigate keratin IF association with cadherin adhesions. Because it is difficult to visualize C-Cadherin adhesion in an intact mesendoderm explant, I plated explants on an artificial C-CadFc substrate. In order to study the dynamics of these adhesions, TIRF microscopy was performed. The results showed that the loss of PG did not completely ablate the recruitment of keratin IFs to C-Cadherin however, the organization of IF network

is slightly disrupted. This indicates a possibility that keratin IF localization to cadherin adhesions could be carried out by more than one protein (especially a protein with a redundant function). PG and β-catenin have been demonstrated to have a redundant function at AJs as well as in WNT signaling involved in *Xenopus* axis specification (Klymkowsky et al., 1999). Also, preliminary studies conducted in skin tissue of mice have shown the presence of β-catenin at desmosomal junctions in absence of PG (Bierkamp et al., 1999). A similar mechanism might be at play in mesendoderm cells where β-catenin is binding to C-cadherin to recruit keratin IFs albeit less efficiently. Further studies are needed to examine this possibility and to more fully understand how keratin IFs are recruited to C-cadherins adhesions. To begin this process, it would be good to look for co-localization of keratin IFs and β-catenin in mesendoderm cells on C-CadFc using TIRF microscopy. Further, the studies should be expanded to the role of other IF-linker proteins such as plakophilin and DP because both are known to facilitate recruitment of IFs at desmosomal junctions (Figure 1.3). Moreover, DP co-localizes with IFs in a manner similar to that of PG ('beads-on-a-string') in SCC9 cell line (Godsel et al., 2005). Immunoprecipitation (IP) experiments could be done to test whether plakophilin or DP binds to C-cadherins.

PG plays a central role in cell-cell adhesions by forming AJ and desmosomal junctions. But the role of PG in cell-ECM adhesion is less well understood. IFs associate with integrins to form hemidesmosomes but the initial study of hemidesmosomes showed the absence of PG at these hemidesmosomal structures in cells (Cowin et al., 1986). This observation, however, could be cell or tissue-specific. Additionally, PG is known to regulate integrin-mediated processes such as secretion of FN (Todorović et al., 2010). This

raises the question whether there is direct interaction between integrins and PG. The observation that the keratin IF-PG complex assembles on FN substrate suggests that there could be a direct interaction between PG and integrins or that PG and integrins are present in the same functional complex. Moreover, Kindlin2, a well-established component of FAs, has been demonstrated to associate with PG at AJ in endothelial cells (Pluskota et al., 2017). Thus, PG could potentially associate with integrin through binding to kindlins or other components of the FA complex in mesendoderm cells. The result that keratin IFs and PG co-localize only on a substrate that can activate integrins further validates the claim that integrins and PG could be in close proximity to each other. Why integrin activation is necessary for keratin IFs and PG co-localization is intriguing and more experiments need to be undertaken to fully understand the basis for the integrin activity requirement. Additionally, integrin expressed (α5β1 and αv) at this stage of gastrulation (Hoffstrom 2002) are not known to bind to IFs and thus further investigation needs to be done to determine if α5β1 and αv are indeed involved in forming keratin IF-PG complexes or whether other integrins are expressed at this stage albeit at low levels. Performing IP experiments using antibodies against integrins on cells plated on FN substrate could potentially test whether of PG and integrins interact.

In summary, this chapter highlights the importance of PG in mesendoderm migration. I have shown that PG is required for regulation of FAs that are required for the organization of actin, recruitment and maintenance of proper organization of keratin IFs at C-cad adhesions. Furthermore, these results show that PG plays an important role in regulating integrin-based FAs and thus suggest the involvement of PG in maintaining mechanical crosstalk between integrin and cadherin adhesion necessary for mesendoderm

migration. Importantly, these results demonstrate a novel interaction between integrin and PG in mesendoderm cells to form hypothetical hemidesmosomal-like junctions. This observation indicates that PG physically links keratin IFs at integrin and cadherin adhesions and thus facilitates mechanically crosstalk between cell-ECM and cell-cell junctions (Figure 6.7).

Figure 3.1: PG MO efficiency.

(A) Representative Western blot of PG expression levels in gastrula stage embryos injected with Control or PG MO, Actin was used as a loading control. Quantification shows PG expression normalized to Actin relative to control embryos (N=4). Data: mean ± SEM, ** $p<0.01$. (B) Representative images of time matched tailbud stage embryos injected with control and PG MO.

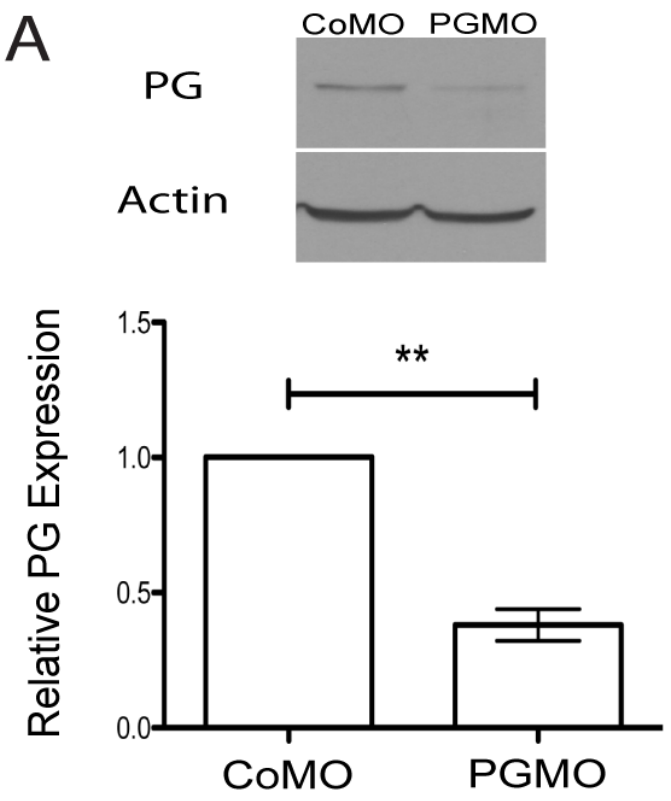
A
CoMO
PGMO
PG
Actin
Relative PG Expression
1.5
1.0
0.5
0.0
**
CoMO
PGMO

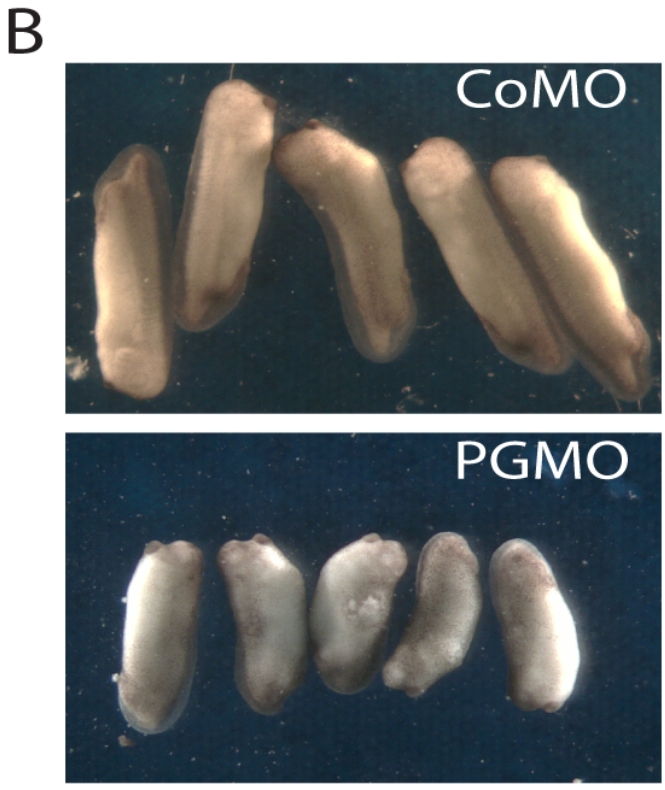
B
CoMO
PGMO

Figure 3.2: Focal adhesion dynamics are altered in PG morphant explants.

(A, C, E and G) Representative TIRF images of mesendoderm explants expressing LifeAct-mCherry (Red) and EGFP-Paxillin (Green). Boxes (A, C, E and G) indicate areas magnified in panels (B-B', D-D", F-F" and H-H"), corresponding to merged (B,D,F and H) and separate LifeAct-mCherry (B', D', F' and K') and EGFP-Paxillin (B'', D'', F'' and K'') channels. (I) Measurement of FA areas was calculated from the first frames of nine separate movies for each condition (9 individual explants per condition imaged from 3 separate experiments). Data: mean ± SEM ***, $p<0.001$. Scale bar = 25um (A, C, E and G) or 10um (B, D, F and H).

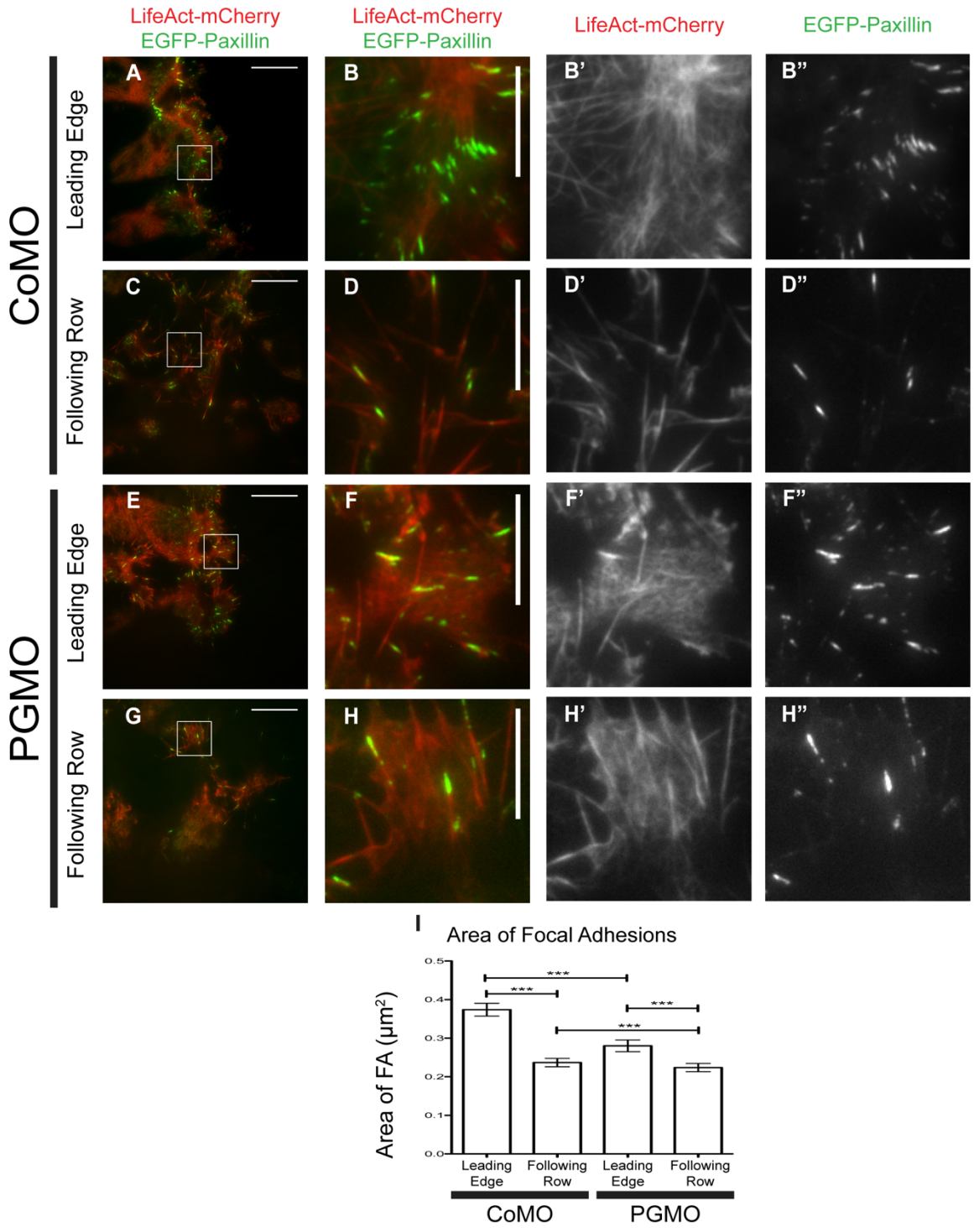
LifeAct-mCherry
EGFP-Paxillin
LifeAct-mCherry
EGFP-Paxillin
LifeAct-mCherry
EGFP-Paxillin
CoMO
PGMO
Leading Edge
Following Row
Leading Edge
Following Row
A
B
B'
B''
C
D
D'
D''
E
F
F'
F''
G
H
H'
H''
I
Area of Focal Adhesions
Area of FA (μm²)
0.5
0.4
0.3
0.2
0.1
0.0
***
***
***
***
Leading Edge
Following Row
Leading Edge
Following Row
CoMO
PGMO

Figure 3.3: Actin morphology is disrupted in PG morphant mesendoderm.

(A-D) Confocal projections of Z-stacks, phalloidin-stained (A and B) control and (C and D) PG morphant explants on FN. Pseudocolors correspond to a fluorescence intensity heat map. Collapsed Z-stack images of representative (A and C) leading edge cells, (B and D) following row protrusion, Arrows in (B) indicate specialized filopodia, white arrowheads in (C) indicate lamellipodial protrusions and red arrowhead indicate collapsed actin in PG morphants. (6 individual explants per condition imaged from 2 separate experiments). Scale bars = 25um (A-D)

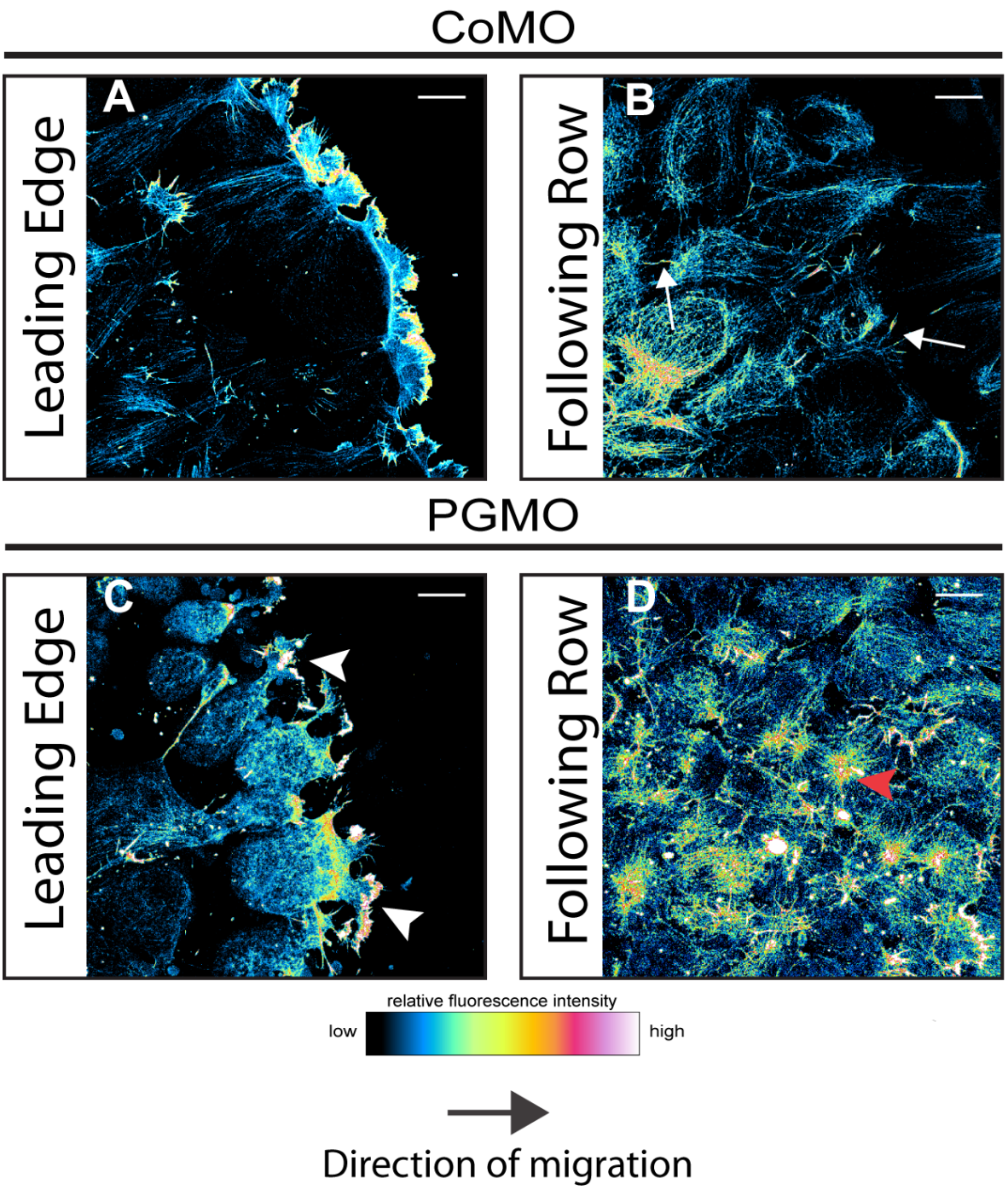
CoMO
Leading Edge
A
Following Row
B
PGMO
Leading Edge
C
Following Row
D
relative fluorescence intensity
low
high
Direction of migration

Figure 3.4: Keratin IFs organization is partially disrupted in PG morphants.

(A-F) Representative TIRF images from time-lapse movies of dissociated mesendoderm cell plated on C-cad substrate. (A-C) control and (D-E) PG morphant dissociated cells. Time points in seconds (secs) from the movies. Arrows in (D-E) indicate fragmented keratin IF networks and arrowheads indicate movement of keratin IFs (Number of cells imaged CoMO = 8 and PGMO = 12 from 2 separate experiments). Scale bars = 25um (A-F).

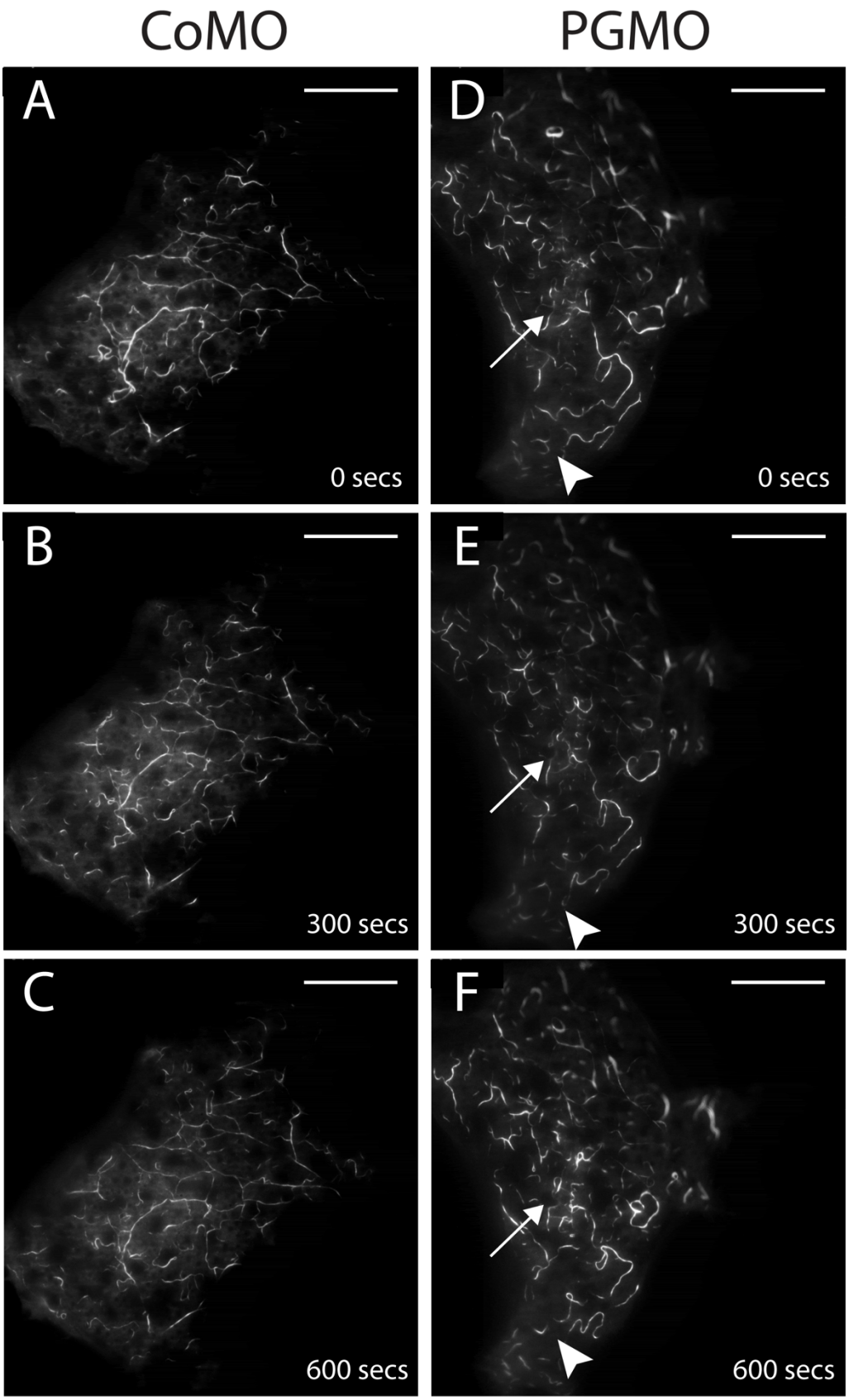
CoMO
PGMO
A
0 secs
D
0 secs
B
300 secs
E
300 secs
C
600 secs
F
600 secs

Figure 3.5: Keratin and PG co-localization on different substrates.

(A, D and G) Representative TIRF images of dissociated mesendoderm cells expressing (B, E and H) myc-PG-EGFP (Green) and (C, F and I) mCherry-krt8 (Red). Boxes (A, D and G) indicate magnified areas in panels (A', D' and G'). Dissociated mesendoderm cells were plated on different substrates (A-C) C-CadFc, (D-F) FN and (G-I) PLL. Arrowheads and arrows indicate co-localization of keratin IFs and PG. (Number of Cells imaged: 2-4 per conditions from at least 2 separate experiments). Scale bar = 25um (A, D and G) and 10um (A', D' and G').

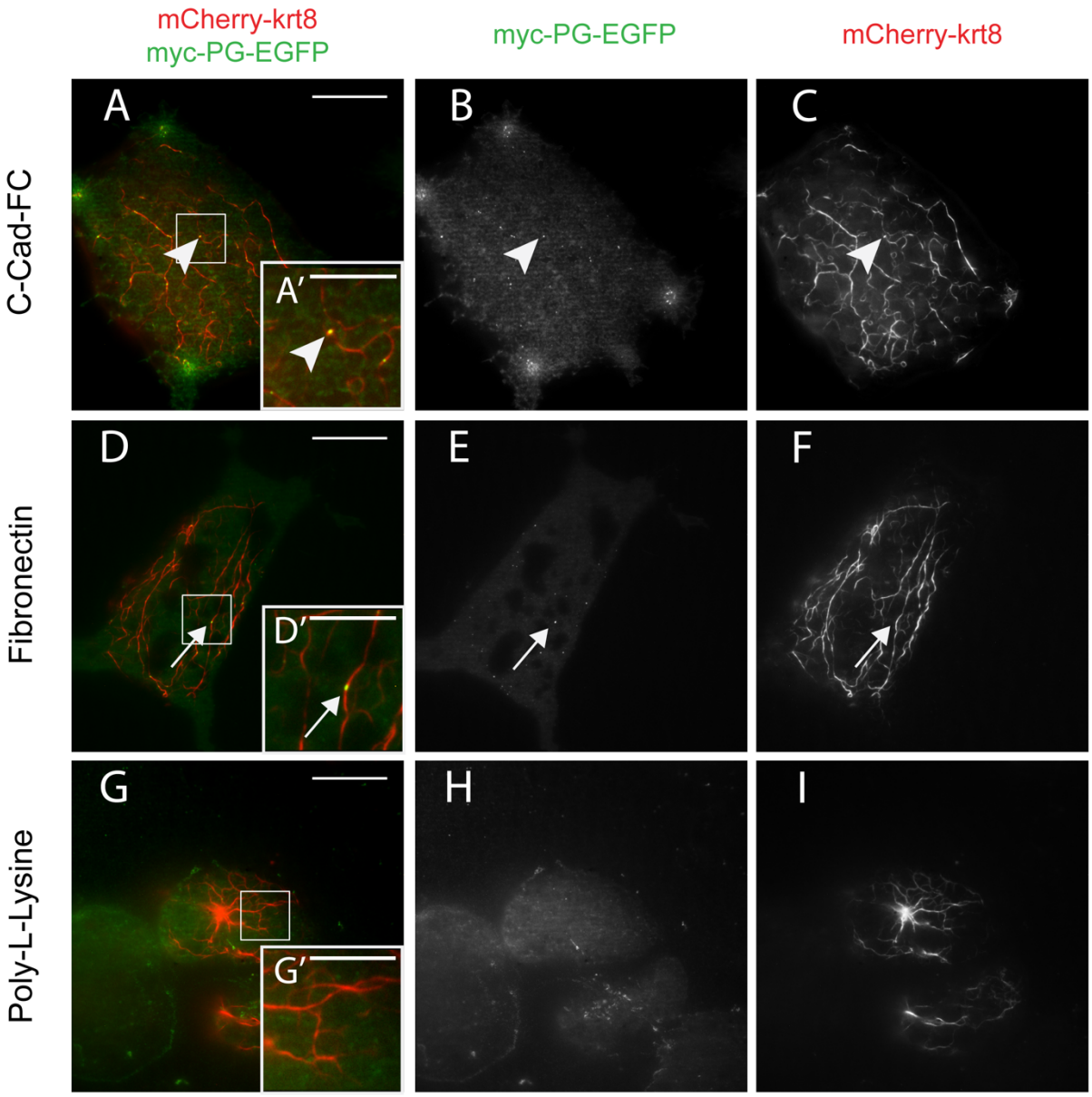
mCherry-krt8
myc-PG-EGFP
myc-PG-EGFP
mCherry-krt8
C-Cad-FC
Fibronectin
Poly-L-Lysine
A
A'
B
C
D
D'
E
F
G
G'
H
I

Figure 3.6: Integrin activation is necessary for Keratin and PG co-localization.

(A) Cartoon of full-length FN molecule and FN bacterial GST-fusion peptides 9.11, 9.11a and HepII. Image modified from Richardson et al., (in preparation). (B, C, D and F) Representative TIRF images of dissociated mesendoderm cells expressing myc-PG-EGFP (Green) and mCherry-krt8 (Red). Boxes (B, C, D and F) indicate areas of remaining panels (B', C', D' and F'). Dissociated mesendoderm cells are plated on different substrate (B) FN, (C) 9.11, (D) 9.11a and (E) HepII. Arrowheads and arrows indicate co-localization of keratin IFs and PG. (Number of Cells imaged: 2-4 per conditions from at least 2 separate experiments). Scale bar = 25um (B, C, D and F) and 10um (B', C', D' and F').

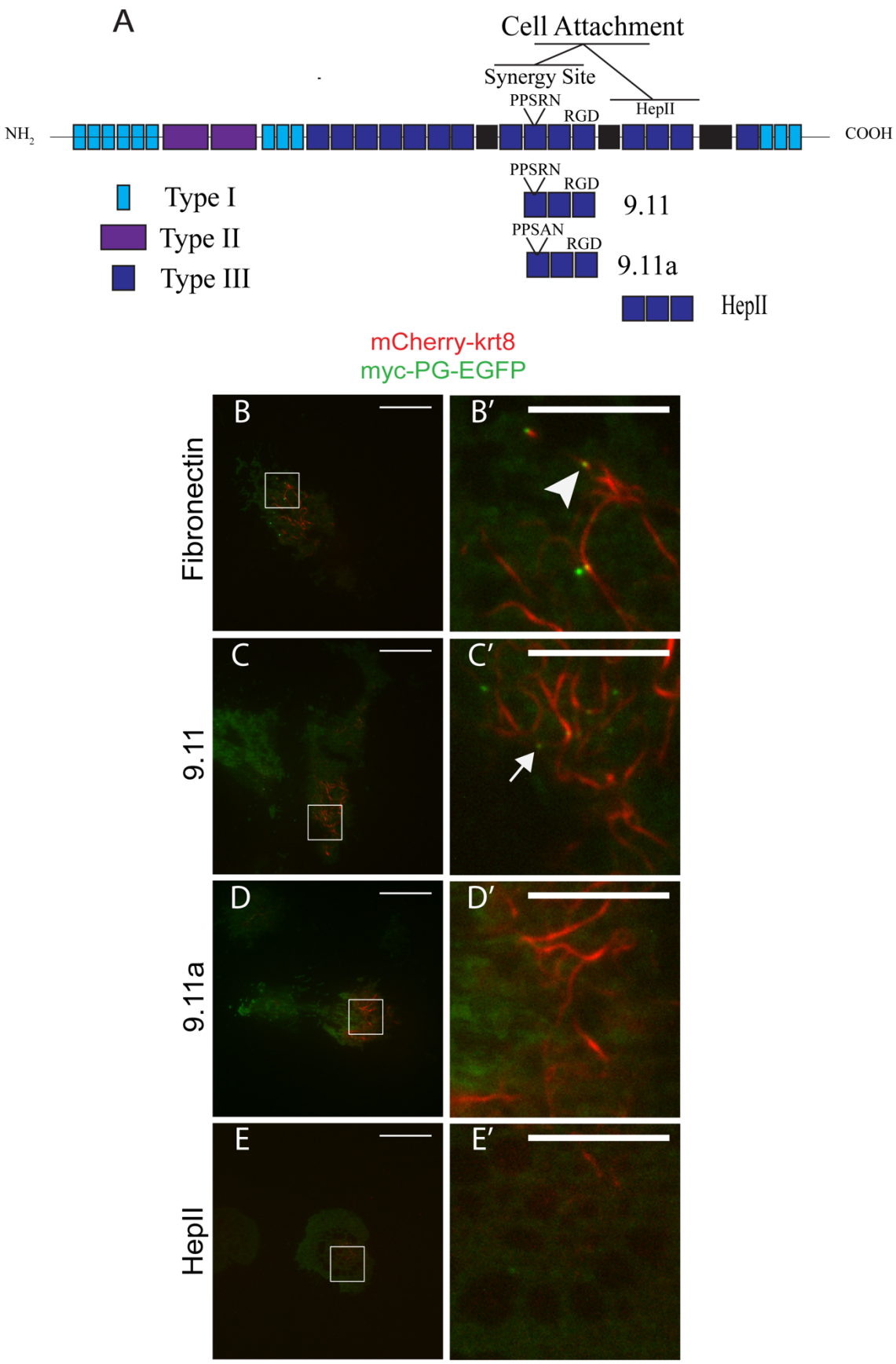
A
Cell Attachment
Synergy Site
PPSRN
RGD
HepII
NH2
COOH
Type I
Type II
Type III
PPSRN
RGD
9.11
PPSAN
RGD
9.11a
HepII
mCherry-krt8
myc-PG-EGFP
Fibronectin
9.11
9.11a
HepII
B
B′
C
C′
D
D′
E
E′

Figure 3.7: Cartoon summary showing PG at integrin and cadherin adhesions.

(A) Cartoon represents collectively migrating mesendoderm tissue exerting traction forces (arrow) using integrin-based adhesions (brown). Cells maintain cohesion through C-cadherin adhesion (dark blue). PG (yellow) assists in the recruitment of keratin IFs (pink) to C-cadherin adhesions bearing tension. PG also links keratin IFs to cell-ECM interface likely through integrins to form hemidesmosomal-like junctions. Since PG links keratin IFs at cadherin and integrin adhesions, it may function to regulate the interaction between these cellular junctions. (B) *En face* view of dissociated mesendoderm cells on FN (green) imaged using a TIRF microscope. Dissociated mesendoderm cells form FAs (brown) in the lamellipodial protrusions (Data not shown). Keratin IFs (pink) localize to the retracting ending of the cell (Based on Figure A.4) and is linked to the FN matrix through PG containing hypothetical hemidesmosomal-like junctions. Based on the imaging of dissociated mesendoderm cells it is clear that FAs and hemidesmosomal-like junctions are spatial separated.

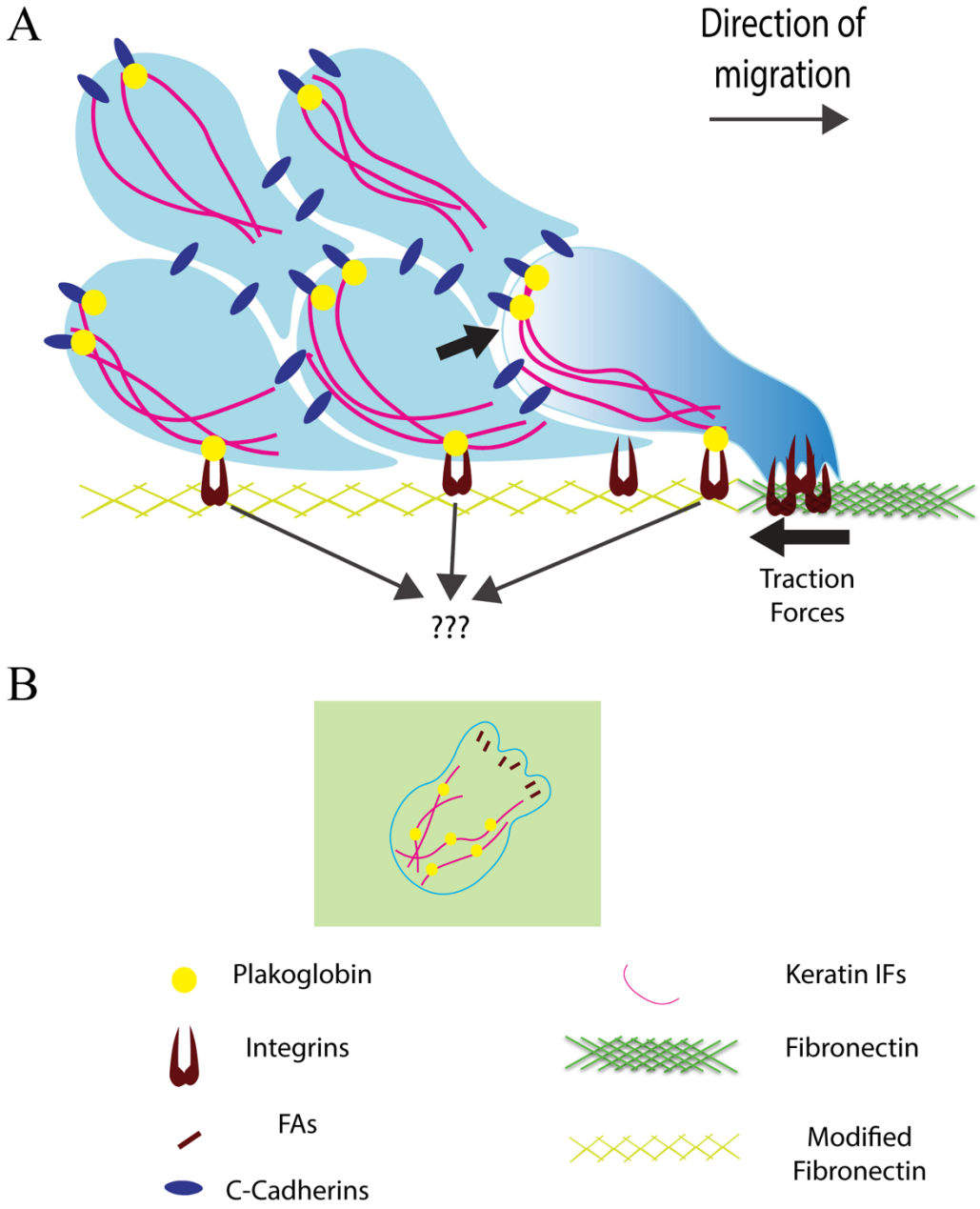
A
Direction of migration
Traction Forces
???
B
Plakoglobin
Integrins
FAs
C-Cadherins
Keratin IFs
Fibronectin
Modified Fibronectin

Appendices

This section contains data that were not included in the Sonavane *et al.,* 2017 but confirms the results shown in Chapter 2. It also contains data from those preliminary experiments that did not yield conclusive results but need to be documented.

Figure A.1: Photoactivation of Rac1 leads to disruption cell-cell junction.

Mesendoderm cells expressing EGFP-PA-Rac1Q61L (not shown) and mCherry-krt8 were dissociated and plated on 10ug/ml FN-coated glass bottom dishes. DIC images of mesendoderm cells and mCherry-krt8 were collected before and after photoactivation. Local photoactivation of Rac1 was done in the region indicated by the red box. Localized Rac1 activation disrupts the cell-cell junction and simultaneously causes reorganization of keratin IFs at the junction. Arrow indicates disrupted cell-cell junction. Scale bar = 25um.

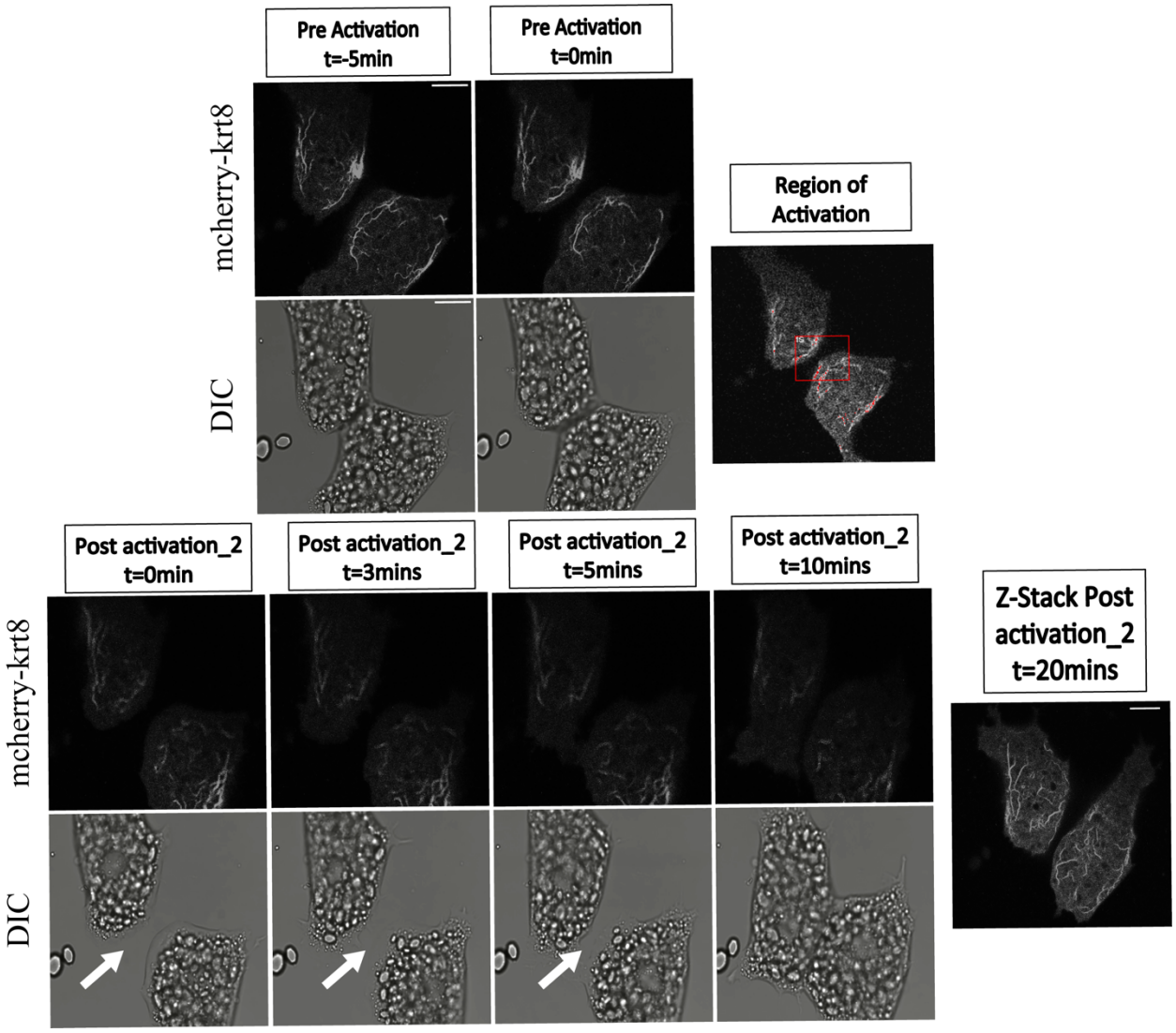
Pre Activation
t=-5min
Pre Activation
t=0min
mcherry-krt8
DIC
Region of
Activation
Post activation_2
t=0min
Post activation_2
t=3mins
Post activation_2
t=5mins
Post activation_2
t=10mins
Z-Stack Post
activation_2
t=20mins
mcherry-krt8
DIC

Figure A.2: Photoactivation of dominant negative Rac1 leads to retraction of the protrusion.

Mesendoderm cells expressing EGFP-PA-Rac1T17N (dnRac1; not shown) and mCherry-krt8 were dissociated and plated on 10ug/ml FN-coated glass bottom dishes. DIC images of mesendoderm cells and mCherry-krt8 were collected before and after photoactivation. Local photoactivation of dnRac1 was done in the region indicated by the red box. Localized activation of dnRac1 at the lamellipodial protrusion results in retraction of the protrusion and reorganization of keratin IFs at the site of retraction. Arrow indicates retraction of the protrusion. Scale bar = 25um.

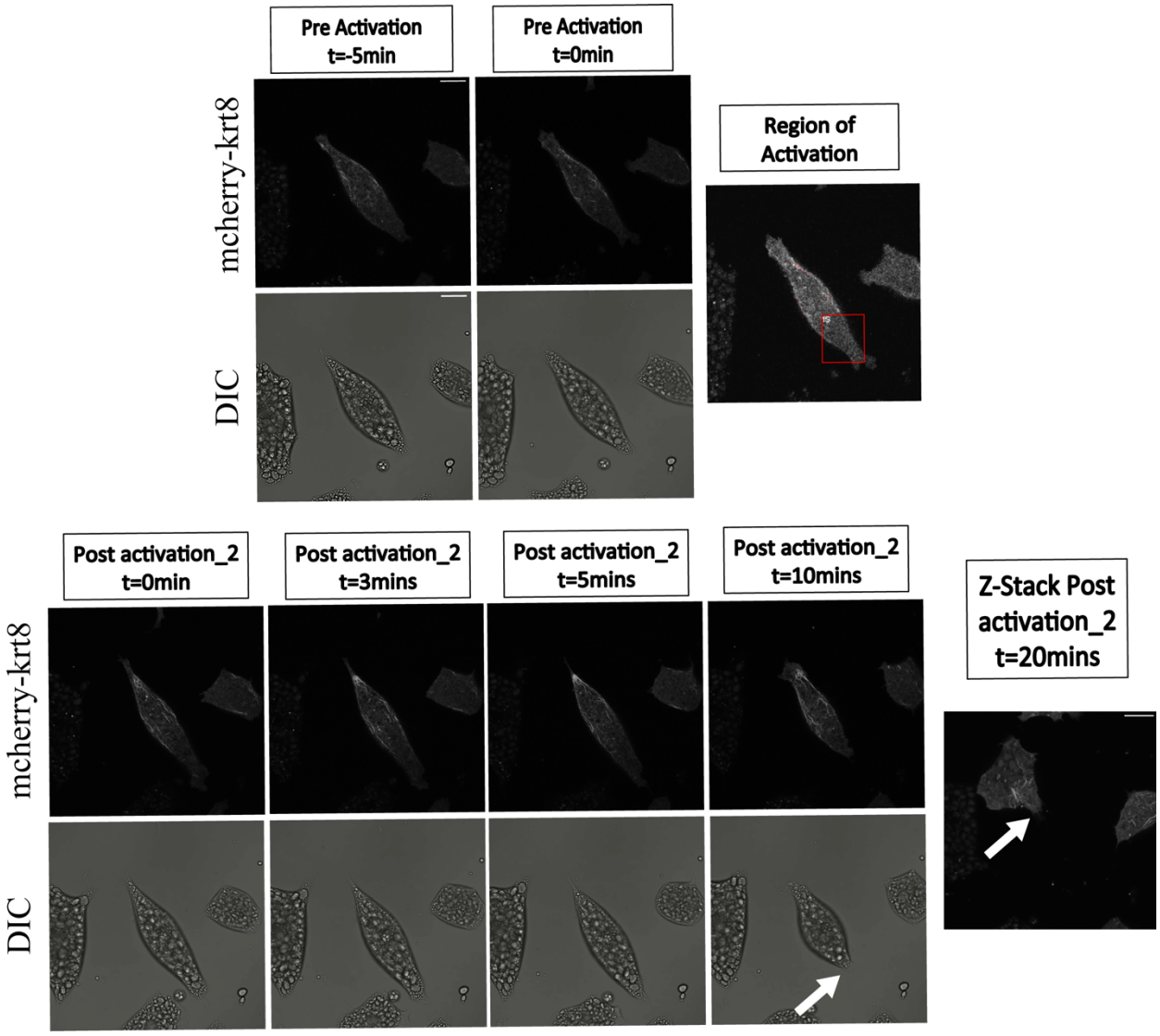
Pre Activation
t=-5min
Pre Activation
t=0min
Region of
Activation
mcherry-krt8
DIC
Post activation_2
t=0min
Post activation_2
t=3mins
Post activation_2
t=5mins
Post activation_2
t=10mins
Z-Stack Post
activation_2
t=20mins
mcherry-krt8
DIC

Figure A.3: Migration rate of Y27632 treated mesendoderm explants.

Migration rates of mesendoderm explants treat with Y27632 inhibitor were calculated to determine whether inhibition of actin stress fibers in krt8 morphants rescues the migration defects in krt8 morphants. Mesendoderm explants were plated on 5ug/ml FN-coated plastic petri dishes and imaged on the AxioObservor. Images were collected every 5 mins for one hour. Migration rates were calculated by dividing the distance traveled by time. From 5 separate experiment with 15 explants for each condition, I was not able to establish a statistically significant difference in migration rates between krt8MO explants treated with either DMSO alone or Y-27632, although it does trend in the direction of a "rescue". There is a lot of variability in migration rates in krt8MO explants and this may account for the lack of significance. Data represents 15 explants per condition spread across 5 independent experiments, * = $p<0.05$.

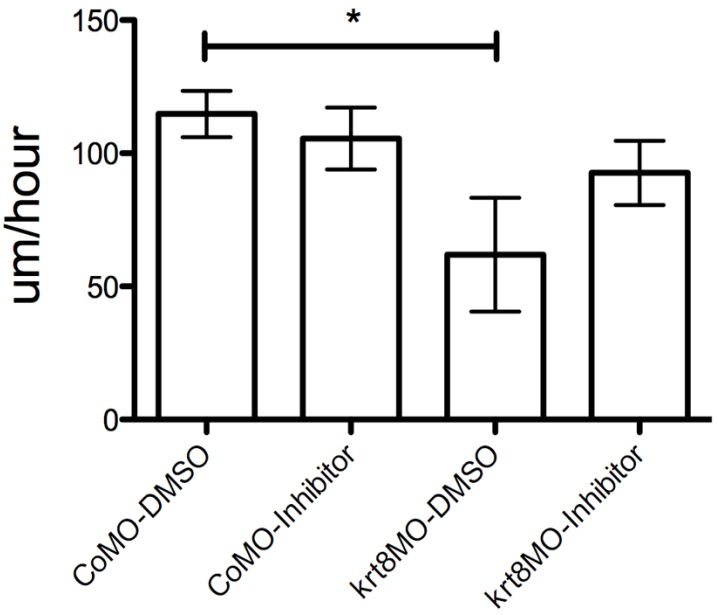
150
100
50
0
um/hour
*
CoMO-DMSO
CoMO-Inhibitor
krt8MO-DMSO
krt8MO-Inhibitor

Figure A.4: Active Rac1 pull-down.

Active Rac1 pull-down experiments were performed to quantitatively measure active Rac1 in mesendoderm cells. Dissociated mesendoderm cells were plated on silicon stretcher coated with C-CadFc to mimic cell-cell adhesions. Cells were allowed to adhere for an hour and then subjected to continuous stretch for varying amounts of time. Cells were lysed immediately after stretch using modified RIPA buffer (Bjerke et al., 2014). Cell lysates were divided into two tubes; the first tube was used to determine total Rac1 levels in the lysates and the second tube was used to perform active Rac1 pulldown. Active Rac1 pulldown was performed using sepharose beads coated with GST-PBD. Lysates were incubated with GST-PBD beads for one hour and then washed with RIPA buffer and loaded on SDS-PAGE. Total Rac1 and active Rac1 were probed with anti-Rac1 antibody (BD Bioscience #610650) at a dilution of 1:1000. Whole embryo lysates (WEL) were treated with GTPγS (Rac1 cannot hydrolysis GTPγS and constantly remains in the active state) or GDP (this causes the displacement of GTP from Rac1 and thus Rac1 constantly remains in the inactive state) as a control for pulldown. This experiment was performed three separate times however, I was not able to achieve a statistically significant result or any trends towards significance.

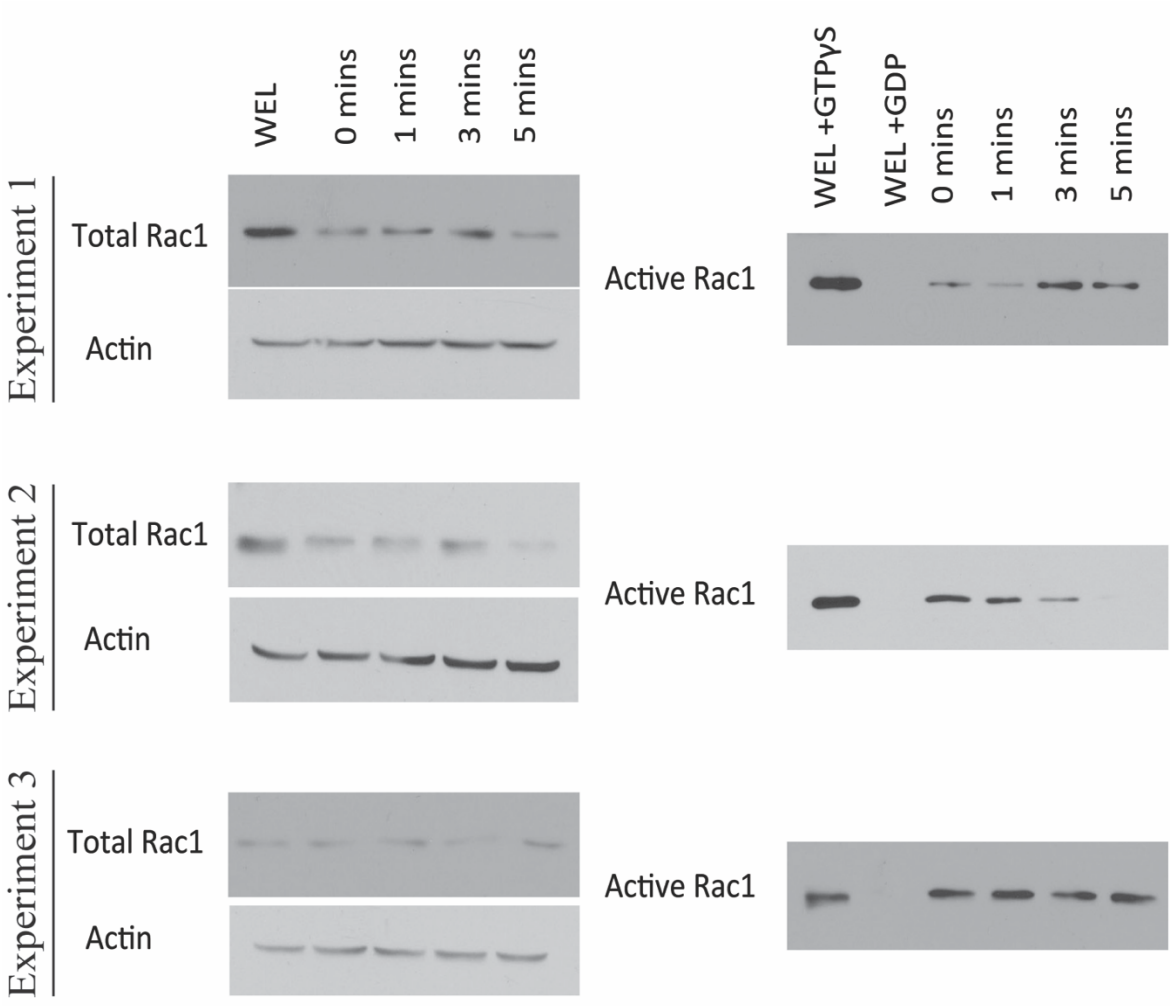
WEL
0 mins
1 mins
3 mins
5 mins
WEL +GTPγS
WEL +GDP
0 mins
1 mins
3 mins
5 mins
Experiment 1
Total Rac1
Actin
Active Rac1
Experiment 2
Total Rac1
Actin
Active Rac1
Experiment 3
Total Rac1
Actin
Active Rac1

Chapter 4

Conclusions and Perspectives

4.1 Overview and summary of major findings.

The work done in this dissertation focuses on the morphogenetic process of mesendoderm migration in gastrulating *Xenopus* embryos. This study was performed with an aim to begin to understand the mechanistic role of mechanical forces in embryonic development. Forces generated during large-scale tissue movement influence cell-cell (cadherins) and cell-ECM (integrins) interactions. Coordinated movements occurring during gastrulation require cooperation between integrins and cadherin adhesions. The results from this study demonstrate that a balance between forces on integrins and cadherins is required for the proper assembly and migration of mesendoderm tissue.

Weber et al., (2012) demonstrated that intercellular tension on C-cadherin is required for directed migration of mesendoderm tissue and identified the formation of a mechanosensitive keratin-cadherin complex as being integral for the formation of polarized protrusions; but the mechanism by which this mechanosensitive complex regulates protrusions was not clarified. In Chapter 2, I showed that migrating mesendoderm tissue organizes to form leader and follower cells. Leader cells generate traction forces necessary for the forward migration of the tissue by forming FAs. In contrast, follower cells exert surprisingly little force on the matrix through FAs, especially in support of forward migration, and instead largely rely on their connections to the leader cells. Thus, the traction force applied by the leader cells generates high tension on C-cadherin adhesions formed between the leader and follower cells, and this coupling between traction force and tension underlies the collective and directed migration of mesendoderm tissue. I also found that keratin IFs are required for maintaining the balance of forces exerted on the matrix and tension across cell junctions during migration. Loss of keratin IFs at cellular adhesions

results in morphological changes to the actin network at both integrin and cadherin adhesions. These data suggest that crosstalk between integrin and cadherin adhesion is critical for migration of mesendoderm tissue.

In Chapter 3, I investigated the role of a cadherin-associated protein PG, a member of the catenin family, in regulating migration of mesendoderm tissue. My results showed that PG is necessary for the organization of cytoskeletal network in the mesendoderm tissue. Indeed, when PG was deficient, I observed disruption of actin morphology in mesendoderm tissue. Moreover, PG in mesendoderm tissue links keratin IFs to classical cadherins to form desmosomal-like junctions rather than true desmosomal junctions. I could mimic this organization using C-CadFc as a substrate for cell attachment and observed co-localization of PG and keratin IFs at discrete punctae. Perhaps my most surprising finding was the co-localization of keratin IFs and PG to "potentially" integrin-containing cell-ECM adhesions to form novel hemidesmosomal-like junctions. When I examined this interaction further using recombinant FN GST fusion peptides, I found that the keratin IFs and PG co-localization only on 9.11 but not on 9.11a or HepII substrates. Indeed it suggests that this interaction requires activation of integrins. I went on to show that PG actively regulates integrin adhesions as evidenced by the observation that loss of PG causes changes in the FA dynamics in the leading-edge cells of mesendoderm tissue. These data suggest that IFs are intimately involved in the crosstalk between cadherin- and integrin-based adhesions and that PG is likely playing an active role in regulating both of the adhesions.

Taken together, the data from this study highlight the importance of mechanical signaling in morphogenesis. Although I have specifically focused on the collective

migration of mesendoderm during gastrulation, similar mechanisms are at play in other physiological and pathological morphogenetic processes. Directed collective migration is observed in many process such as mesendoderm migration in zebrafish (Dumortier et al., 2012), posterior lateral line primordia (pLLP) migration in zebrafish (Haas and Gilmour, 2006), border cell migration in *Drosophila* oocytes (Cai et al., 2014), neural crest migration in *Xenopus* (Scarpa et al., 2015; Theveneau et al., 2010), wound healing and angiogenesis (Friedl and Gilmour, 2009; Mayor and Etienne-Manneville, 2016). Furthermore, metastatic transformed cells migrate collectively during cancer invasion (Friedl and Gilmour, 2009). Common features, as well as specific differences, have emerged concerning how collectively migrating cells sense and respond to mechanical and chemical cues necessary for directed migration. However, there are a lot of gaps in our understanding of these mechanisms that are yet to be filled. Below, I compare and contrast *Xenopus* mesendoderm and other collectively migrating cells based on the principles that have emerged from my work and that of others and point out future directions and implications of the results described in chapter 2 and 3.

4.2 Emergence of leader and follower cells in collectively migrating cells.

Mesendoderm tissue organizes into leader and follower cell during migration (Chapter 2). Similarly, other examples of collective migrating populations such as pLLP and epithelial cells, also assemble into leader and follower cells. Although I have shown that this organization is dependent on the mechanical forces experienced by the cells during migration, there are details that are yet to be clarified in order to fully understand how forces regulate the assembly of mesendoderm tissue.

Leading the way.

Single migratory cells can follow a gradient of diffusible molecules through chemotaxis. Directional migration of groups of cells can also be guided by chemotaxis. Mesendoderm cells sense a gradient of platelet derived growth factor (PDGF) ligand bound to the FN matrix in the BCR, and PDGF signaling is required for directional migration (Nagel et al., 2004). Integrin signaling can activate PDGF receptor in a ligand-independent manner (Richardson et al., in preparation). Leader cells in mesendoderm explants exert high traction forces by forming broad lamellipodial protrusions and integrin-based FAs. However, is a PDGF gradient sufficient for the formation and maintenance of leader cells in mesendoderm cells? *Ex vivo* mesendoderm explants on a FN-coated glass migrate directionally without a gradient of PDGF. But dissociated mesendoderm cells on the same FN-coated glass form random protrusions and show lack of persistent migration. This suggests that cell-cell contacts are crucial for directional migration. Dissociated mesendoderm cells are indistinguishable from each other; these cells have the potential to form directed protrusions when pulled using a magnetic bead coated with C-CadFc (Weber et al., 2012) similar to leader cells. Additionally, surgical removal of leader cells causes the cells at the newly formed edge of the explant to adopt leader cell characteristics (Figure 2.7). Thus, in mesendoderm tissue, PDGF can initiate directional migration *in vivo*, but PDGF is not necessary for the maintenance of leader cells in mesendoderm tissue.

As the mesendoderm cells migrate into the open space of the blastocoel cavity, cells at the edge of the tissue experience high tension on the cell-cell junctions and this tension acts as a positive feedback loop for these cells to maintain leader cell characteristics. The

guidance of migration by differential tension on the cell-cell junction is termed cohesotaxis (Weber et al., 2012) and is also observed during border cell migration and cancer invasion. Tension on E-cadherin adhesions is necessary for border cells to lead nurse cell (follower cells) during collective migration (Cai et al., 2014). In transformed cells, tension on P-cadherin adhesions is required for directional migration (Plutoni et al., 2016).

Unlike mesendoderm cells, the organization of pLLP into leader and follower cells is primarily dependent on a gradient of the chemokine sdf1 (as known as Cxcl12a). Cells at the migrating front of the pLLP sense the sdf1 gradient via the Cxcr4b receptor (David et al., 2002; Haas and Gilmour, 2006) and activate Wnt/beta-catenin mediated signaling, which results in these cells becoming leader cells (Aman and Piotrowski, 2008). The leader cells secrete fgf3/10 ligands, which are sensed by the rest of the cells; these ligands suppress the expression of Cxcr4b and thus drive the rest of the cells to become "non-leader" cells (Lecaudey et al., 2008).

Keratin IFs in mesendoderm cells are recruited to the C-cadherin adhesions in response to mechanical stress. Keratin IFs help to resist high tension at the cell-cell junction between the leader and follower and are essential for the maintenance of leader cell and follower cell organization in the tissue (Figure 2.13). Upon loss of keratin IFs, cellular adhesions are unable to resist tension and thus follower cells exert high traction forces similar to that of leader cells (Figure 2.3). This suggests that tension on C-cadherins also actively inhibits follower cells from becoming leader cells. Owing to the complex geometry of the mesendoderm tissue it would be difficult to quantitatively measure the differences in cell-cell adhesion strength between leader-follower cells and follower-follower cells and determine whether this causes differential behavior in the leader and follower cells.

However, FRET-based tension biosensors (Vinculin or cadherin biosensors) should be considered as a way to determine if there is a difference in tension across these junctions (Conway et al., 2013; Grashoff et al., 2010).

Contact inhibition of locomotion (CIL) is a feature observed in fibroblasts wherein cells avoid moving onto each other and instead move in opposite directions as cell-cell contact is initiated (Abercrombie and Heaysman, 1954). During neural crest collective migration, cells undergo EMT and exhibit CIL. Neural crest cells actively protrude away from sites of cell-cell contact (Bahm et al., 2017; Theveneau et al., 2010). Furthermore, leader cells of the neural crest show change in cell stiffness as measured using AFM and this change is necessary for initiation of migration (Blaue et al., 2018). Similarly, CIL is observed in mesendoderm cell-pairs on FN matrix; cells in the cell-pair polarize in the direction away from the C-cadherin adhesions (Weber et al., 2012). An interesting question for future investigation is whether CIL changes mesendoderm cell stiffness and if so is that necessary for migration? In order to begin to test this hypothesis, we need to determine if there is a change in cell stiffness upon CIL. This could be determined by measuring the stiffness of single cells and cells within cell-pairs and a reaggregated monolayer of mesendoderm cells. Reaggregated monolayers would potentially mimic behaviors in intact mesendoderm tissue and would not have geometrical constraints of multiple cells layer like that in the intact mesendoderm tissue. This would help us to determine whether there is a difference in cell stiffness between leader cells at the edge and follower cells at the center of the aggregate-follower cells.

Do following row cells contribute to collective migration?

In mesendoderm, both leader and follower cells form lamellipodial protrusions (Davidson et al., 2002; Weber et al., 2012). However, only protrusions of leader cells are persistent; protrusions in follower cells are highly dynamic (Figure 2.5). Moreover, leader cells primarily exert the traction forces required for forward migration whereas, traction forces exerted by the following rows are minimal and these traction forces are randomly oriented (Figure 2.3). Thus, based on these results I hypothesize that, unlike in the pLLP, protrusions of mesendoderm follower cells do not contribute to forward migration; instead the primary function of the follower cells is to resist the tension across leader cell junctions. But mesendoderm tissue also consists of cells that are not directly in contact with the blastocoel roof (referred to as upper following row or UFR cells; Figure 2.14). Because of the geometry of the mesendoderm explants, it is difficult to visualize cellular dynamics in the mesendoderm cells that are not directly juxtaposed to the FN matrix. Visualizing of fixed donut explants (Figure 2.1) showed the presence of bands of actin stress fibers that span neighboring cells in the UFR cells (Figure 2.15). Traction force results of donut explants show that forces required for forward migration are restricted to the leading edge of the explant but the magnitude is lower than that of the DMZ explants (Compare figure 2.3 and 2.4). Additionally, donut explants completely close in absence of any substrate (data not shown). Based on these observations, I hypothesize that actin network in the UFR may provide the tangential forces required for the closing of the mesendoderm tissue.

In collectively migrating epithelial sheets and pLLP, both leader and follower cells extend protrusions in the direction of migration similar to mesendoderm tissue (Dalle Nogare et al., 2014; Farooqui and Fenteany, 2005; Tambe et al., 2011; Trepat et al., 2009). However, in contrast to mesendoderm tissue, cells in the center of the epithelial cluster

exert traction force on the matrix and actively contribute to the migration of the sheet (Tambe et al., 2011; Trepat et al., 2009). Leader cells in pLLP experience bilateral stretching in the direction of migration due to the chemokine gradient in the front and attachment of follower cells in the back. The severing of follower cells causes the leading edges to stall; migration resumes only when follower cells migrate toward the leader cells and establish contact (Dalle Nogare et al., 2014). This suggests that during pLLP migration both leader and follower cells actively participate in collective migration, unlike mesendoderm tissue.

During cancer invasion, cancer-associated fibroblast cells lead migration of transformed cells by remodeling the ECM and laying tracts for the migration of the follower cells. This remodeling of ECM requires matrix metalloproteinases (MMPs; Gaggioli et al., 2007). What may be a similar reorganization/degradation of FN matrix is observed when leader cells migrate in mesendoderm. If this change is dependent on MMPs, it could be tested by using inhibitors against MMPs (Shi and Sottile, 2011). Due to lack of FN matrix, follower cells may not be able to form strong integrin adhesions to exert traction forces (Figure 2.3 and 2.8) necessary for forward migration.

Interestingly, follower cells form long and dynamic specialized filopodia. These specialized filopodia resemble cytonemes first described in *Drosophila* (Kornberg and Roy, 2014; Ramírez-Weber and Kornberg, 1999; Roy et al., 2014). Cytonemes are thin actin-based protrusions involved in morphogen signaling. In *Xenopus*, these structures are observed during early stages of development and are required for cytoplasmic exchange (Danilchik et al., 2013). Whether these filopodial structures in follower cells are sensing morphogen can be determined by visualizing if fluorescently tagged morphogens are

present in filopodial structure of mesendoderm explants plated on a conditioned substrate using TIRF microscopy.

4.3 Molecular mechanism of cell polarization during collective migration.

During collective migration, cells have to maintain cell-cell and cell-ECM adhesions. These cells constantly receive mechanical and chemical inputs. The question that then arises is how do cells integrate these inputs during collective migration? In Chapter 1, I have addressed how mechanical forces influence activation of integrins, cadherin clustering and changes in cytoskeletal networks. In this section, I will discuss some common signaling pathways activated during collective migration and expand on how these pathways may be relevant in the context of mesendoderm migration.

Rho GTPases Signaling.

The Rho family of small GTPase proteins such as Cdc42, Rac1 and RhoA are key regulators of polarity during cell migration (Ridley, 2015). Rho GTPase signaling is activated through both integrin and cadherin-based adhesions. Increasing evidence suggests that Rho GTPases actively regulate collective migration (Plutoni et al., 2016; Reffay et al., 2014; Scarpa et al., 2015; Yamaguchi et al., 2015). Rho GTPases cycle between a GTP bound active state and GDP bound inactive state (Nethe and Hordijk, 2010). The spatial localization of these proteins within the cells is dependent on the activation status (MacHacek et al., 2009). Activation of Cdc42 mediated by the Rho family GEF, β-pix, and P-cadherin signaling is necessary for collective migration of the transformed C2C12 cell line (Plutoni et al., 2016). Spatial activation of RhoA is necessary

for the formation of the contractile actomyosin network at the leading edge of collectively migrating MDCK cells. During metastasis, cancer-associated fibroblasts lead metastatic follower cells in RhoA dependent manner (Gaggioli et al., 2007).

Rac1 activity is necessary for the formation of lamellipodial protrusions (Jou and Nelson, 1998; Nobes and Hall, 1995). Context-dependent integrin and cadherin signaling can either activate Rac1 (Del Pozo et al., 2002; Nakagawa et al., 2001) or downregulate Rac1 signaling (Kitt and Nelson, 2011; Nishiya et al., 2005). Results from chapter 2 show increased Rac1 activity in the lamellipodial protrusions of leader cells in the mesendoderm tissue. This activation probably occurs through integrin α5β1signaling (Davidson et al., 2002). A similar result was recently confirmed by Hayashi et al., (2018). This study shows Rac1 activation in leader cell through continuous Ca^{2+} ion stimulation. Whether integrins and Ca^{2+} signaling independently activate Rac1 requires further investigation. Additionally, in collectively migrating MDCK cells, integrin β1 mediated activation of Rac1 is necessary for the formation of leader cells (Yamaguchi et al., 2015). Furthermore, nuclear transport of merlin induces activation of Rac1 and promotes the formation of lamellipodial protrusions (Das et al., 2015). Thus, Rac1 signaling has been demonstrated to play important role in regulating lamellipodial protrusions during collective cell migration.

In leader cells of mesendoderm tissue, Rac1 activity is highest at the lamellipodial protrusions; whereas, a region of low of Rac1 activity coincides with the keratin IFs at the rear C-cadherin adhesion. Rac1 and keratin IFs display an antagonistic relationship in mesendoderm cells. Indeed, loss of keratin IFs causes disruption of the Rac1 activity gradient in leader cells whereas activation Rac1 leads to disassembly of keratin IFs. Similar

an antagonism between Rac1 and vimentin IFs is observed in fibroblast cells. Spatial activation of Rac1 causes vimentin phosphorylation and subsequent disassembly of vimentin IFs (Helfand et al., 2011). Protein kinase C delta mediated phosphorylation of keratin IFs leads to disassembly of keratin IFs in epithelial cells (Ridge et al., 2005). Does Rac1 activation cause phosphorylation of keratin IFs similar to that observed in epithelial cells? It would be possible to observe whether there is a change in keratin IF phosphorylation in presence of constitutively active or dominant negative Rac1. If phosphorylation of keratin IFs increases in presence of constitutively active Rac1, it could explain how active Rac1 inhibits assembly of keratin IFs at the lamellipodial protrusions (Figure 4.4). Another question that arises is how do keratin IFs downregulate Rac1 activity at the rear of mesendoderm cells? During wound healing, epithelial krt6/17 sequesters SH2 domain containing Src kinase and suppresses Src activity (Rotty and Coulombe, 2012). Src kinase acts downstream of integrins and is necessary for Rac1 activation (Figure 4.4; Choma et al., 2007; Huveneers and Danen, 2009; Kawakatsu et al., 2005). It is possible that krt8/18 also binds and suppresses Src activity in mesendoderm to inhibit Rac1 activation in mesendoderm cells (Figure 4.4).

Interaction between cytoskeletal networks.

Cytoskeletal changes are important for cell migration. However, to what extent do these cytoskeletal networks interact with each other in migrating mesendoderm tissue? Fak acts downstream of integrin signaling and is known to regulate the formation of a mechanosensitive cadherin-keratin complex in mesendoderm cells. Knockdown of Fak causes disorganization of keratin IFs and disrupts actin morphology (Bjerke et al., 2014).

This is similar to the actin stress fibers observed when krt8 levels are reduced in mesendoderm cells (Figure 2.9). However, it is necessary to determine whether changes in actin morphology are due to changes in signaling pathways or whether actin and keratin network are physically coupled and therefore loss of keratin IFs leads to reorganization of actin. This could be addressed by acutely perturbing the keratin IF network during mesendoderm migration. One possible way to do this would be to employ Chromophore assisted light inactivation (CALI). CALI uses a fluorescent protein to locally induce the formation of reactive oxygen species (ROS). Generation of ROS disrupts molecular complex associated with the fluorescently-tagged protein (Jacobson et al., 2008; Takemoto et al., 2013). CALI could be used to acutely perturb keratin IFs and observe changes in actin morphology (Figure 4.1). If actin and keratin networks are linked, acute perturbation of keratin IFs network would lead to severe changes in actin organization.

It has been established that actin, microtubule and IF cytoskeletal networks are connected to each other through the protein plectin. (Wiche, 1998). Plectins also function to recruit IFs at integrin-based adhesions (Borradori and Sonnenberg, 1999). Loss of plectins in cultured cells results in MAP kinase signaling and formation of actin stress fibers (Osmanagic-Myers et al., 2006). Furthermore, plectin and vimentin IFs regulate lamellipodial dynamics, actin organization and FA turnover through FAK signaling in fibroblast cells (Gregor et al., 2014). Mesendoderm tissue shows a change in FA dynamics and actin morphology in absence of keratin IFs. Loss of keratin IFs could alter the global functioning of plectin. Thus, in the context of mesendoderm migration, it is possible that plectin could mediate an interaction between actin and keratin cytoskeletal network (Figure 4.5) and regulate FA dynamics at the leading edge of the tissue.

Additionally, vimentin IFs regulate the retrograde flow of actin in fibroblast cells (Costigliola et al., 2017) and inhibit the formation of stress fibers by downregulating RhoA signaling (Jiu et al., 2017). In contrast, Solo kinase binds to keratin IFs and regulates the formation of actin stress fibers in epithelial cell lines. Knockdown of keratin IFs or Solo kinase results in a reduction in actin stress fibers (Fujiwara et al., 2016). Thus, evidence suggest that keratin IFs are both required for formation and inhibition of actin stress fibers. It is possible that the interaction between keratin IFs and actin could be cell-type specific. However, these studies demonstrate that IFs can actively participate in signaling and regulate migratory behavior by governing actin dynamics. Similarly, keratin IFs in the mesendoderm not only resist tension at C-cadherin adhesion but actively regulate cell polarity through signaling.

Role of catenins in migration.

As mentioned in Chapter 3, the catenin family of proteins are recruited to cadherin adhesions. However, catenins can also regulate migratory behavior in single cells and collectively migrating cells (Vassilev et al., 2017; Weber et al., 2012). In mesendoderm, loss of PG (γ-catenin) causes disruption of cell polarity (Weber et al., 2012) and partial loss of keratin IFs from the site of C-cadherin adhesions (Figure 3.4). Injection of MO does not completely knockdown expression of proteins. The partial loss of keratin IFs from the site of cadherin adhesion could be due to insufficient knockdown of PG levels. Thus, to determine whether PG is required for the recruitment keratin IFs to C-Cadherin junctions, acute perturbation of PG can be performed using CALI. However, at the desmosomal junctions, PG does not directly bind to IFs. DP directly binds to the IFs and recruits IFs to

the desmosomal junctions (Figure 1.3). Whether DP is involved in the recruitment of keratin IFs to C-cadherin needs to be tested. Preliminary evidence shows DP expression at gastrula stages in *Xenopus* embryos (Figure 4.2). Expression was determined in the whole embryo, animal caps and mesendoderm tissue specifically using anti-DP antibody (Abcam #16434). However, mesendoderm tissue does not show a band but this could be due to uneven loading (Tubulin band intensity is also weak in mesendoderm tissue). In order to determine the specificity of the anti-DP antibody, titration and secondary alone controls were also performed. Further investigation can be done by performing immunoprecipitation (IP) experiments using antibodies to C-cadherin to demonstrate whether DP binds to C-cadherin.

β-catenin and α-catenin are reported to localize to lamellipodial protrusions and guide directional migration of neural crest cells in mice. The rearward translocation of α-catenin from the lamellipodial protrusion requires β-catenin and this movement of α-catenin activates RhoA, which in turn regulates actomyosin in the neural crest cell (Vassilev et al., 2017). Similarly, β-catenin staining is observed in mesendoderm cells (data not shown). In order to determine whether α-catenin and β-catenin also function to regulate mesendoderm migration, live cell imaging of fluorescently tagged α-catenin and β-catenin could be performed. The movement of these proteins within the mesendoderm cells could be correlated to the changes in the cytoskeletal network.

Preliminary immunostaining experiments show PG staining at lamellipodial protrusions in mesendoderm cells (Figure 4.3). Is PG activating Rho GTPase signaling or interacting with other components of the lamellipodial protrusions to regulate mesendoderm migration? The results presented in Chapter 3 show that loss of PG leads to

changes in FAs dynamics in the leader cells of mesendoderm tissue and that cells are unable to exert traction forces necessary for mesendoderm migration. This suggests that PG regulates integrin-based adhesions. Furthermore, co-localization of keratin IFs and PG to form hemidesmosomal-like junction in dissociated mesendoderm plated on FN matrix and that the formation of this hemidesmosomal-like junction requires activation of integrins (Figure 3.6). These observations suggest that PG may regulate the mechanical crosstalk between integrin and cadherin adhesions by physically coupling cell-ECM and cell-cell adhesions (Figure 3.7). CALI experiments could be performed using myc-PG-Supernova construct to disrupt these hemidesmosomal-like junctions and observe the effect on organization and migration of mesendoderm tissue. Disruption of these junctions could lead to detachment of keratin IFs from the junctions and decoupling of integrin and cadherin adhesions; this, in turn, would cause changes in the distribution of traction forces due to an imbalance of forces between integrin and cadherin adhesions.

4.4 Conclusions

Morphogenesis plays important roles in both physiological and pathological processes. By studying morphogenetic movement in embryonic development, we can gain better insight into the mechanisms that are misregulated in developmental disorders and how diseases such as cancer progress. The work presented in this dissertation primarily focuses on the migration of mesendoderm tissue and the forces that are generated during this process. I have identified novel roles for keratin IFs and PG, components of the mechanosensitive cadherin complex, in regulating collective migration of mesendoderm tissue. Both keratin IFs and PG are involved in tension mediated organization of the

mesendoderm tissue. This study also highlights the importance of achieving the proper balance of forces between cell-cell and cell-ECM adhesions during morphogenesis. Thus, these data provide key mechanistic insights on how forces contribute to regulate coordinated cellular behaviors during morphogenesis.

Figure 4.1: Expression of Supernova-krt8 in dissociated mesendoderm cells.

Supernova is variant of KillerRed fluorescent protein and has an excitation/emission maxima at 579/610nm. Supernova-krt8 construct was generated to perform CALI. Expression of Supernova-krt8 was tested by injecting 250pg of RNA each encoding Supernova-krt8 and EGFP-krt8. Mesendoderm tissue expressing the RNA was dissociated in CMF MBS and plated on 10ug/ml FN-coated glass bottom dish. Images of mesendoderm were collected on Nikon C1 confocal microscope. (A-C) Representative image of mesendoderm cells expressing (A) EGFP-krt8 and (B) Supernova-krt8. (C) shows the merge of the two channels and complete overlap of EGFP-krt9 and Supernova-krt8 (yellow). This shows the Supernova-krt8 construct can synthesize krt8, which can be incorporated into the keratin IF network by mesendoderm cells successfully.

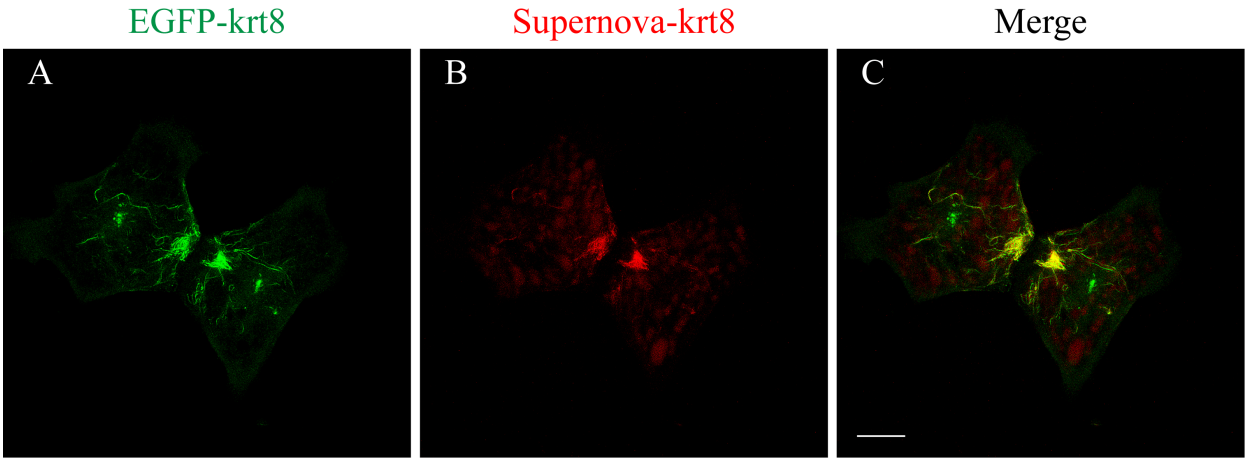
EGFP-krt8
Supernova-krt8
Merge
A
B
C

Figure 4.2 Expression of DP in gastrula stage embryos.

(A) Western blot analysis was done to determine levels of DP expression in whole embryos, animal cap and mesendoderm tissue. Arrow indicates DP (molecular weight: ~330kDa). (B) Titration of WEL was done to determine the specificity of the anti-DP antibody (1:500 dilution). Lysate volume equivalent to 2 embryos, 1 embryo and 0.5 embryo was loaded on the gel and probed with the anti-DP antibody. Arrow indicates DP band intensity, which decreases as the volume loaded on the gel decreases. (C) In order to ensure that proteins with large molecular weight are not excluded while performing this analysis, levels of FN (~220kDa) were also detected. 4H2 antibody was used to probe for FN (1:3000 dilution). (D) Secondary alone control to determine the specificity of the anti-DP antibody. Blot was probed with anti-mouse secondary antibody alone. Secondary antibody alone does not recognize any band at 300kDa. (A-D) Tubulin was used as loading control. Anti-Tubulin antibody (Clone DM1A Sigma) was used at a dilution of 1:10,000. Analysis of tubulin blot was done using LICOR instruments (Secondary antibody: Donkey anti-mouse IRDye 800CW).

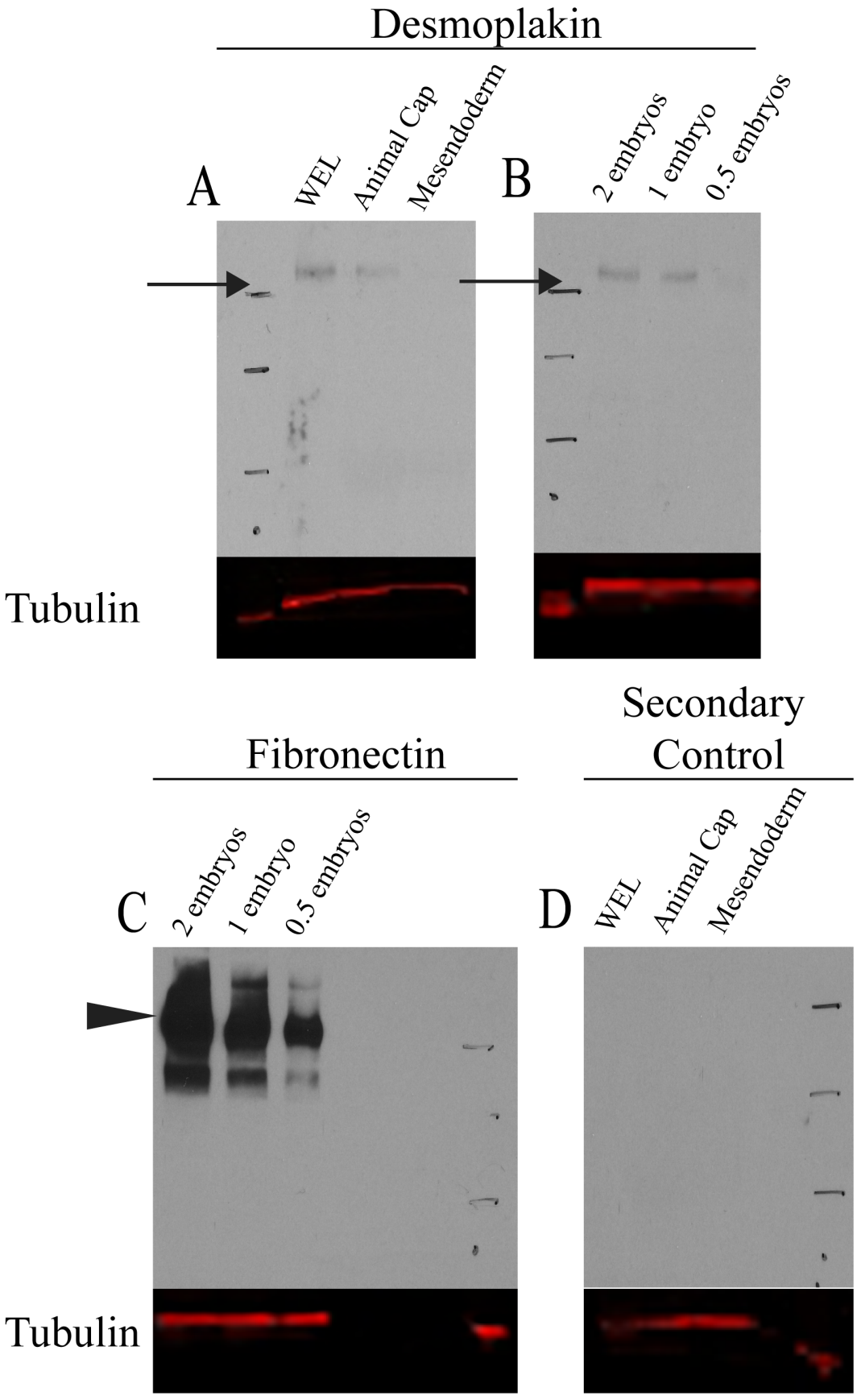
Desmoplakin
A
WEL
Animal Cap
Mesendoderm
B
2 embryos
1 embryo
0.5 embryos
Tubulin
Secondary Control
Fibronectin
C
2 embryos
1 embryo
0.5 embryos
D
WEL
Animal Cap
Mesendoderm
Tubulin

Figure 4.3: PG staining at the lamellipodial protrusions.

(A) Representative images of mesendoderm explants fixed and stained with (B) PG (BD Biosciences #610253; green) and (C) Pan keratin (Thermo Fischer #PA1-27114; red) primary antibodies. Primary antibody staining was followed by followed by secondary antibodies (Anti-mouse Alexa 488 against PG and Anti-Rabbit Alexa 555 against keratin). Arrows in (A and B) indicate PG staining the lamellipodial protrusions. (D) Image of fixed mesendoderm explant probed with only secondary antibodies (Anti-mouse Alexa 488 and Anti-Rabbit Alexa 555). Secondary alone control was done to ensure the specificity of PG staining in the lamellipodial protrusions.

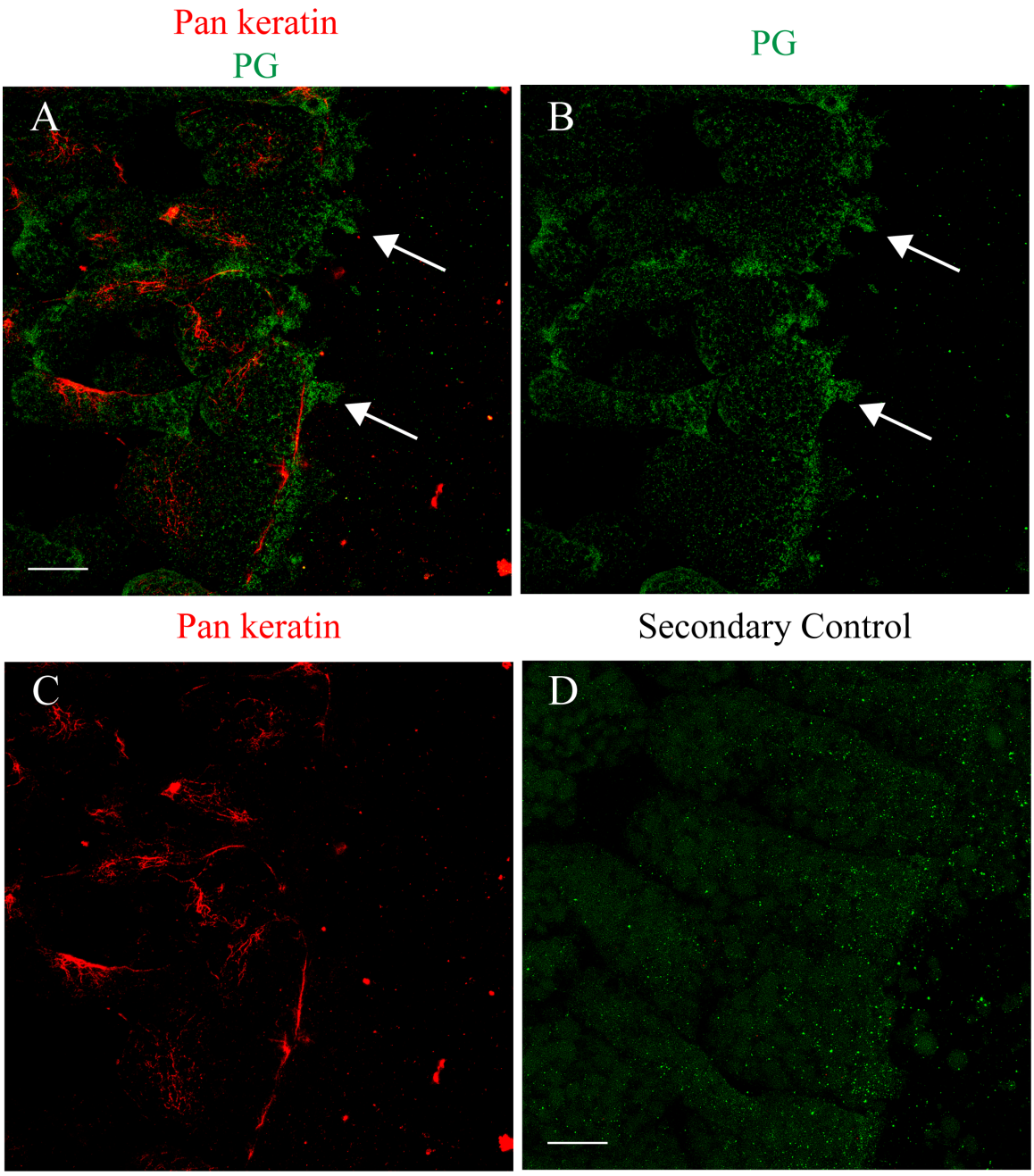
Pan keratin
PG
PG
A
B
Pan keratin
Secondary Control
C
D

Figure 4.4: A proposed model of signaling networks in collectively migrating mesendoderm tissue.

The cartoon shows a cross section of mesendoderm tissue migrating on FN matrix along with key components of the signaling networks proposed to play important role in regulating cell polarity and interaction between cytoskeletal interaction.

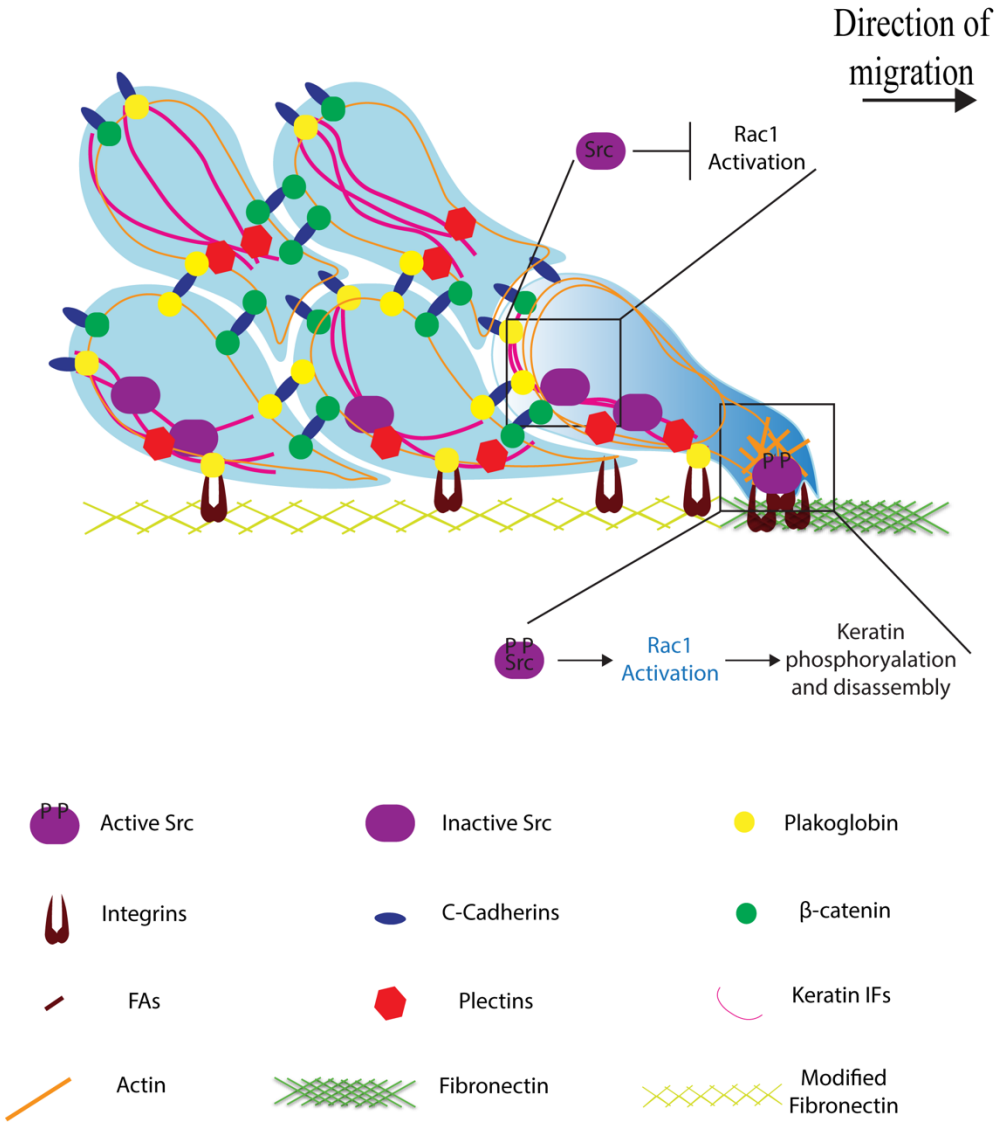
Direction of migration
Src
Rac1 Activation
P P
P P Src
Rac1 Activation
Keratin phosphoryalation and disassembly
P P Active Src
Inactive Src
Plakoglobin
Integrins
C-Cadherins
β-catenin
FAs
Plectins
Keratin IFs
Actin
Fibronectin
Modified Fibronectin

Reference:

Abercrombie, M. and Heaysman, J. E. (1954). Observations on the social behaviour of cells in tissue culture. II. Monolayering of fibroblasts. *Exp. Cell Res.* **6**, 293–306.

Aegerter-Wilmsen, T., Heimlicher, M. B., Smith, A. C., de Reuille, P. B., Smith, R. S., Aegerter, C. M. and Basler, K. (2012). Integrating force-sensing and signaling pathways in a model for the regulation of wing imaginal disc size. *Development* **139**, 3221–3231.

Albert Basson, M. (2012). Signaling in cell differentiation and morphogenesis. *Cold Spring Harb. Perspect. Biol.* **4**, 1–21.

Allen, E., Yu, Q. C. and Fuchs, E. (1996). Mice expressing a mutant desmosomal cadherin exhibit abnormalities in desmosomes, proliferation, and epidermal differentiation. *J. Cell Biol.* **133**, 1367–1382.

Aman, A. and Piotrowski, T. (2008). Wnt/β-Catenin and Fgf Signaling Control Collective Cell Migration by Restricting Chemokine Receptor Expression. *Dev. Cell* **15**, 749–761.

Andresen Eguiluz, R. C., Kaylan, K. B., Underhill, G. H. and Leckband, D. E. (2017). Substrate stiffness and VE-cadherin mechano-transduction coordinate to regulate endothelial monolayer integrity. *Biomaterials* **140**, 45–57.

Aplin, A. E. (2003). Cell adhesion molecule regulation of nucleocytoplasmic trafficking. *FEBS Lett.* **534**, 11–14.

Arnsdorf, E. J., Tummala, P., Kwon, R. Y. and Jacobs, C. R. (2009a). Mechanically induced osteogenic differentiation - the role of RhoA, ROCKII and cytoskeletal dynamics. *J. Cell Sci.* **122**, 546–553.

Arnsdorf, E. J., Tummala, P. and Jacobs, C. R. (2009b). Non-canonical Wnt signaling and N-cadherin related β-catenin signaling play a role in mechanically induced osteogenic cell fate. *PLoS One* **4**, e5388.

Bahm, I., Barriga, E. H., Frolov, A., Theveneau, E., Frankel, P. and Mayor, R. (2017). PDGF controls contact inhibition of locomotion by regulating N-cadherin during neural crest migration. *Development* **144**, 2456–2468.

Barriga, E. H., Franze, K., Charras, G. and Mayor, R. (2018). Tissue stiffening coordinates morphogenesis by triggering collective cell migration in vivo. *Nature* **554**, 523–527.

Barry, A. K., Tabdili, H., Muhamed, I., Wu, J., Shashikanth, N., Gomez, G. A., Yap, A. S., Gottardi, C. J., de Rooij, J., Wang, N., and Leckband, D.E. (2014). α-Catenin cytomechanics - role in cadherin-dependent adhesion and mechanotransduction. *J. Cell Sci.* **127**, 1779–1791.

Beck, J. N., Singh, A., Rothenberg, A. R., Elisseeff, J. H. and Ewald, A. J. (2013). The independent roles of mechanical, structural and adhesion characteristics of 3D

hydrogels on the regulation of cancer invasion and dissemination. *Biomaterials* **34**, 9486–9495.

Beloussov, L. V, Dorfman, J. G. and Cherdantzev, V. G. (1975). Mechanical stresses and morphological patterns in amphibian embryos. *J. Embryol. Exp. Morphol.* **34**, 559–574.

Beningo, K. A., Dembo, M., Kaverina, I., Small, J. V. and Wang, Y. L. (2001). Nascent focal adhesions are responsible for the generation of strong propulsive forces in migrating fibroblasts. *J. Cell Biol.* **153**, 881–887.

Bertet, C., Sulak, L. and Lecuit, T. (2004). Myosin-dependent junction remodelling controls planar cell intercalation and axis elongation. *Nature* **429**, 667–671.

Bierkamp, C., Mclaughlin, K. J., Schwarz, H., Huber, O. and Kemler, R. (1996). Embryonic heart and skin defects in mice lacking plakoglobin. *Dev. Biol.* **180**, 780–785.

Bierkamp, C., Schwarz, H., Huber, O. and Kemler, R. (1999). Desmosomal localization of β-catenin in the skin of plakoglobin null-mutant mice. *Development* **126**, 371–381.

Bischoff, M., Gradilla, A. C., Seijo, I., Andrés, G., Rodríguez-Navas, C., González-Méndez, L. and Guerrero, I. (2013). Cytonemes are required for the establishment of a normal Hedgehog morphogen gradient in Drosophila epithelia. *Nat. Cell Biol.* **15**, 1269–1281.

Bjerke, M. A., Dzamba, B., Wang, C. and DeSimone, D. W. (2014). FAK Is required for tension-dependent organization of collective cell movements in *Xenopus* mesendoderm. *Dev. Biol.* **394**, 1–17.

Blaue, C., Kashef, J. and Franz, C. M. (2018). Cadherin-11 promotes neural crest cell spreading by reducing intracellular tension—Mapping adhesion and mechanics in neural crest explants by atomic force microscopy. *Semin. Cell Dev. Biol.* **73**, 95–106.

Borghi, N., Lowndes, M., Maruthamuthu, V., Gardel, M. L. and Nelson, W. J. (2010). Regulation of cell motile behavior by crosstalk between cadherin- and integrin-mediated adhesions. *Proc. Natl. Acad. Sci.* **107**, 13324–13329.

Borghi, N., Sorokina, M., Shcherbakova, O. G., Weis, W. I., Pruitt, B. L., Nelson, W. J. and Dunn, A. R. (2012). E-cadherin is under constitutive actomyosin-generated tension that is increased at cell-cell contacts upon externally applied stretch. *Proc. Natl. Acad. Sci.* **109**, 12568–12573.

Borradori, L. and Sonnenberg, A. (1999). Structure and function of hemidesmosomes: More than simple adhesion complexes. *J. Invest. Dermatol.* **112**, 411–418.

Boselli, F., Freund, J. B. and Vermot, J. (2015). Blood flow mechanics in cardiovascular development. *Cell. Mol. Life Sci.* **72**, 2545–2559.

Bosveld, F., Bonnet, I., Guirao, B., Tlili, S., Wang, Z., Petitalot, A., Marchand, R., Bardet, P.-L., Marcq, P., Graner, F., et al. (2012). Mechanical control of morphogenesis by Fat/Dachsous/Four-jointed planar cell polarity pathway. *Science*

336, 724–7.

Bosveld, F., Markova, O., Guirao, B., Martin, C., Wang, Z., Pierre, A., Balakireva, M., Gaugue, I., Ainslie, A., Christophorou, N., Lubensky, D.K., Minc, N. and Bellaïche. (2016). Epithelial tricellular junctions act as interphase cell shape sensors to orient mitosis. *Nature* **530**, 495–498.

Boucaut, J. C., Johnson, K. E., Darribere, T., Shi, D. L., Riou, J. F., Bache, H. B. and Delarue, M. (1990). Fibronectin-rich fibrillar extracellular matrix controls cell migration during amphibian gastrulation. *Int. J. Dev. Biol.* **34**, 139–147.

Brand, T. (2003). Heart development: Molecular insights into cardiac specification and early morphogenesis. *Dev. Biol.* **258**, 1–19.

Brangwynne, C. P., MacKintosh, F. C., Kumar, S., Geisse, N. A., Talbot, J., Mahadevan, L., Parker, K. K., Ingber, D. E. and Weitz, D. A. (2006). Microtubules can bear enhanced compressive loads in living cells because of lateral reinforcement. *J. Cell Biol.* **173**, 733–741.

Brugués, A., Anon, E., Conte, V., Veldhuis, J. H., Gupta, M., Colombelli, J., Muñoz, J. J., Brodland, G. W., Ladoux, B. and Trepat, X. (2014). Forces driving epithelial wound healing. *Nat. Phys.* **10**, 683–690.

Buckley, C. D., Tan, J., Anderson, K. L., Hanein, D., Volkmann, N., Weis, W. I., Nelson, W. J. and Dunn, A. R. (2014). The minimal cadherin-catenin complex binds to actin filaments under force. *Science (80-.).* **346**,.

Butler, J. P., Tolic-Norrelykke, I. M., Fabry, B. and Fredberg, J. J. (2002). Traction fields, moments, and strain energy that cells exert on their surroundings. *AJP Cell Physiol.* **282**, C595–C605.

Butler, L. C., Blanchard, G. B., Kabla, A. J., Lawrence, N. J., Welchman, D. P., Mahadevan, L., Adams, R. J. and Sanson, B. (2009). Cell shape changes indicate a role for extrinsic tensile forces in Drosophila germ-band extension. *Nat. Cell Biol.* **11**, 859–864.

Cai, D., Chen, S. C., Prasad, M., He, L., Wang, X., Choesmel-Cadamuro, V., Sawyer, J. K., Danuser, G. and Montell, D. J. (2014). Mechanical feedback through E-cadherin promotes direction sensing during collective cell migration. *Cell* **157**, 1146–1159.

Califano, J. P. and Reinhart-King, C. A. (2010). Exogenous and endogenous force regulation of endothelial cell behavior. *J. Biomech.* **43**, 79–86.

Campbell, K. and Casanova, J. (2016). A common framework for EMT and collective cell migration. *Development* **143**, 4291–4300.

Campbell, I. D. and Humphries, M. J. (2011). Integrin structure, activation, and interactions. *Cold Spring Harb. Perspect. Biol.* **3**, 1–14.

Campinho, P., Behrndt, M., Ranft, J., Risler, T., Minc, N. and Heisenberg, C. P. (2013). Tension-oriented cell divisions limit anisotropic tissue tension in epithelial

spreading during zebrafish epiboly. *Nat. Cell Biol.* **15**, 1405–1414.

Carisey, A., Tsang, R., Greiner, A. M., Nijenhuis, N., Heath, N., Nazgiewicz, A., Kemkemer, R., Derby, B., Spatz, J. and Ballestrem, C. (2013). Vinculin regulates the recruitment and release of core focal adhesion proteins in a force-dependent manner. *Curr. Biol.* **23**, 271–281.

Case, L. B. and Waterman, C. M. (2015). Integration of actin dynamics and cell adhesion by a three-dimensional, mechanosensitive molecular clutch. *Nat. Cell Biol.* **17**, 955–963.

Caussinus, E., Colombelli, J. and Affolter, M. (2008). Tip-Cell Migration Controls Stalk-Cell Intercalation during Drosophila Tracheal Tube Elongation. *Curr. Biol.* **18**, 1727–1734.

Cavey, M. and Lecuit, T. (2016). Molecular Bases of Cell – Cell Junctions Stability and Dynamics. 1–19.

Cetera, M., Ramirez-San Juan, G. R., Oakes, P. W., Lewellyn, L., Fairchild, M. J., Tanentzapf, G., Gardel, M. L. and Horne-Badovinac, S. (2014). Epithelial rotation promotes the global alignment of contractile actin bundles during Drosophila egg chamber elongation. *Nat. Commun.* **5**, 1–12.

Chanet, S. and Martin, A. C. (2014). Mechanical Force Sensing in Tissues. *Prog Mol Biol Transl Sci.* **126**, 317–352.

Cheffings, T. H., Burroughs, N. J. and Balasubramanian, M. K. (2016). Actomyosin Ring Formation and Tension Generation in Eukaryotic Cytokinesis. *Curr. Biol.* **26**, R719–R737.

Chen, Y. and Periasamy, A. (2006). Intensity range based quantitative FRET data analysis to localize protein molecules in live cell nuclei. *J. Fluoresc.* **16**, 95–104.

Chen, P., Melchior, C., Brons, N. H. C., Schlegel, N., Caen, J. and Kieffer, N. (2001). Probing conformational changes in the I-like domain and the cysteine-rich repeat of human β3 integrins following disulfide bond disruption by cysteine mutations. Identification of cysteine 598 involved in αIIbβ3 activation. *J. Biol. Chem.* **276**, 38628–38635.

Chen, C. S., Tan, J. and Tien, J. (2004). Mechanotransduction at Cell-Matrix and Cell-Cell Contacts. *Annu. Rev. Biomed. Eng.* **6**, 275–302.

Cheung, K. J., Gabrielson, E., Werb, Z. and Ewald, A. J. (2013). Collective invasion in breast cancer requires a conserved basal epithelial program. *Cell* **155**, 1639–1651.

Cheung, K. J., Padmanaban, V., Silvestri, V., Schipper, K., Cohen, J. D., Fairchild, A. N., Gorin, M. A., Verdone, J. E., Pienta, K. J., Bader, J. S., et al. (2016). Polyclonal breast cancer metastases arise from collective dissemination of keratin 14-expressing tumor cell clusters. *Proc. Natl. Acad. Sci.* **113**, E854–E863.

Choi, C. K., Vicente-Manzanares, M., Zareno, J., Whitmore, L. A., Mogilner, A. and Horwitz, A. R. (2008). Actin and α-actinin orchestrate the assembly and maturation

of nascent adhesions in a myosin II motor-independent manner. *Nat. Cell Biol.* **10**, 1039–1050.

Choi, H. J., Gross, J. C., Pokutta, S. and Weis, W. I. (2009). Interactions of plakoglobin and β-catenin with desmosomal cadherins: Basis of selective exclusion of α- and β-catenin from desmosomes. *J. Biol. Chem.* **284**, 31776–31788.

Choma, D. P., Milano, V., Pumiglia, K. M. and DiPersio, C. M. (2007). Integrin α3β1-dependent activation of FAK/Src regulates Rac1-mediated keratinocyte polarization on laminin-5. *J. Invest. Dermatol.* **127**, 31–40.

Choquet, D., Felsenfeld, D. P. and Sheetz, M. P. (1997). Extracellular matrix rigidity causes strengthening of integrin- cytoskeleton linkages. *Cell* **88**, 39–48.

Chrzanowska-Wodnicka, M. and Burridge, K. (1996). Drives the Contractility Formation of Stress Fibers and Focal Adhesions. *J. Cell Biol.* **133**, 1403–1415.

Chung, B. M., Rotty, J. D. and Coulombe, P. A. (2013). Networking galore: Intermediate filaments and cell migration. *Curr. Opin. Cell Biol.* **25**, 600–612.

Clark, K., Langeslag, M., Figdor, C. G. and van Leeuwen, F. N. (2007). Myosin II and mechanotransduction: a balancing act. *Trends Cell Biol.* **17**, 178–186.

Collins, C. and Nelson, W. J. (2015). Running with neighbors: Coordinating cell migration and cell-cell adhesion. *Curr. Opin. Cell Biol.* **36**, 62–70.

Conway, D. E., Breckenridge, M. T., Hinde, E., Gratton, E., Chen, C. S. and Schwartz, M. A. (2013). Fluid shear stress on endothelial cells modulates mechanical tension across VE-cadherin and PECAM-1. *Curr. Biol.* **23**, 1024–1030.

Costigliola, N., Ding, L., Burckhardt, C. J., Han, S. J., Gutierrez, E., Mota, A., Groisman, A., Mitchison, T. J. and Danuser, G. (2017). Vimentin fibers orient traction stress. *Proc. Natl. Acad. Sci.* **114**, 5195–5200.

Coulombe, P. A. and Lee, C. H. (2012). Defining keratin protein function in skin epithelia: Epidermolysis bullosa simplex and its aftermath. *J. Invest. Dermatol.* **132**, 763–775.

Coulombe, P. A., Hutton, M. E., Vassar, R. and Fuchs, E. (1991). A function for keratins and a common thread among different types of epidermolysis bullosa simplex diseases. *J. Cell Biol.* **115**, 1661–1674.

Cowin, P., Kapprell, H. P., Franke, W. W., Tamkun, J. and Hynes, R. O. (1986). Plakoglobin: A protein common to different kinds of intercellular adhering junctions. *Cell* **46**, 1063–1073.

Crest, J., Diz-Muñoz, A., Chen, D. Y., Fletcher, D. A. and Bilder, D. (2017). Organ sculpting by patterned extracellular matrix stiffness. *Elife* **6**,.

Daley, W. P., Kohn, J. M. and Larsen, M. (2011). A focal adhesion protein-based mechanochemical checkpoint regulates cleft progression during branching morphogenesis. *Dev. Dyn.* **240**, 2069–2083.

Dalle Nogare, D., Somers, K., Rao, S., Matsuda, M., Reichman-Fried, M., Raz, E. and Chitnis, A. B. (2014). Leading and trailing cells cooperate in collective migration of the zebrafish posterior lateral line primordium. *Development* **141**, 3188–3196.

Danilchik, M., Williams, M. and Brown, E. (2013). Blastocoel-spanning filopodia in cleavage-stage *Xenopus* laevis: Potential roles in morphogen distribution and detection. *Dev. Biol.* **382**, 70–81.

Das, T., Safferling, K., Rausch, S., Grabe, N., Boehm, H. and Spatz, J. P. (2015). A molecular mechanotransduction pathway regulates collective migration of epithelial cells. *Nat. Cell Biol.* **17**, 276–287.

David, N. B., Sapède, D., Saint-Etienne, L., Thisse, C., Thisse, B., Dambly-Chaudière, C., Rosa, F. M. and Ghysen, A. (2002). Molecular basis of cell migration in the fish lateral line: role of the chemokine receptor CXCR4 and of its ligand, SDF1. *Proc. Natl. Acad. Sci. U. S. A.* **99**, 16297–16302.

Davidson, L. A., Hoffstrom, B. G., Keller, R. and DeSimone, D. W. (2002). Mesendoderm extension and mantle closure in *Xenopus* laevis gastrulation: Combined roles for integrin α5β1, fibronectin, and tissue geometry. *Dev. Biol.* **242**, 109–129.

Davidson, L. A., Keller, R. and DeSimone, D. W. (2004). Assembly and remodeling of the fibrillar fibronectin extracellular matrix during gastrulation and neurulation in *Xenopus* laevis. *Dev. Dyn.* **231**, 888–895.

Del Pozo, M. A., Kiosses, W. B., Alderson, N. B., Meller, N., Hahn, K. M. and Schwartz, M. A. (2002). Integrins regulate GTP-Rac localized effector interactions through dissociation of Rho-GDI. *Nat. Cell Biol.* **4**, 232–239.

Del Rio, A., Perez-Jimenez, R., Liu, R., Roca-Cusachs, P., Fernandez, J. M. and Sheetz, M. P. (2009). Stretching single talin rod molecules activates vinculin binding. *Science (80-.).* **323**, 638–641.

DeMaio, L., Tarbell, J. M., Scaduto, R. C., Gardner, T. W. and Antonetti, D. a (2004). A transmural pressure gradient induces mechanical and biological adaptive responses in endothelial cells. *Am. J. Physiol. Heart Circ. Physiol.* **286**, H731-41.

Desai, R., Sarpal, R., Ishiyama, N., Pellikka, M., Ikura, M. and Tepass, U. (2013). Monomeric α-catenin links cadherin to the actin cytoskeleton. *Nat. Cell Biol.* **15**, 261–273.

Diaz-Gonzalez, F., Hughes, P. E., Diaz-Gonzalez, F., Leong, L., Wu, C., McDonald, J. A., Shattil, S. J. and Ginsberg, M. H. (1996). Breaking the Integrin Hinge. *J. Biol. Chem.* **271**, 6571–6574.

Dicko, M., Saramito, P., Blanchard, G. B., Lye, C. M., Sanson, B. and Étienne, J. (2017). Geometry can provide long-range mechanical guidance for embryogenesis. *PLoS Comput. Biol.* **13**, 1–30.

Dimitriadis, E. K., Horkay, F., Maresca, J., Kachar, B. and Chadwick, R. S. (2002). Determination of elastic moduli of thin layers of soft material using the atomic force

microscope. *Biophys. J.* **82**, 2798–2810.

Dowling, J., Yu, Q. C. and Fuchs, E. (1996). Beta4 integrin is required for hemidesmosome formation, cell adhesion and cell survival. *J. Cell Biol.* **134**, 559–72.

Drees, F., Pokutta, S., Yamada, S., Nelson, W. J. and Weis, W. I. (2005). α-catenin is a molecular switch that binds E-cadherin-β-catenin and regulates actin-filament assembly. *Cell* **123**, 903–915.

Du, X., Plow, E. F., Frelinger, A. L., O'Toole, T. E., Loftus, J. C. and Ginsberg, M. H. (1991). Ligands "activate" integrin αIIbβ3 (platelet GPIIb-IIIa). *Cell* **65**, 409–416.

du Roure, O., Saez, A., Buguin, A., Austin, R. H., Chavrier, P., Silberzan, P. and Ladoux, B. (2005). Force mapping in epithelial cell migration. *Proc. Natl. Acad. Sci.* **102**, 2390–2395.

Dufour, S., Mège, R. M. and Thiery, J. P. (2013). α-catenin, vinculin, and F-actin in strengthening E-cadherin cell-cell adhesions and mechanosensing. *Cell Adhes. Migr.* **7**, 345–350.

Dumbauld, D. W., Lee, T. T., Singh, A., Scrimgeour, J., Gersbach, C. A., Zamir, E. A., Fu, J., Chen, C. S., Curtis, J. E., Craig, S. W., and García, A.J. (2013). How vinculin regulates force transmission. *Proc. Natl. Acad. Sci.* **110**, 9788–9793.

Dumortier, J. G., Martin, S., Meyer, D., Rosa, F. M. and David, N. B. (2012). Collective mesendoderm migration relies on an intrinsic directionality signal transmitted through cell contacts. *Proc. Natl. Acad. Sci.* **109**, 16945–16950.

Dzamba, B. J., Jakab, K. R., Marsden, M., Schwartz, M. a and DeSimone, D. W. (2009). Cadherin adhesion, tissue tension, and noncanonical Wnt signaling regulate fibronectin matrix organization. *Dev. Cell* **16**, 421–32.

Eckert, B. S. and Yeagle, P. L. (1988). Acrylamide treatment of PtKl cells causes dephosphorylation of keratin polypeptides. *Cell Motil. Cytoskeleton* **11**, 24–30.

Eder, D., Aegerter, C. and Basler, K. (2017). Forces controlling organ growth and size. *Mech. Dev.* **144**, 53–61.

Elting, M. W., Hueschen, C. L., Udy, D. B. and Dumont, S. (2014). Force on spindle microtubule minus ends moves chromosomes. *J. Cell Biol.* **206**, 245–256.

Engler, A. J., Sen, S., Sweeney, H. L. and Discher, D. E. (2006). Matrix elasticity directs stem cell lineage specification. *Cell* **126**, 677–89.

Even-Ram, S., Doyle, A. D., Conti, M. A., Matsumoto, K., Adelstein, R. S. and Yamada, K. M. (2007). Myosin IIA regulates cell motility and actomyosin-microtubule crosstalk. *Nat. Cell Biol.* **9**, 299–309.

Ewald, A. J., Brenot, A., Duong, M., Chan, B. S. and Werb, Z. (2008). Collective Epithelial Migration and Cell Rearrangements Drive Mammary Branching Morphogenesis. *Dev. Cell* **14**, 570–581.

Fagotto, F., Funayama, N., Glück, U. and Gumbiner, B. M. (1996). Binding to

cadherins antagonizes the signaling activity of β-catenin during axis formation in *Xenopus*. *J. Cell Biol.* **132**, 1105–1114.

Fagotto, F., Guger, K. and Gumbiner, B. M. (1997). Induction of the primary dorsalizing center in *Xenopus* by the Wnt/GSK/β-catenin signaling pathway, but not by Vg1, Activin or Noggin. *Development* **124**, 453–460.

Farooqui, R. and Fenteany, G. (2005). Multiple rows of cells behind an epithelial wound edge extend cryptic lamellipodia to collectively drive cell-sheet movement. *J. Cell Sci.* **118**, 51–63.

Fata, J. E., Werb, Z. and Bissell, M. J. (2003). Regulation of mammary gland branching morphogenesis by the extracellular matrix and its remodeling enzymes. *Breast Cancer Res.* **6**, 1.

Fernandez-Gonzalez, R., Simoes, S. de M., Röper, J. C., Eaton, S. and Zallen, J. A. (2009). Myosin II Dynamics Are Regulated by Tension in Intercalating Cells. *Dev. Cell* **17**, 736–743.

Fink, J., Carpi, N., Betz, T., Bétard, A., Chebah, M., Azioune, A., Bornens, M., Sykes, C., Fetler, L., Cuvelier, D., and Matthieu, P. (2011). External forces control mitotic spindle positioning. *Nat. Cell Biol.* **13**, 771–778.

Forth, S. and Kapoor, T. M. (2017). The mechanics of microtubule networks in cell division. *J. Cell Biol.* **216**, 1525–1531.

Franke, J. D., Montague, R. A. and Kiehart, D. P. (2005). Nonmuscle myosin II generates forces that transmit tension and drive contraction in multiple tissues during dorsal closure. *Curr. Biol.* **15**, 2208–2221.

Franz, J. K. and Franke, W. W. (1986). Cloning of cDNA and amino acid sequence of a cytokeratin expressed in oocytes of *Xenopus* laevis. *Proc. Natl. Acad. Sci. U. S. A.* **83**, 6475–9.

Franz, J. K., Gall, L., Williams, M. A., Picheral, B. and Franke, W. W. (1983). Intermediate-size filaments in a germ cell: Expression of cytokeratins in oocytes and eggs of the frog *Xenopus*. *Proc. Natl. Acad. Sci. U. S. A.* **80**, 6254–8.

Friedl, P. and Gilmour, D. (2009). Collective cell migration in morphogenesis, regeneration and cancer. *Nat. Rev. Mol. Cell Biol.* **10**, 445–57.

Friedl, P., Wolf, K. and Lammerding, J. (2011). Nuclear mechanics during cell migration. *Curr. Opin. Cell Biol.* **23**, 55–64.

Friedland, J. C., Lee, M. H. and Boettiger, D. (2009). Mechanically activated integrin switch controls α5β1 function. *Sci. STKE* **323**, 642.

Fujiwara, S., Ohashi, K., Mashiko, T., Kondo, H. and Mizuno, K. (2016). Interplay between Solo and keratin filaments is crucial for mechanical force-induced stress fiber reinforcement. *Mol. Biol. Cell* **27**, 954–966.

Gaggioli, C., Hooper, S., Hidalgo-Carcedo, C., Grosse, R., Marshall, J. F.,

Harrington, K. and Sahai, E. (2007). Fibroblast-led collective invasion of carcinoma cells with differing roles for RhoGTPases in leading and following cells. *Nat. Cell Biol.* **9**, 1392–1400.

Galbraith, C. G. and Sheetz, M. P. (1999). Keratocytes pull with similar forces on their dorsal and ventral surfaces. *J. Cell Biol.* **147**, 1313–1323.

Gallicano, G. I., Bauer, C. and Fuchs, E. (2001). Rescuing desmoplakin function in extra-embryonic ectoderm reveals the importance of this protein in embryonic heart, neuroepithelium, skin and vasculature. *Development* **128**, 929–41.

Georges-Labouesse, E., Messaddeq, N., Yehia, G., Cadalbert, L., Dierich, A. and Le Meur, M. (1996). Absence of integrin α6 leads to epidermolysis bullosa and neonatal death in mice. *Nat. Genet.* **13**, 370–373.

Girard, P. R. and Nerem, R. M. (1995). Shear stress modulates endothelial cell morphology and F-actin organization through the regulation of focal adhesion-associated proteins. *J. Cell. Physiol.* **163**, 179–193.

Godsel, L. M., Hsieh, S. N., Amargo, E. V, Bass, A. E., Pascoe-mcgillicuddy, L. T., Huen, A. C., Thorne, M. E., Gaudry, C. A., Park, J. K., Myung, K., et al. (2005). Desmoplakin assembly dynamics in four dimensions: multiple phases differentially regulated by intermediate filaments and actin. *J. Cell Biol.* 1045–1059.

Graham, D. M. and Burridge, K. (2016). Mechanotransduction and nuclear function. *Curr. Opin. Cell Biol.* **40**, 98–105.

Grashoff, C., Hoffman, B. D., Brenner, M. D., Zhou, R., Parsons, M., Yang, M. T., McLean, M. A., Sligar, S. G., Chen, C. S., Ha, T., et al. (2010). Measuring mechanical tension across vinculin reveals regulation of focal adhesion dynamics. *Nature* **466**, 263–266.

Gregor, M., Osmanagic-Myers, S., Burgstaller, G., Wolfram, M., Fischer, I., Walko, G., Resch, G. P., Jörgl, A., Herrmann, H. and Wiche, G. (2014). Mechanosensing through focal adhesion-anchored intermediate filaments. *FASEB J.* **28**, 715–729.

Grimes, D. T. and Burdine, R. D. (2017). Left–Right Patterning: Breaking Symmetry to Asymmetric Morphogenesis. *Trends Genet.* **33**, 616–628.

Grossmann, K. S., Grund, C., Huelsken, J., Behrend, M., Erdmann, B., Franke, W. W. and Birchmeier, W. (2004). Requirement of plakophilin2 for heart morphogenesis and cardiac junction formation. *J. Cell Biol.* **167**, 149–160.

Guger, K. A. and Gumbiner, B. M. (1995). β-Catenin has Wnt-like activity and mimics the Nieuwkoop signaling center in *Xenopus* dorsal-ventral patterning. *Dev. Biol.* **172**, 115–125.

Guilluy, C., Osborne, L. D., Van Landeghem, L., Sharek, L., Superfine, R., Garcia-Mata, R. and Burridge, K. (2014). Isolated nuclei adapt to force and reveal a mechanotransduction pathway in the nucleus. *Nat. Cell Biol.* **16**, 376–381.

Gumbiner, B. M. (2005). Regulation of cadherin-mediated adhesion in morphogenesis.

Nat. Rev. Mol. Cell Biol. **6**, 622–34.

Gumbiner, B. M. and McCrea, P. D. (1993). Catenins as mediators of the cytoplasmic functions of cadherins. *J. Cell Sci. Suppl.* **17**, 155–158.

Gutzeit, H. (1990). The microfilament pattern in the somatic follicle cells of mid - vitellogenic ovarian follicles of Drosophila . *Eur J Cell Biol.* **53**, 349–56.

Haas, P. and Gilmour, D. (2006). Chemokine Signaling Mediates Self-Organizing Tissue Migration in the Zebrafish Lateral Line. *Dev. Cell* **10**, 673–680.

Haigo, S. L. and Bilder, D. (2011). Global tissue revolutions in a morphogenetic movement controlling elongation. *Science (80-.).* **331**, 1071–1074.

Hansen, S. D., Kwiatkowski, A. V., Ouyang, C.-Y., Liu, H., Pokutta, S., Watkins, S. C., Volkmann, N., Hanein, D., Weis, W. I., Mullins, R. D., et al. (2013). αE-catenin actin-binding domain alters actin filament conformation and regulates binding of nucleation and disassembly factors. *Mol. Biol. Cell* **24**, 3710–3720.

Happe, C. L. and Engler, A. J. (2016). Mechanical Forces Reshape Differentiation Cues That Guide Cardiomyogenesis. *Circ. Res.* **118**, 296–310.

Hara, Y., Nagayama, K., Yamamoto, T. S., Matsumoto, T., Suzuki, M. and Ueno, N. (2013). Directional migration of leading-edge mesoderm generates physical forces: Implication in *Xenopus* notochord formation during gastrulation. *Dev. Biol.* **382**, 482–495.

Hastings, N. E., Simmers, M. B., Mcdonald, O. G., Wamhoff, B. R. and Blackman, B. R. (2007). Atherosclerosis-prone hemodynamics differentially regulates endothelial and smooth muscle cell phenotypes and promotes pro-inflammatory priming. *Am. J. Physiol.* 1824–1833.

Hayashi, K., Yamamoto, T. S. and Ueno, N. (2018). Intracellular calcium signal at the leading edge regulates mesodermal sheet migration during *Xenopus* gastrulation. *Sci. Rep.* **8**,.

Heasman, J., Kofron, M. and Wylie, C. (2000). β-catenin signaling activity dissected in the early *Xenopus* embryo: A novel antisense approach. *Dev. Biol.* **222**, 124–134.

Heisenberg, C. P. and Bellaïche, Y. (2013). Forces in tissue morphogenesis and patterning. *Cell* **153**,.

Helfand, B. T., Mendez, M. G., Murthy, S. N. P., Shumaker, D. K., Grin, B., Mahammad, S., Aebi, U., Wedig, T., Wu, Y. I., Hahn, K. M., et al. (2011). Vimentin organization modulates the formation of lamellipodia. *Mol. Biol. Cell* **22**, 1274–89.

Herrmann, H., Bär, H., Kreplak, L., Strelkov, S. V and Aebi, U. (2007). Intermediate filaments: from cell architecture to nanomechanics. *Nat. Rev. Mol. Cell Biol.* **8**, 562–73.

Hirsh, G., Dzamba, B.J., Sonavane, P.R., Allen, C.M. and DeSimone, D.W.

Plakoglobin is required for normal expression and assembly of fibronectin fibrills (in preparation).

Hodgson, L., Shen, F. and Hahn, K. (2010). Biosensors for characterizing the dynamics of rho family GTPases in living cells. *Curr. Protoc. Cell Biol.* **Chapter 14**, Unit 14.11.1-26.

Hoffstrom, Benjamin Gerald. 2002. Integrin function during *Xenopus* laevis gastrulation. Ph.D. diss., University of Virginia,

Homan, S. M., Martinez, R., Benware, A. and LaFlamme, S. E. (2002). Regulation of the association of α6β4 with vimentin intermediate filaments in endothelial cells. *Exp. Cell Res.* **281**, 107–114.

Hove Jay R., Koster Reinhard W. Forouhar Arian S. Acevedo-Bolton Gabriel, F. S. E. G. M. (2003). Intracardiac fluid forces are an essential epigenetic factor for embryonic cardiogenesis. *Nature* **421**,.

Huang, J., Deng, H., Peng, X., Li, S., Xiong, C. and Fang, J. (2012). Cellular traction force reconstruction based on a self-adaptive filtering scheme. *Cell. Mol. Bioeng.* **5**, 205–216.

Huang, D. L., Bax, N. A., Buckley, C. D., Weis, W. I. and Dunn, A. R. (2017). Vinculin forms a directionally asymmetric catch bond with F-actin. *Science (80-.).* **357**, 703–706.

Huen, A. C., Park, J. K., Godsel, L. M., Chen, X., Bannon, L. J., Amargo, E. V., Hudson, T. Y., Mongiu, A. K., Leigh, I. M., Kelsell, D. P., et al. (2002). Intermediate filament-membrane attachments function synergistically with actin-dependent contacts to regulate intercellular adhesive strength. *J. Cell Biol.* **159**, 1005–1017.

Humphries, M. J. (2002). Insights into integrin-ligand binding and activation from the first crystal structure. *Arthritis Res.* **4 Suppl 3**, S69–S78.

Humphries, J. D., Wang, P., Streuli, C., Geiger, B., Humphries, M. J. and Ballestrem, C. (2007). Vinculin controls focal adhesion formation by direct interactions with talin and actin. *J. Cell Biol.* **179**, 1043–1057.

Hunter, M. V. and Fernandez-Gonzalez, R. (2017). Coordinating cell movements in vivo: junctional and cytoskeletal dynamics lead the way. *Curr. Opin. Cell Biol.* **48**, 54–62.

Huveneers, S. and Danen, E. H. J. (2009). Adhesion signaling - crosstalk between integrins, Src and Rho. *J. Cell Sci.* **122**, 1059–1069.

Huveneers, S., Oldenburg, J., Spanjaard, E., van der Krogt, G., Grigoriev, I., Akhmanova, A., Rehmann, H. and de Rooij, J. (2012). Vinculin associates with endothelial VE-cadherin junctions to control force-dependent remodeling. *J. Cell Biol.* **196**, 641–652.

Hynes, R. O. (2002). Integrins: Bidirectional, allosteric signaling machines. *Cell* **110**, 673–

687.

Ilić, D., Furuta, Y., Kanazawa, S., Takeda, N., Sobue, K., Nakatsuji, N., Nomura, S., Fujimoto, J., Okada, M. and Yamamoto, T. (1995). Reduced cell motility and enhanced focal adhesion contact formation in cells from FAK-deficient mice. *Nature* **377**, 539–544.

Inaki, M., Vishnu, S., Cliffe, A. and Rorth, P. (2012). Effective guidance of collective migration based on differences in cell states. *Proc. Natl. Acad. Sci.* **109**, 2027–2032.

Irwin McLean, W. H., Pulkkinen, L., Smith, F. J. D., Rugg, E. L., Lane, E. B., Bullrich, F., Burgeson, R. E., Amano, S., Hudson, D. L., Owaribe, K., McMilla, J. R., Eady, R. A. J., Leigh, I. M., and Christiano, A. M. and Uitto, J. (1996). Loss of plectin causes epidermolysis bullosa with muscular dystrophy: cDNA cloning and genomic organization. *Genes Dev.* **10**, 1724–1735.

Iskratsch, T., Wolfenson, H. and Sheetz, M. P. (2014). Appreciating force and shape-the rise of mechanotransduction in cell biology. *Nat. Rev. Mol. Cell Biol.* **15**, 825–833.

Jacobson, K., Rajfur, Z., Vitriol, E. and Hahn, K. (2008). Chromophore-assisted laser inactivation in cell biology. *Trends Cell Biol.* **18**, 443–450.

Jiu, Y., Peränen, J., Schaible, N., Cheng, F., Eriksson, J. E., Krishnan, R. and Lappalainen, P. (2017). Vimentin intermediate filaments control actin stress fiber assembly through GEF-H1 and RhoA. *J. Cell Sci.* **130**, 892–902.

Jou, T. S. and Nelson, W. J. (1998). Effects of regulated expression of mutant RhoA and Rac1 small GTPases on the development of epithelial (MDCK) cell polarity. *J. Cell Biol.* **142**, 85–100.

Karnovsky, a and Klymkowsky, M. W. (1995). Anterior axis duplication in *Xenopus* induced by the over-expression of the cadherin-binding protein plakoglobin. *Proc. Natl. Acad. Sci. U. S. A.* **92**, 4522–6.

Kawakatsu, T., Ogita, H., Fukuhara, T., Fukuyama, T., Minami, Y., Shimizu, K. and Takai, Y. (2005). Vav2 as a Rac-GDP/GTP exchange factor responsible for the nectin-induced, c-Src- and Cdc42-mediated activation of Rac. *J. Biol. Chem.* **280**, 4940–4947.

Keller, R., Davidson, L., Edlund, A., Elul, T., Ezin, M., Shook, D. and Skoglund, P. (2000). Mechanisms of convergence and extension by cell intercalation. *Philos. Trans. R. Soc. B Biol. Sci.* **355**, 897–922.

Keller, R., Davidson, L. a and Shook, D. R. (2003). How we are shaped: the biomechanics of gastrulation. *Differentiation.* **71**, 171–205.

Kemler, R. Hierholzer, A. Kanzler, B. Kuppig, S. Hansen, S. Hansen, K. Taketo, MM. de Vries, WN. Knowles, BB. Solter, D. (2004). Stabilization of β-catenin in the mouse zygote leads to premature epithelial-mesenchymal transition in the epiblast. *Development* **131**, 5817–5824.

Kerr, J. P., Robison, P., Shi, G., Bogush, A. I., Kempema, A. M., Hexum, J. K., Becerra, N., Harki, D. A., Martin, S. S., Raiteri, R., Prosser, B. L. and Ward, C. W. (2015). Detyrosinated microtubules modulate mechanotransduction in heart and skeletal muscle. *Nat. Commun.* **6**,.

Kiehart, D. P., Galbraith, C. G., Edwards, K. A., Rickoll, W. L. and Montague, R. A. (2000). Multiple forces contribute to cell sheet morphogenesis for dorsal closure in Drosophila. *J. Cell Biol.* **149**, 471–490.

Kitt, K. N. and Nelson, W. J. (2011). Rapid suppression of activated Rac1 by cadherins and nectins during de novo cell-cell adhesion. *PLoS One* **6**, e17841.

Klymkowsky, M. W., Shook, D. R. and Maynell, L. a (1992). Evidence that the deep keratin filament systems of the *Xenopus* embryo act to ensure normal gastrulation. *Proc. Natl. Acad. Sci. U. S. A.* **89**, 8736–8740.

Klymkowsky, M. W., Williams, B. O., Barish, G. D., Varmus, H. E. and Vourgourakis, Y. E. (1999). Membrane-anchored plakoglobins have multiple mechanisms of action in Wnt signaling. *Mol. Biol. Cell* **10**, 3151–69.

Knutsdottir, H., Zmurchok, C., Bhaskar, D., Palsson, E., Dalle Nogare, D., Chitnis, A. B. and Edelstein-Keshet, L. (2017). Polarization and migration in the zebrafish posterior lateral line system. *PLoS Comput. Biol.* **13**, 1–26.

Kofron, M., Heasman, J., Lang, S. A. and Wylie, C. C. (2002). Plakoglobin is required for maintenance of the cortical actin skeleton in early *Xenopus* embryos and for Cdc42-mediated wound healing. *J. Cell Biol.* **158**, 695–708.

Kondapalli, J., Flozak, A. S. and Albuquerque, M. L. C. (2004). Laminar Shear Stress Differentially Modulates Gene Expression of p120 Catenin , Kaiso Transcription Factor , and Vascular Endothelial Cadherin in Human Coronary Artery Endothelial Cells. *J. Biol. Chem.* **279**, 11417–11424.

Kornberg, T. B. and Roy, S. (2014). Cytonemes as specialized signaling filopodia. *Development* **141**, 729–736.

Kowalczyk, A. P., Bornslaeger, E. A., Borgwardt, J. E., Palka, H. L., Dhaliwal, A. S., Corcoran, C. M., Denning, M. F. and Green, K. J. (1997). The amino-terminal domain of desmoplakin binds to plakoglobin and clusters desmosomal cadherin-plakoglobin complexes. *J. Cell Biol.* **139**, 773–784.

Kowalczyk, a P., Navarro, P., Dejana, E., Bornslaeger, E. a, Green, K. J., Kopp, D. S. and Borgwardt, J. E. (1998). VE-cadherin and desmoplakin are assembled into dermal microvascular endothelial intercellular junctions: a pivotal role for plakoglobin in the recruitment of desmoplakin to intercellular junctions. *J. Cell Sci.* **111**, 3045–3057.

Kowalczyk, A. P., Hatzfeld, M., Bornslaeger, E. A., Kopp, D. S., Borgwardt, J. E., Corcoran, C. M., Settler, A. and Green, K. J. (1999). The head domain of plakophilin-1 binds to desmoplakin and enhances its recruitment to desmosomes. Implications for cutaneous disease. *J. Biol. Chem.* **274**, 18145–18148.

Krens, S. F. G., Veldhuis, J. H., Barone, V., Čapek, D., Maître, J.-L., Brodland, G. W. and Heisenberg, C.-P. (2017). Interstitial fluid osmolarity modulates the action of differential tissue surface tension in progenitor cell segregation during gastrulation. *Development* **144**, 1798–1806.

Krieg, M., Arboleda-Estudillo, Y., Puech, P. H., Käfer, J., Graner, F., Müller, D. J. and Heisenberg, C. P. (2008). Tensile forces govern germ-layer organization in zebrafish. *Nat. Cell Biol.* **10**, 429–436.

Kröger, C., Loschke, F., Schwarz, N., Windoffer, R., Leube, R. E. and Magin, T. M. (2013). Keratins control intercellular adhesion involving PKC-α-mediated desmoplakin phosphorylation. *J. Cell Biol.* **201**, 681–692.

Kumar, A., Ouyang, M., Van den Dries, K., McGhee, E. J., Tanaka, K., Anderson, M. D., Groisman, A., Goult, B. T., Anderson, K. I. and Schwartz, M. A. (2016). Talin tension sensor reveals novel features of focal adhesion force transmission and mechanosensitivity. *J. Cell Biol.* **213**, 371–383.

Ladoux, B., Nelson, W. J., Yan, J. and Mège, R. M. (2015). The mechanotransduction machinery at work at adherens junctions. *Integr. Biol.* **7**, 1109–1119.

Lagendijk, A. K., Gomez, G. A., Baek, S., Hesselson, D., Hughes, W. E., Paterson, S., Conway, D. E., Belting, H. G., Affolter, M., Smith, K. A., Schwartz, M. A., Yap, A. S. and Hogan, B. M. (2017). Live imaging molecular changes in junctional tension upon VE-cadherin in zebrafish. *Nat. Commun.* **8**,.

Lauffenburger, D. A. and Horwitz, A. F. (1996). Cell migration: A physically integrated molecular process. *Cell* **84**, 359–369.

Lawson, C., Lim, S. T., Uryu, S., Chen, X. L., Calderwood, D. A. and Schlaepfer, D. D. (2012). FAK promotes recruitment of talin to nascent adhesions to control cell motility. *J. Cell Biol.* **196**, 223–232.

Le Duc, Q., Shi, Q., Blonk, I., Sonnenberg, A., Wang, N., Leckband, D. and De Rooij, J. (2010). Vinculin potentiates E-cadherin mechanosensing and is recruited to actin-anchored sites within adherens junctions in a myosin II-dependent manner. *J. Cell Biol.* **189**, 1107–1115.

Lecaudey, V., Cakan-Akdogan, G., Norton, W. H. J. and Gilmour, D. (2008). Dynamic Fgf signaling couples morphogenesis and migration in the zebrafish lateral line primordium. *Development* **135**, 2695–2705.

Leckband, D. E. and de Rooij, J. (2014). Cadherin Adhesion and Mechanotransduction. *Annu. Rev. Cell Dev. Biol.* **30**, 291–315.

Lecuit, T., Lenne, P.-F. and Munro, E. (2011). Force Generation, Transmission, and Integration during Cell and Tissue Morphogenesis. *Annu. Rev. Cell Dev. Biol.* **27**, 157–184.

LeGoff, L., Rouault, H. and Lecuit, T. (2013). A global pattern of mechanical stress polarizes cell divisions and cell shape in the growing *Drosophila* wing disc. *Development* **140**, 4051–4059.

Leonard, M., Chan, Y. and Menko, A. S. (2008). Identification of a novel intermediate filament-linked N-cadherin/γ-catenin complex involved in the establishment of the cytoarchitecture of differentiated lens fiber cells. *Dev. Biol.* **319**, 298–308.

Lesman, A., Notbohm, J., Tirrell, D. A. and Ravichandran, G. (2014). Contractile forces regulate cell division in three-dimensional environments. *J. Cell Biol.* **205**, 155–162.

Li, D., Zhang, W., Liu, Y., Haneline, L. S. and Shou, W. (2012). Lack of plakoglobin in epidermis leads to keratoderma. *J. Biol. Chem.* **287**, 10435–10443.

Li, J., Wang, Z., Chu, Q., Jiang, K., Li, J. and Tang, N. (2018). The Strength of Mechanical Forces Determines the Differentiation of Alveolar Epithelial Cells. *Dev. Cell* **44**, 297–312.e5.

Liu, Z., Tan, J. L., Cohen, D. M., Yang, M. T., Sniadecki, N. J., Ruiz, S. A., Nelson, C. M. and Chen, C. S. (2010). Mechanical tugging force regulates the size of cell-cell junctions. *Proc. Natl. Acad. Sci.* **107**, 9944–9949.

Lowery, J., Kuczmarski, E. R., Herrmann, H. and Goldma, R. D. (2015). Intermediate filaments play a pivotal role in regulating cell architecture and function. *J. Biol. Chem.* **290**, 17145–17153.

Lu, P., Takai, K., Weaver, V. M. and Werb, Z. (2011). Extracellular matrix degradation and remodeling in development and disease. *Cold Spring Harb Perspect Biol* **3**, 1–24.

Lyons, J. S., Joca, H. C., Law, R. A., Williams, K. M., Kerr, J. P., Shi, G., Khairallah, R. J., Martin, S. S., Konstantopoulos, K., Ward, C. W., and Stains, J. P. (2017). Microtubules tune mechanotransduction through NOX2 and TRPV4 to decrease sclerostin abundance in osteocytes. *Sci. Signal.* **10**,.

MacHacek, M., Hodgson, L., Welch, C., Elliott, H., Pertz, O., Nalbant, P., Abell, A., Johnson, G. L., Hahn, K. M. and Danuser, G. (2009). Coordination of Rho GTPase activities during cell protrusion. *Nature* **461**, 99–103.

Machesky, L. M., Mullins, R. D., Higgs, H. N., Kaiser, D. a, Blanchoin, L., May, R. C., Hall, M. E. and Pollard, T. D. (1999). Scar, a WASp-related protein, activates nucleation of actin filaments by the Arp2/3 complex. *Proc. Natl. Acad. Sci. U. S. A.* **96**, 3739–3744.

Maître, J. L., Berthoumieux, H., Krens, S. F. G., Salbreux, G., Jülicher, F., Paluch, E. and Heisenberg, C. P. (2012). Adhesion functions in cell sorting by mechanically coupling the cortices of adhering cells. *Science (80-.).* **338**, 253–256.

Malet-engra, G., Yu, W., Oldani, A., Rey-barroso, J., Gov, N. S., Scita, G. and Paolo, S. (2015). Report Collective Cell Motility Promotes Chemotactic Prowess and Resistance to Chemorepulsion. *Curr. Biol.* 242–250.

Mammoto, T. and Ingber, D. E. (2010). Mechanical control of tissue and organ development. *Development* **137**, 1407–1420.

Mammoto, T., Mammoto, A. and Ingber, D. E. (2013). Mechanobiology and

Developmental Control. *Annu. Rev. Cell Dev. Biol.* **29**, 27–61.

Mao, Y., Tournier, A. L., Hoppe, A., Kester, L., Thompson, B. J. and Tapon, N. (2013). Differential proliferation rates generate patterns of mechanical tension that orient tissue growth. *EMBO J.* **32**, 2790–2803.

Marsden, M. and DeSimone, D. W. (2001). Regulation of cell polarity, radial intercalation and epiboly in *Xenopus*: novel roles for integrin and fibronectin. *Development* **128**, 3635–3647.

Marsden, M. and DeSimone, D. W. (2003). Integrin-ECM interactions regulate cadherin-dependent cell adhesion and are required for convergent extension in *Xenopus*. *Curr. Biol.* **13**, 1182–1191.

Maruthamuthu, V., Sabass, B., Schwarz, U. S. and Gardel, M. L. (2011). Cell-ECM traction force modulates endogenous tension at cell – cell contacts.

Mauck, R. L., Yuan, X. and Tuan, R. S. (2006). Chondrogenic differentiation and functional maturation of bovine mesenchymal stem cells in long-term agarose culture. *Osteoarthr. Cartil.* **14**, 179–189.

Mayor, R. and Carmona-Fontaine, C. (2010). Keeping in touch with contact inhibition of locomotion. *Trends Cell Biol.* **20**, 319–328.

Mayor, R. and Etienne-Manneville, S. (2016). The front and rear of collective cell migration. *Nat. Rev. Mol. Cell Biol.* **17**, 97–109.

McGrath, J. A., McMillan, J. R., Shemanko, C. S., Runswick, S. K., Leigh, I. M., Lane, E. B., Garrod, D. R. and Eady, R. A. J. (1997). Mutations in the plakophilin 1 gene result in ectodermal dysplasia/skin fragility syndrome. *Nat. Genet.* **17**, 244.

Mendez, M. G., Restle, D. and Janmey, P. A. (2014). Vimentin enhances cell elastic behavior and protects against compressive stress. *Biophys. J.* **107**, 314–323.

Merriam, J. M., Rubenstein, A. B. and Klymkowsky, M. W. (1997). Cytoplasmically anchored plakoglobin induces a WNT-like phenotype in *Xenopus*. *Dev. Biol.* **185**, 67–81.

Mertz, A. F., Che, Y., Banerjee, S., Goldstein, J. M., Rosowski, K. A., Revilla, S. F., Niessen, C. M., Marchetti, M. C., Dufresne, E. R. and Horsley, V. (2013). Cadherin-based intercellular adhesions organize epithelial cell-matrix traction forces. *Proc. Natl. Acad. Sci.* **110**, 842–847.

Miller, C. J. and Davidson, L. A. (2013). The interplay between cell signalling and mechanics in developmental processes. *Nat. Rev. Genet.* **14**, 733–744.

Miyake, Y., Inoue, N., Nishimura, K., Kinoshita, N., Hosoya, H. and Yonemura, S. (2006). Actomyosin tension is required for correct recruitment of adherens junction components and zonula occludens formation. *Exp. Cell Res.* **312**, 1637–1650.

Moore, K. A., Huang, S., Kong, Y. P., Sunday, M. E. and Ingber, D. E. (2002). Control of embryonic lung branching morphogenesis by the Rho activator, cytotoxic

necrotizing factor 1. *J. Surg. Res.* **104**, 95–100.

Moore, K. A., Polte, T., Huang, S., Shi, B., Alsberg, E., Sunday, M. E. and Ingber, D. E. (2005). Control of basement membrane remodeling and epithelial branching morphogenesis in embryonic lung by Rho and cytoskeletal tension. *Dev. Dyn.* **232**, 268–281.

Moosmann, J., Ershov, A., Altapova, V., Baumbach, T., Prasad, M. S., Labonne, C., Xiao, X., Kashef, J. and Hofmann, R. (2013). X-ray phase-contrast in vivo microtomography probes new aspects of *Xenopus* gastrulation. *Nature* **497**, 374–377.

Morita, H., Grigolon, S., Bock, M., Krens, S. F. G., Salbreux, G. and Heisenberg, C. P. (2017). The Physical Basis of Coordinated Tissue Spreading in Zebrafish Gastrulation. *Dev. Cell* **40**, 354–366.e4.

Morrison, S. J. and Kimble, J. (2006). Asymmetric and symmetric stem-cell divisions in development and cancer. *Nature* **441**, 1068–1074.

Mould, A. P., Askari, J. A., Barton, S., Kline, A. D., McEwan, P. A., Craig, S. E. and Humphries, M. J. (2002). Integrin activation involves a conformational change in the α1 helix of the β subunit A-domain. *J. Biol. Chem.* **277**, 19800–19805.

Nagel, M. Tahinci, E. Symes, K. Winklbauer, R. (2004). Guidance of mesoderm cell migration in the *Xenopus* gastrula requires PDGF signaling. *Development* **131**, 2727–2736.

Nakagawa, M., Fukata, M., Yamaga, M., Itoh, N. and Kaibuchi, K. (2001). Recruitment and activation of Rac1 by the formation of E-cadherin-mediated cell-cell adhesion sites. *J. Cell Sci.* **114**, 1829–38.

Nelson, W. J. (2008). Regulation of cell–cell adhesion by the cadherin–catenin complex. *Biochem. Soc. Trans.* **36**, 149–155.

Nestor-Bergmann, A., Goddard, G. and Woolner, S. (2014). Force and the spindle: Mechanical cues in mitotic spindle orientation. *Semin. Cell Dev. Biol.* **34**, 133–139.

Nethe, M. and Hordijk, P. L. (2010). The role of ubiquitylation and degradation in RhoGTPase signalling. *J. Cell Sci.* **123**, 4011–8.

Niessen, C. M., Leckband, D. and Yap, A. S. (2011). Tissue Organization by Cadherin Adhesion Molecules: Dynamic Molecular and Cellular Mechanisms of Morphogenetic Regulation. *Physiol. Rev.* **91**, 691–731.

Nieuwkoop P., F. J. (1994). *Normal Table of Xenopus Laevis (Daudin): A Systematical & Chronological Survey of the Development from the Fertilized Egg till the End of Metamorphosis*.

Nishiya, N., Kiosses, W. B., Han, J. and Ginsberg, M. H. (2005). An α4integrin-paxillin-Arf-GAP complex restricts Rac activation to the leading edge of migrating cells. *Nat. Cell Biol.* **7**, 343–352.

Nobes, C. D. and Hall, A. (1995). Rho, Rac, and Cdc42 GTPases regulate the assembly

of multimolecular focal complexes associated with actin stress fibers, lamellipodia, and filopodia. *Cell* **81**, 53–62.

Nobes, C. D. and Hall, A. (1999). Rho GTPases control polarity, protrusion, and adhesion during cell movement. *J. Cell Biol.* **144**, 1235–1244.

Nonaka, S., Shiratori, H., Saijoh, Y. and Hamada, H. (2002). Determination of left-right patterning of the mouse embryo by artificial nodal flow. *Nature* **418**, 96–99.

Noria, S., Cowan, D. B., Gotlieb, A. I. and Langille, B. L. (1999). Transient and Steady-State Effects of Shear Stress on Endothelial Cell Adherens Junctions. *Circ. Res.* **85**, 504–514.

Noria, S., Xu, F., McCue, S., Jones, M., Gotlieb, A. I. and Langille, B. L. (2004). Assembly and Reorientation of Stress Fibers Drives Morphological Changes to Endothelial Cells Exposed to Shear Stress. *Am. J. Pathol.* **164**, 1211–1223.

Olson, E. N. and Nordheim, A. (2010). Linking actin dynamics and gene transcription to drive cellular motile functions. *Nat. Rev. Mol. Cell Biol.* **11**, 353–365.

Osmanagic-Myers, S., Gregor, M., Walko, G., Burgstaller, G., Reipert, S. and Wiche, G. (2006). Plectin-controlled keratin cytoarchitecture affects MAP kinases involved in cellular stress response and migration. *J. Cell Biol.* **174**, 557–568.

Palazzo, A. F., Eng, C. H., Schlaepfer, D. D., Marcantonio, E. E. and Gundersen, G. G. (2004). Localized Stabilization of Microtubules by Integrin- and FAK-Facilitated Rho Signaling. *Science (80-.).* **303**, 836–839.

Panadero, J. A., Lanceros-Mendez, S. and Ribelles, J. L. G. (2016). Differentiation of mesenchymal stem cells for cartilage tissue engineering: Individual and synergetic effects of three-dimensional environment and mechanical loading. *Acta Biomater.* **33**, 1–12.

Parsons, S. J. and Parsons, J. T. (2004). Src family kinases, key regulators of signal transduction. *Oncogene* **23**, 7906–7909.

Pasapera, A. M., Schneider, I. C., Rericha, E., Schlaepfer, D. D. and Waterman, C. M. (2010). Myosin II activity regulates vinculin recruitment to focal adhesions through FAK-mediated paxillin phosphorylation. *J. Cell Biol.* **188**, 877–890.

Paszek, M. J., Boettiger, D., Weaver, V. M. and Hammer, D. A. (2009). Integrin clustering is driven by mechanical resistance from the glycocalyx and the substrate. *PLoS Comput. Biol.* **5**,.

Patil, S., Jedsadayanmata, A., Wencel-Drake, J. D., Wang, W., Knezevic, I. and Lam, S. C. T. (1999). Identification of a talin-binding site in the integrin β3subunit distinct from the NPLY regulatory motif of post-ligand binding functions. The talin N-terminal head domain interacts with the membrane-proximal region of the β3cytoplasmic tail. *J. Biol. Chem.* **274**, 28575–28583.

Petridou, N. I. and Skourides, P. A. (2014). FAK transduces extracellular forces that orient the mitotic spindle and control tissue morphogenesis. *Nat. Commun.* **5**, 5240.

Pfister, K., Shook, D. R., Chang, C., Keller, R. and Skoglund, P. (2016). Molecular model for force production and transmission during vertebrate gastrulation. *Development* **143**, 715–727.

Pines, M., Das, R., Ellis, S. J., Morin, A., Czerniecki, S., Yuan, L., Klose, M., Coombs, D. and Tanentzapf, G. (2012). Mechanical force regulates integrin turnover in Drosophila in vivo. *Nat. Cell Biol.* **14**, 935–943.

Pinheiro, D., Hannezo, E., Herszterg, S., Bosveld, F., Gaugue, I., Balakireva, M., Wang, Z., Cristo, I., Rigaud, S. U., Markova, O., et al. (2017). Transmission of cytokinesis forces via E-cadherin dilution and actomyosin flows. *Nature* **545**, 103–107.

Plotnikov, S. V., Pasapera, A. M., Sabass, B. and Waterman, C. M. (2012). Force fluctuations within focal adhesions mediate ECM-rigidity sensing to guide directed cell migration. *Cell* **151**, 1513–1527.

Plouhinec, J.-L., Zakin, L., Moriyama, Y. and De Robertis, E. M. (2013). Chordin forms a self-organizing morphogen gradient in the extracellular space between ectoderm and mesoderm in the *Xenopus* embryo. *Proc. Natl. Acad. Sci.* **110**, 20372–20379.

Pluskota, E., Bledzka, K. M., Bialkowska, K., Szpak, D., Soloviev, D. A., Jones, S. V, Verbovetskiy, D. and Plow, E. F. (2017). Kindlin-2 interacts with endothelial adherens junctions to support vascular barrier integrity. *J. Physiol.* **20**, 6443–6462.

Plutoni, C., Bazellieres, E., Le Borgne-Rochet, M., Comunale, F., Brugues, A., Séveno, M., Planchon, D., Thuault, S., Morin, N., Bodin, S., Trepat, X. and Gauthier-Rouvière, C. (2016). P-cadherin promotes collective cell migration via a Cdc42-mediated increase in mechanical forces. *J. Cell Biol.* **212**, 199–217.

Prager-Khoutorsky, M., Lichtenstein, A., Krishnan, R., Rajendran, K., Mayo, A., Kam, Z., Geiger, B. and Bershadsky, A. D. (2011). Fibroblast polarization is a matrix-rigidity-dependent process controlled by focal adhesion mechanosensing. *Nat. Cell Biol.* **13**, 1457–1465.

Przybyla, L., Muncie, J. M. and Weaver, V. M. (2016). Mechanical Control of Epithelial-to-Mesenchymal Transitions in Development and Cancer. *Annu. Rev. Cell Dev. Biol.* **32**, 527–554.

Rajagopalan, P., Marganski, W. A., Brown, X. Q. and Wong, J. Y. (2004). Direct comparison of the spread area, contractility, and migration of balb/c 3T3 fibroblasts adhered to fibronectin- and RGD-modified substrata. *Biophys. J.* **87**, 2818–2827.

Ramírez-Weber, F. A. and Kornberg, T. B. (1999). Cytonemes: Cellular processes that project to the principal signaling center in Drosophila imaginal discs. *Cell* **97**, 599–607.

Ramms, L., Fabris, G., Windoffer, R., Schwarz, N., Springer, R., Zhou, C., Lazar, J., Stiefel, S., Hersch, N., Schnakenberg, U., Magin, T. M., Leube, R. E., Merkel, R. and Hoffman, B. (2013). Keratins as the main component for the mechanical integrity

of keratinocytes. *Proc. Natl. Acad. Sci.* **110**, 18513–18518.

Ramos, J. W. and DeSimone, D. W. (1996). *Xenopus* embryonic cell adhesion to fibronectin: Position-specific activation of RGD/synergy site-dependent migratory behavior at gastrulation. *J. Cell Biol.* **134**, 227–240.

Rappaport, R. (1999). Absence of furrowing activity following regional cortical tension reduction in sand dollar blastomere and fertilized egg fragment surfaces. *Dev. Growth Differ.* **41**, 441–447.

Rappaport, R. and Rappaport, B. N. (1974). Establishment of cleavage furrows by the mitotic spindle. *J. Exp. Zool.* **189**, 189–196.

Rausch, S., Das, T., Soiné, J. R. D., Hofmann, T. W., Boehm, C. H. J., Schwarz, U. S., Boehm, H. and Spatz, J. P. (2013). Polarizing cytoskeletal tension to induce leader cell formation during collective cell migration. *Biointerphases* **8**,.

Rauzi, M., Krzic, U., Saunders, T. E., Krajnc, M., Ziherl, P., Hufnagel, L. and Leptin, M. (2015). Embryo-scale tissue mechanics during Drosophila gastrulation movements. *Nat. Commun.* **6**,.

Reffay, M., Parrini, M. C., Cochet-Escartin, O., Ladoux, B., Buguin, A., Coscoy, S., Amblard, F., Camonis, J. and Silberzan, P. (2014). Interplay of RhoA and mechanical forces in collective cell migration driven by leader cells. *Nat. Cell Biol.* **16**, 217–223.

Richardson, C.M., Dzamba, B.J., Sonavane, P.R. and DeSeimone, D.W. Integrin and ligand-independent PDGFr signaling synergistically contributes to directional migration of *Xenopus* mesendoderm (in preparation).

Ridge, K. M., Linz, L., Flitney, F. W., Kuczmarski, E. R., Chou, Y. H., Omary, M. B., Sznajder, J. I. and Goldman, R. D. (2005). Keratin 8 phosphorylation by protein kinase C δ regulates shear stress-mediated disassembly of keratin intermediate filaments in alveolar epithelial cells. *J. Biol. Chem.* **280**, 30400–30405.

Ridley, A. J. (2015). Rho GTPase signalling in cell migration. *Curr. Opin. Cell Biol.* **36**, 103–112.

Ridley, A. J., Paterson, H. F., Johnston, C. L., Diekmann, D. and Hall, A. (1992). The small GTP-binding protein rac regulates growth factor-induced membrane ruffling. *Cell* **70**, 401–410.

Riedl, J., Crevenna, A. H., Kessenbrock, K., Yu, J. H., Neukirchen, D., Bista, M., Bradke, F., Jenne, D., Holak, T. A., Werb, Z., Sixt, M. and Wedlich-Soldner, R. (2008). Lifeact: A versatile marker to visualize F-actin. *Nat. Methods* **5**, 605–607.

Robison, P., Caporizzo, M. A., Ahmadzadeh, H., Bogush, A. I., Chen, C. Y., Margulies, K. B., Shenoy, V. B. and Prosser, B. L. (2016). Detyrosinated microtubules buckle and bear load in contracting cardiomyocytes. *Science (80-.).* **352**,.

Roca-Cusachs, P., del Rio, A., Puklin-Faucher, E., Gauthier, N. C., Biais, N. and

Sheetz, M. P. (2013). Integrin-dependent force transmission to the extracellular matrix by -actinin triggers adhesion maturation. *Proc. Natl. Acad. Sci.* **110**, E1361–E1370.

Rotty, J. D. and Coulombe, P. A. (2012). A wound-induced keratin inhibits Src activity during keratinocyte migration and tissue repair. *J. Cell Biol.* **197**, 381–389.

Roy, S., Huang, H., Liu, S. and Kornberg, T. B. (2014). Cytoneme-mediated contact-dependent transport of the Drosophila decapentaplegic signaling protein. *Science (80-.).* **343**,.

Rozario, T. and DeSimone, D. W. (2010). The extracellular matrix in development and morphogenesis: A dynamic view. *Dev. Biol.* **341**, 126–140.

Rozario, T., Dzamba, B., Weber, G. F., Davidson, L. A. and DeSimone, D. W. (2009). The physical state of fibronectin matrix differentially regulates morphogenetic movements in vivo. *Dev. Biol.* **327**, 386–398.

Ruiz, P., Brinkmann, V., Ledermann, B., Behrend, M., Grund, C., Thalhammer, C., Vogel, F., Birchmeier, C., Günthert, U., Franke, W. W., and Birchmeier, W. (1996). Targeted mutation of plakoglobin in mice reveals essential functions of desmosomes in the embryonic heart. *J. Cell Biol.* **135**, 215–25.

Rupprecht, J.-F., Ong, K. H., Yin, J., Huang, A., Dinh, H.-H.-Q., Singh, A. P., Zhang, S., Yu, W. and Saunders, T. E. (2017). Geometric constraints alter cell arrangements within curved epithelial tissues. *Mol. Biol. Cell* mbc.E17-01-0060.

Sakai, T., Larsen, M. and Yamada, K. M. (2003). Fibronectin requirement in branching morphogenesis. *Nature* **423**, 876–881.

Sanghvi-Shah, R. and Weber, G. F. (2017). Intermediate Filaments at the Junction of Mechanotransduction, Migration, and Development. *Front. Cell Dev. Biol.* **5**,.

Scarpa, E., Szabó, A., Bibonne, A., Theveneau, E., Parsons, M. and Mayor, R. (2015). Cadherin Switch during EMT in Neural Crest Cells Leads to Contact Inhibition of Locomotion via Repolarization of Forces. *Dev. Cell* **34**, 421–434.

Schaller, M. D. (2001). Paxillin: A focal adhesion-associated adaptor protein. *Oncogene* **20**, 6459–6472.

Schnatwinkel, C. and Niswander, L. (2013). Multiparametric image analysis of lung-branching morphogenesis. *Dev. Dyn.* **242**, 622–637.

Schwartz, M. a and DeSimone, D. W. (2008). Cell adhesion receptors in mechanotransduction. *Curr. Opin. Cell Biol.* **20**, 551–6.

Schwarz, U. S. and Gardel, M. L. (2012). United we stand: integrating the actin cytoskeleton and cell-matrix adhesions in cellular mechanotransduction. *J. Cell Sci.* **125**, 3051–60.

Seltmann, K., Roth, W., Loschke, F., Lederer, M., Hüttelmaier, S. and Magin, T. M. (2013). Keratins mediate localization of hemidesmosomes and repress cell motility. *J*

Invest Dermatol **133**, 181–190.

Shi, F. and Sottile, J. (2011). MT1-MMP regulates the turnover and endocytosis of extracellular matrix fibronectin. *J. Cell Sci.* **124**, 4039–4050.

Shindo, A. and Wallingford, J. B. (2014). PCP and septins compartmentalize collective cell movement. *Science (80-.).* **343**, 649–652.

Shraiman, B. I. (2005). Mechanical feedback as a possible regulator of tissue growth. *Proc. Natl. Acad. Sci.* **102**, 3318–3323.

Shyer, A. E., Rodrigues, A. R., Schroeder, G. G., Kassianidou, E., Kumar, S. and Harland, R. M. (2017). Emergent cellular self-organization and mechanosensation initiate follicle pattern in the avian skin. *Science (80-.).* **357**, 811–815.

Simmons, C. A., Matlis, S., Thornton, A. J., Chen, S., Wang, C. Y. and Mooney, D. J. (2003). Cyclic strain enhances matrix mineralization by adult human mesenchymal stem cells via the extracellular signal-regulated kinase (ERK1/2) signaling pathway. *J. Biomech.* **36**, 1087–1096.

Skoglund, P., Rolo, A., Chen, X., Gumbiner, B. M. and Keller, R. (2008). Convergence and extension at gastrulation require a myosin IIB-dependent cortical actin network. *Development* **135**, 2435–2444.

Smith, M. L., Gourdon, D., Little, W. C., Kubow, K. E., Eguiluz, R. A., Luna-Morris, S. and Vogel, V. (2007). Force-induced unfolding of fibronectin in the extracellular matrix of living cells. *PLoS Biol.* **5**, 2243–2254.

Smith, E. M., Mitsi, M., Nugent, M. A. and Symes, K. (2009). PDGF-A interactions with fibronectin reveal a critical role for heparan sulfate in directed cell migration during *Xenopus* gastrulation. *Proc. Natl. Acad. Sci.* **106**, 21683–21688.

Smutny, M., Ákos, Z., Grigolon, S., Shamipour, S., Ruprecht, V., Čapek, D., Behrndt, M., Papusheva, E., Tada, M., Hof, B., Vicsek, T., Salbreux, G. and Heisenberg, C. P. (2017). Friction forces position the neural anlage. *Nat. Cell Biol.* **19**, 306–317.

Solon, J., Kaya-Çopur, A., Colombelli, J. and Brunner, D. (2009). Pulsed Forces Timed by a Ratchet-like Mechanism Drive Directed Tissue Movement during Dorsal Closure. *Cell* **137**, 1331–1342.

Stamos, J. L. and Weis, W. I. (2013). The β-catenin destruction complex. *Cold Spring Harb. Perspect. Biol.* **5**,.

Stanganello, E. and Scholpp, S. (2016). Role of cytonemes in Wnt transport. *J. Cell Sci.* **129**, 665–672.

Streichan, S. J., Hoerner, C. R., Schneidt, T., Holzer, D. and Hufnagel, L. (2014). Spatial constraints control cell proliferation in tissues. *Proc. Natl. Acad. Sci. U. S. A.* **111**, 5586–91.

Stricker, J., Aratyn-Schaus, Y., Oakes, P. W. and Gardel, M. L. (2011). Spatiotemporal constraints on the force-dependent growth of focal adhesions. *Biophys. J.* **100**, 2883–

2893.

Sumigray, K., Zhou, K. and Lechler, T. (2014). Cell-cell adhesions and cell contractility are upregulated upon desmosome disruption. *PLoS One* **9**, 1–8.

Takahashi, K. and Coulombe, P. A. (1996). A transgenic mouse model with an inducible skin blistering disease phenotype. *Proc. Natl. Acad. Sci. U. S. A.* **93**, 14776–14781.

Takemoto, K., Matsuda, T., Sakai, N., Fu, D., Noda, M., Uchiyama, S., Kotera, I., Arai, Y., Horiuchi, M., Fukui, K., Ayabe, T., Inagaki, F., Suzuki, H. and Nagai, T. (2013). SuperNova, a monomeric photosensitizing fluorescent protein for chromophore-assisted light inactivation. *Sci. Rep.* **3**, 1–7.

Tambe, D. T., Corey Hardin, C., Angelini, T. E., Rajendran, K., Park, C. Y., Serra-Picamal, X., Zhou, E. H., Zaman, M. H., Butler, J. P., Weitz, D. A., Fredberg, J. J. and Trepat, X. (2011). Collective cell guidance by cooperative intercellular forces. *Nat. Mater.* **10**, 469–475.

Tanentzapf, G. and Brown, N. H. (2006). An interaction between integrin and the talin FERM domain mediates integrin activation but not linkage to the cytoskeleton. *Nat. Cell Biol.* **8**, 601–606.

Tang, Z., Hu, Y., Wang, Z., Jiang, K., Zhan, C., Marshall, W. F. and Tang, N. (2018). Mechanical Forces Program the Orientation of Cell Division during Airway Tube Morphogenesis. *Dev. Cell*.

Theveneau, E. and Mayor, R. (2013). Collective cell migration of epithelial and mesenchymal cells. *Cell. Mol. Life Sci.* **70**, 3481–3492.

Theveneau, E., Marchant, L., Kuriyama, S., Gull, M., Moepps, B., Parsons, M. and Mayor, R. (2010). Collective Chemotaxis Requires Contact-Dependent Cell Polarity. *Dev. Cell* **19**, 39–53.

Thomas, W. A., Boscher, C., Chu, Y. S., Cuvelier, D., Martinez-Rico, C., Seddiki, R., Heysch, J., Ladoux, B., Thiery, J. P., Mege, R. M., and Dufour, S. (2013). α-Catenin and vinculin cooperate to promote high E-cadherin-based adhesion strength. *J. Biol. Chem.* **288**, 4957–4969.

Todorović, V., Desai, B. V, Patterson, M. J. S., Amargo, E. V, Dubash, A. D., Yin, T., Jones, J. C. R. and Green, K. J. (2010). Plakoglobin regulates cell motility through Rho- and fibronectin-dependent Src signaling. *J. Cell Sci.* **123**, 3576–86.

Tojkander, S., Gateva, G. and Lappalainen, P. (2012). Actin stress fibers - assembly, dynamics and biological roles. *J. Cell Sci.* **125**, 1855–1864.

Trepat, X., Wasserman, M. R., Angelini, T. E., Millet, E., Weitz, D. a., Butler, J. P. and Fredberg, J. J. (2009). Physical forces during collective cell migration. *Nat. Phys.* **5**, 426–430.

Tse, J. M., Cheng, G., Tyrrell, J. A., Wilcox-Adelman, S. A., Boucher, Y., Jain, R. K. and Munn, L. L. (2012). Mechanical compression drives cancer cells toward invasive phenotype. *Proc. Natl. Acad. Sci.* **109**, 911–916.

Tseng, Q., Duchemin-Pelletier, E., Deshiere, A., Balland, M., Guillou, H., Filhol, O. and Thery, M. (2012). Spatial organization of the extracellular matrix regulates cell-cell junction positioning. *Proc. Natl. Acad. Sci.* **109**, 1506–1511.

Tsuchida, J., Ueki, S., Takada, Y., Saito, Y. and Takagi, J. (1998). The "ligand-induced conformational change" of α5β1 integrin. Relocation of α5 subunit to uncover the β1 stalk region. *J. Cell Sci.* **111 (Pt 1**, 1759–66.

Turner, C. E. (2000). Paxillin and focal adhesion signalling. *Nat. Cell Biol.* **2**, 231–236.

Tzima, E., Irani-Tehrani, M., Kiosses, W. B., Dejana, E., Schultz, D. A., Engelhardt, B., Cao, G., DeLisser, H. and Schwartz, M. A. (2005). A mechanosensory complex that mediates the endothelial cell response to fluid shear stress. *Nature* **437**, 426–431.

Ukropec, J. A., Hollinger, M. K. and Woolkalis, M. J. (2002). Regulation of VE-Cadherin Linkage to the Cytoskeleton in Endothelial Cells Exposed to Fluid Shear Stress. *Exp. Cell Res.* **247**, 240–247.

Uruno, T., Liu, J., Zhang, P., Fan, Y. X., Egile, C., Li, R., Mueller, S. C. and Zhan, X. (2001). Activation of Arp2/3 complex-mediated actin polymerization by cortactin. *Nat. Cell Biol.* **3**, 259–266.

Valgeirsdóttir, S., Claesson-Welsh, L., Bongcam-Rudloff, E., Hellman, U., Westermark, B. and Heldin, C. H. (1998). PDGF induces reorganization of vimentin filaments. *J. Cell Sci.* **111 (Pt 1**, 1973–1980.

Vasilyev, A., Liu, Y., Mudumana, S., Mangos, S., Lam, P. Y., Majumdar, A., Zhao, J., Poon, K. L., Kondrychyn, I., Korzh, V. and Drummond, A. (2009). Collective cell migration drives morphogenesis of the kidney nephron. *PLoS Biol.* **7**,.

Vassilev, V., Platek, A., Hiver, S., Enomoto, H. and Takeichi, M. (2017). Catenins Steer Cell Migration via Stabilization of Front-Rear Polarity. *Dev. Cell* **43**, 463–479.e5.

Vicente-Manzanares, M., Choi, C. K. and Horwitz, A. R. (2009). Integrins in cell migration - the actin connection. *J. Cell Sci.* **122**, 1473–1473.

Wang, Y., Jin, G., Miao, H., Li, J. Y.-S., Usami, S. and Chien, S. (2006). Integrins regulate VE-cadherin and catenins: dependence of this regulation on Src, but not on Ras. *Proc. Natl. Acad. Sci. U. S. A.* **103**, 1774–9.

Wang, X., He, L., Wu, Y. I., Hahn, K. M. and Montell, D. J. (2010). Light-mediated activation reveals a key role for Rac in collective guidance of cell movement in vivo. *Nat. Cell Biol.* **12**, 591–7.

Wang, S., Sekiguchi, R., Daley, W. P. and Yamada, K. M. (2017). Patterned cell and matrix dynamics in branching morphogenesis. *J. Cell Biol.* **216**, 559–570.

Webb, D. J., Parsons, J. T. and Horwitz, A. F. (2002). Adhesion assembly, disassembly and turnover in migrating cells - Over and over and over again. *Nat. Cell Biol.* **4**,.

Webb, D. J., Donais, K., Whitmore, L. A., Thomas, S. M., Turner, C. E., Parsons, J. T. and Horwitz, A. F. (2004). FAK-Src signalling through paxillin, ERK and MLCK

regulates adhesion disassembly. *Nat. Cell Biol.* **6**, 154–161.

Weber, G. F., Bjerke, M. a and DeSimone, D. W. (2011). Integrins and cadherins join forces to form adhesive networks. *J. Cell Sci.* **124**, 1183–93.

Weber, G. F., Bjerke, M. a and DeSimone, D. W. (2012). A mechanoresponsive cadherin-keratin complex directs polarized protrusive behavior and collective cell migration. *Dev. Cell* **22**, 104–15.

Wiche, G. (1998). Role of plectin in cytoskeleton organization and dynamics. *J. Cell Sci.* **111**, 2477–2486.

Winklbauer, R. and Nagel, M. (1991) Directional mesoderm cell migration in the *Xenopus* gastrula. *Dev. Biol.* **148**, 573-589

Winklbauer, R. and Selchow, A. (1992). Motile behavior and protrusive activity of migratory mesoderm cells from the *Xenopus* gastrula. *Dev. Biol.* **150**, 335–351.

Winklbauer, R., Selchow, A., Nagel, M. and Angres, B. (1992). Cell interaction and its role in mesoderm cell migration during *Xenopus* gastrulation. *Dev. Dyn.* **195**, 290–302.

Winklbauer, R., Nagel, M., Selchow, A. and Wacker, S. (1996). Mesoderm migration in the *Xenopus* gastrula. *Int. J. Dev. Biol.* **40**, 305–311.

Wolf, K., Wu, Y. I., Liu, Y., Geiger, J., Tam, E., Overall, C., Stack, M. S. and Friedl, P. (2007). Multi-step pericellular proteolysis controls the transition from individual to collective cancer cell invasion. *Nat. Cell Biol.* **9**, 893–904.

Wozniak, M. A. and Chen, C. S. (2009). Mechanotransduction in development: A growing role for contractility. *Nat. Rev. Mol. Cell Biol.* **10**, 34–43.

Wyatt, T. P. J., Harris, A. R., Lam, M., Cheng, Q., Bellis, J., Dimitracopoulos, A., Kabla, A. J., Charras, G. T. and Baum, B. (2015). Emergence of homeostatic epithelial packing and stress dissipation through divisions oriented along the long cell axis. *Proc. Natl. Acad. Sci.* **112**, 5726–5731.

Wylie, C., Kofron, M., Payne, C., Anderson, R., Hosobuchi, M., Joseph, E. and Heasman, J. (1996). Maternal beta-catenin establishes a "dorsal signal" in early *Xenopus* embryos. *Development* **122**, 2987–2996.

Xiong, F., Ma, W., Hiscock, T. W., Mosaliganti, K. R., Tentner, A. R., Brakke, K. A., Rannou, N., Gelas, A., Souhait, L., Swinburne, I. A., et al. (2014). Interplay of cell shape and division orientation promotes robust morphogenesis of developing epithelia. *Cell* **159**, 415–427.

Yamada, S. and Nelson, W. J. (2007). Localized zones of Rho and Rac activities drive initiation and expansion of epithelial cell-cell adhesion. *J. Cell Biol.* **178**, 517–527.

Yamaguchi, N., Mizutani, T., Kawabata, K. and Haga, H. (2015). Leader cells regulate collective cell migration via Rac activation in the downstream signaling of integrin β1 and PI3K. *Sci. Rep.* **5**, 1–8.

Yan, B. and Smith, J. W. (2001). Mechanism of integrin activation by disulfide bond reduction. *Biochemistry* **40**, 8861–8867.

Yang, J. and Weinberg, R. A. (2008). Epithelial-Mesenchymal Transition: At the Crossroads of Development and Tumor Metastasis. *Dev. Cell* **14**, 818–829.

Yao, M., Qiu, W., Liu, R., Efremov, A. K., Cong, P., Seddiki, R., Payre, M., Lim, C. T., Ladoux, B., Mège, R. M. and Yan, J. (2014). Force-dependent conformational switch of α -catenin controls vinculin binding. *Nat. Commun.* **5**,.

Yin, T., Getsios, S., Caldelari, R., Kowalczyk, A. P., Müller, E. J., Jones, J. C. R. and Green, K. J. (2005). Plakoglobin suppresses keratinocyte motility through both cell-cell adhesion-dependent and -independent mechanisms. *Proc. Natl. Acad. Sci. U. S. A.* **102**, 5420–5.

Yonemura, S., Itoh, M., Nagafuchi, A. and Tsukita, S. (1995). Cell-to-cell adherens junction formation and actin filament organization: similarities and differences between non-polarized fibroblasts and polarized epithelial cells. *J. Cell Sci.* **108**, 127–142.

Yonemura, S., Wada, Y., Watanabe, T., Nagafuchi, A. and Shibata, M. (2010). α-Catenin as a tension transducer that induces adherens junction development. *Nat. Cell Biol.* **12**, 533–542.

Yu, J. C. and Fernandez-Gonzalez, R. (2016). Local mechanical forces promote polarized junctional assembly and axis elongation in Drosophila. *Elife* **5**,.

Zhang, H., Landmann, F., Zahreddine, H., Rodriguez, D., Koch, M. and Labouesse, M. (2011). A tension-induced mechanotransduction pathway promotes epithelial morphogenesis. *Nature* **471**, 99–103.

Zhurinsky, J., Shtutman, M. and Ben-Ze'ev, A. (2000). Plakoglobin and β-catenin: protein interactions, regulation and biological roles. *J. Cell Sci.* **113 (Pt 1**, 3127–3139.